UNIVERSIDAD SAN FRANCISCO DE QUITO USFQ

Colegio de Ciencias e Ingenierías

Vibration Analysis of the human temporal bone when using Bone Conduction headphone applying the finite element method

Marco David Ramírez Ortiz

Ingeniería Mecánica

Trabajo de integración curricular presentado como requisito
para la obtención del título de
Ingeniero Mecánico

Quito, 06 de diciembre de 2019

UNIVERSIDAD SAN FRANCISCO DE QUITO USFQ

COLEGIO DE CIENCIAS E INGENIERÍAS

HOJA DE CALIFICACIÓN
DE TRABAJO DE INTEGRACIÓN CURRICULAR

Vibration Analysis of a human temporal bone when using Bone Conduction headphones applying the finite element method

Marco David Ramírez Ortiz

Calificación:

Nombre del profesor, Título académico Patricio Chiriboga, Ph.D.

Firma del profesor: _____

Nombre del profesor, Título académico Marco León, M. Sc.

Firma del profesor: _____

Quito, 06 de diciembre de 2019

Derechos de Autor

Por medio del presente documento certifico que he leído todas las Políticas y Manuales de la Universidad San Francisco de Quito USFQ, incluyendo la Política de Propiedad Intelectual USFQ, y estoy de acuerdo con su contenido, por lo que los derechos de propiedad intelectual del presente trabajo quedan sujetos a lo dispuesto en esas Políticas.

Asimismo, autorizo a la USFQ para que realice la digitalización y publicación de este trabajo en el repositorio virtual, de conformidad a lo dispuesto en el Art. 144 de la Ley Orgánica de Educación Superior.

Firma del estudiante: _____

Nombres y apellidos: Marco David Ramírez Ortiz

Código: 118309

Cédula de identidad: 1803845278

Lugar y fecha: Quito, 06 de diciembre de 2019

RESUMEN

Los auriculares Bone Conduction (BC) y Bone Conduction se han fabricado y estudiado durante más de una década, ya que esta tecnología está creciendo en el mundo de los audiófilos, se necesita la necesidad de una mejor calidad de los auriculares y el sonido que es transmitido. Es necesario no solo comprender mejor cómo se produce la vibración causada por los auriculares, sino también cómo mejorar la calidad del sonido que pueden proporcionar los auriculares. En este documento, se analiza la conducción ósea en un hueso temporal seco de la cabeza humana, evaluando la propagación de la vibración a través de la simulación por computadora con el método de elementos finitos FEM usando Ansys 2017 Student Edition. Para hacerlo, se prueba un hueso temporal real usando auriculares de conducción ósea que se encuentran en el mercado actual y un acelerómetro triaxial junto con un DAQ de National Instruments y LabView 2018 Student Edition, comparando ambos resultados. En la primera parte del estudio, usando un hueso temporal real, auriculares BC y un acelerómetro triaxial, se realiza una prueba para ver cómo el transductor propaga vibraciones a través del hueso, una configuración para todos los componentes que simulan una cabeza humana está hecho. En la segunda parte del estudio, utilizando el software Ansys 2017 Student Edition, se encuentran frecuencias naturales y modos de vibración y también se realiza una simulación del efecto producido por los auriculares BC sobre el hueso temporal, se utiliza todo el rango de frecuencia audible humana para este propósito. Los resultados obtenidos son comparables entre estas dos partes: la simulación FE y la prueba con el hueso real. Se encuentran cinco modos vibratorios usando Ansys 2017 dentro de ese rango audible. Los gráficos de desplazamiento para tres ejes se realizan en Ansys y LabView. Los resultados muestran cómo estos gráficos son comparables entre sí utilizando un gráfico superpuesto, donde los picos de desplazamiento en ambos casos corresponden a los modos vibratorios que se encuentran extrayendo las frecuencias naturales en Ansys. Aunque los resultados obtenidos con LabView tienen ruido de varias fuentes, ambos gráficos tienen las mismas tendencias de desplazamiento. Toda esta investigación e investigación se realizó teniendo en cuenta los estudios médicos y biomecánicos realizados previamente.

Palabras clave: Conducción Ósea, Auriculares, Vibraciones, FEM, Cabeza Humana, Hueso temporal

ABSTRACT

Bone Conduction (BC) and Bone Conduction headphones have been made and studied for more than a decade, as this technology is growing in the audiophile world, the necessity of better quality of headphones and sound is needed. It is necessary not only to have a better understanding on how the vibration caused by the headphones occur but also how to improve the quality of sound that the headphones can provide. In this paper, bone conduction on a dry temporal bone of the human head is analyzed, evaluating the vibration propagation through computer simulation with finite element method FEM using Ansys 2017 Student Edition. In order to do so, a real temporal bone is tested using bone conduction headphones found in today's market and a triaxial accelerometer in conjunction with a National Instruments DAQ and LabView 2018 Student Edition, comparing both results. In the first portion of the study, using a real temporal bone, BC headphones and a the triaxial accelerometer a test is performed in order to see how the transducer is propagating vibrations through the bone, a set up for all the components simulating a human head is made. In the second part of the study, using Ansys 2017 Student Edition software, natural frequencies and vibrational modes are found and also a simulation of the effect produced by the BC headphones over the temporal bone is made, the whole human audible frequency range is used for this purpose. The results obtained are comparable between these two parts: the FE simulation and the test using the real bone. Five vibrational modes are found using Ansys 2017 within that audible range. Displacement plots for three axes are made in Ansys and LabView. Results show how these graphics are comparable to one another using an overlapped plot, where the peaks for displacement in both cases correspond to the vibrational modes found extracting the natural frequencies in Ansys. Although the results obtained using LabView have noise from various sources, both graphics have the same displacement tendencies. All this research and investigation was made taking in consideration medical, as well as biomechanical studies previously done.

Key Words: Bone Conduction, Headphones, Vibrations, FEM, Human Head, Temporal Bone

TABLE OF CONTENTS

1. Introduction 10
2. Methodology 27
2.1. Finite Element Analysis 27
2.2. Real Bone Analysis 40
3. Results and data analysis 50
3.1. Finite Element Analysis 50
3.2. Real Bone Analysis 56
4. Discussion 71
5. Conclusions 74
6. Bibliographic references 75
7. Annexes 77
6.1. Photos from the Real Bone test 77
6.2. Photo of the PCB Piezotronics calibration data cards for the accelerometer 81
6.3. MATLAB raw acceleration data bandpass filter code 82
6.4. MATLAB filtered acceleration signal Integration and FFT code 84

TABLE INDEX

Table 1. Table of densities for different cranial bones (Peterson, Dechow, 2003). 19
Table 2. Table for the elastic moduli for different cranial bones (Peterson, Dechow, 2003). 20
Table 3. Table for Poisson's ratios for different cranial bones (Peterson, Dechow, 2003).....21
Table 4. Table for direction of the greatest stiffness for different cranial bones (Peterson, Dechow, 2003).....21
Table 5. Mechanical properties of polyurethane (Kim, 2014) 22
Table 6. Temporal Bone structures differences (Jen-Fang, 2011) 24
Table 7. Temporal bone material properties.....31

FIGURE INDEX

Figure 1. Structure of the inner ear (Khetrapal, 2018). 12
Figure 2. Structure of the human skull (Encyclopedia Britannica, 2011). 14
Figure 3. Borders of the temporal bone (Jones, 2018). 17
Figure 4. Lateral view of the human skull, the temporal bone is shown in a red color (Jones, 2018). .17
Figure 5. Parts of the temporal bone (Jones, 2018). 18
Figure 6. Coronal section of the temporal bone (Jones, 2018) 18
Figure 7. Displacement caused by a vibratory system in a dry skull using FEM (Kim, 2014) 22
Figure 8. Acceleration caused by a vibratory system in a dry skull using FEM (Kim, 2014) 23
Figure 9. 3D image of the mastoid (Jen-Fang, 2011) 24
Figure 10. Frequency response on the surface of mastoid at 15 degrees, 0 degree and -15 degree (Jen-Fang, 2011) 25
Figure 11. Point cloud file of a real temporal bone scanned using EinScan Pro 28
Figure 12. Point cloud file of a real temporal bone scanned using EinScan Pro zoomed 28
Figure 13. Mesh of the point cloud file of the temporal bone 29
Figure 14. Mesh of the point cloud file of the temporal bone zoomed 29
Figure 15. Final full mesh of the point cloud file of the temporal bone 30
Figure 16. Final adaptive mesh of the temporal bone 30
Figure 17. Temporal bone mesh converted into a BRep solid 31
Figure 18. Ansys Workbench with Modal module 32
Figure 19. Engineering data for the mechanical properties of the temporal bone 33
Figure 20. Ansys - Mechanical Geometry window 33
Figure 21. Ansys - Mechanical Temporal Bone mesh geometry and settings 34
Figure 22. Details and settings of the Modal Analysis in Ansys 34
Figure 23. Zygomaticotemporal suture fixed support on the Modal module 35
Figure 24. Squamosal suture fixed support on the Modal module 35
Figure 25. Sphenosquamosal suture fixed support on the Modal module 36
Figure 26. Zygomaticotemporal suture fixed support on the Modal module 36
Figure 27. Harmonic Response modules connected to Modal module in Ansys Workbench 37
Figure 28. Harmonic Response module connected to Modal module in Ansys - Mechanical 38
Figure 29. Pressure area over the temporal bone used in the Harmonic Response Module 38
Figure 30. Nodal point tracking the displacement caused by the Harmonic Response Module 39
Figure 31. Skull model with a parietal, zygomatic, sphenoid and occipital bones 40
Figure 32. Skull cut with the real temporal bone scanned 41
Figure 33. 3D skull model with the cut for the real temporal bone 41
Figure 34. Stand base for the 3D printed skull and temporal bone isometric view 42
Figure 35. Base and skull for 3D printing 42
Figure 36. Location of the BC headphone right transducer. 43
Figure 37. Location of the accelerometer on the temporal bone 43
Figure 38. Final skull-temporal bone Set-up 44
Figure 39. LabView 2018 code used in conjunction with DAQ Assistant 45
Figure 40. DAQ Assistant settings for X axis 45
Figure 41. DAQ Assistant settings for Y axis 46
Figure 42. DAQ Assistant settings for Z axis 46
Figure 43. Spectral Measurement Set-up 47

Figure 44. LabView Front Panel for the raw and spectral measurements plots 47
Figure 45. Ansys Modal Module, vibrational mode number 1, at 12309 Hz 50
Figure 46. Ansys Modal Module, vibrational mode number 2, at 13097 Hz 51
Figure 47. Ansys Modal Module, vibrational mode number 3, at 14969 Hz 51
Figure 48. Ansys Modal Module, vibrational mode number 4, at 19554 Hz 52
Figure 49. Ansys Modal Module, vibrational mode number 5, at 18686 Hz 52
Figure 50. Total deformation for 1 Hz – 10 kHz in the Harmonic Response module 53
Figure 51. Total deformation for 10 kHz – 20 kHz in the Harmonic Response module 54
Figure 52. Y axis real displacement in the nodal tracking point caused by the Harmonic Response ...54
Figure 53. X axis real displacement in the nodal tracking point caused by the Harmonic Response ...55
Figure 54. Z axis real displacement in the nodal tracking point caused by the Harmonic Response ...55
Figure 55. Raw and Spectral plot for the first set 1 Hz to 10 kHz from LabView number 1 56
Figure 56. Raw and Spectral plot for the first set 1 Hz to 10 kHz from LabView number 2 57
Figure 57. Raw and Spectral plot for the first set 1 Hz to 10 kHz from LabView number 3 57
Figure 58. Raw and Spectral plot for the first set 1 Hz to 10 kHz from LabView number 4 58
Figure 59. Raw and Spectral plot for the first set 1 Hz to 10 kHz from LabView number 5 58
Figure 60. Raw and Spectral plot for the first set 1 Hz to 10 kHz from LabView number 6 59
Figure 61. Raw and Spectral plot for the first set 1 Hz to 10 kHz from LabView number 7 59
Figure 62. Raw and Spectral plot for the first set 1 Hz to 10 kHz from LabView number 8 60
Figure 63. Raw and Spectral plot for the first set 1 Hz to 10 kHz from LabView number 9 60
Figure 64. Raw and Spectral plot for the first set 1 Hz to 10 kHz from LabView number 10 61
Figure 65. Raw and Spectral plot for second set 20 kHz to 10 kHz from LabView number 1 61
Figure 66. Raw and Spectral plot for second set 20 kHz to 10 kHz from LabView number 2 62
Figure 67. Raw and Spectral plot for second set 20 kHz to 10 kHz from LabView number 3 62
Figure 68. Raw and Spectral plot for second set 20 kHz to 10 kHz from LabView number 4 63
Figure 69. Raw and Spectral plot for second set 20 kHz to 10 kHz from LabView number 5 63
Figure 70. Raw and Spectral plot for second set 20 kHz to 10 kHz from LabView number 6 64
Figure 71. Raw and Spectral plot for second set 20 kHz to 10 kHz from LabView number 7 64
Figure 72. Raw and Spectral plot for second set 20 kHz to 10 kHz from LabView number 8 65
Figure 73. Raw and Spectral plot for second set 20 kHz to 10 kHz from LabView number 9 65
Figure 74. Raw and Spectral plot for second set 20 kHz to 10 kHz from LabView number 10 66
Figure 75. Raw acceleration signal for each axis plotted using MATLAB 67
Figure 76. Filtered acceleration signal for each axis plotted using MATLAB 67
Figure 77. Displacement caused by the BC headphones for each axis plotted using MATLAB 68
Figure 78. Displacement Spectrum for each axis plotted using MATLAB 68
Figure 79. Comparison of Displacement Spectrum between the real bone test and Ansys FE first axis 69
Figure 80. Comparison of Displacement Spectrum between the real bone test and Ansys FE second axis 70
Figure 81. Comparison of Displacement Spectrum between the real bone test and Ansys FE third axis 70

1. INTRODUCTION

Interest in Bone Conduction hearing has been gaining popularity over the last decade, these devices provide the user the ability to interact with sounds of the natural environment and also sounds of an external device at the same time, allowing both sounds to be clear and hearable. This feature makes bone conduction sound transmissions a natural pathway for hearing. The open hearing sound has been already achieved by open back headphones, although, this type of headphones provides natural environment sound, they block the entire ear in order to achieve this purpose (Ogiso, 2014). Bone conduction headphones, on the other hand, are thought as the most useful method to let the user have the ear untouched, performing in a similar way as other traditional headphones, but through bone vibrations. As this technology is relativity new, bone conduction headphones have been used by athletes focused on marathon, sprint running, mountain claiming and snow related sports, although this science open new possibilities for other applications, just to name a few: military communications, autism and other psychological diseases and more importantly hearing loss disorders.

When the human auditory system receives acoustic stimulations, they are converted into auditory sensations, knowing that the auditory system is composed by two ears and the associated neural network that perceives incoming sounds in form of mechanical vibrations, these acoustics stimulations are converted into neural impulses, which at the same time travel along the auditory nerves arriving to the brain, where they translated into auditory sensations in the cortex. To achieve these process, two pathways get the job done, which are: air conduction (AC) and bone conduction (BC). AC happens when an acoustic signal goes through the outer and middle ear arriving to the cochlea, meanwhile, BC happens when an acoustic signal vibrates the bones of the human skull stimulating the cochlea. Both pathways use the same conversion mechanism in the cochlea (Lowy, 1942). The AC pathway is the primary

form of sound reception of acoustic information by a human, and most living creatures, with normal hearing and uncovered ears. These occurs by using the middle and the external ear mechanisms which are designed to help enhancing the acoustic information by transforming the incoming acoustic soundwaves into mechanical vibrations delivering them to the cochlea, where these are perceived and analyzed. The BC pathway bypasses these two mechanisms, the middle and external ear, in other words, the acoustic signals go directly to the cochlea through the vibrations of skull, this result in a 40dB in the high and mid frequencies and 70dB in low frequencies less effective than the AC pathway (Henry, Letowski, 2007), this means that the AC pathway still a better way for humans to hear incoming audio signals from the environment and from an external source such as headphones. For an instance, when a person is in a loud environment, could be a factory with machines working and the ear is totally obstructed using earplugs, the amount of sound energy that enter through the AC pathway to the ear canal is reduced, but it has no effect on the amount of sound energy absorbed by the BC pathway. In other words, BC is much more effective when the audio signal is transmitted directly to a human head, these include all the bones that compose the skull itself including the teeth.

As it was mentioned before, the auditory system involves two ear mechanisms, left and right, these are connected to the brain by a network of auditory fibers. Ear mechanisms consist of three parts which are: the external ear, the middle ear and the inner ear and these are consequently connected. The ear canal where the mentioned mechanisms are located has an S shaped tube and altogether has resonance capabilities providing about 5 to 20dB amplification in a frequency range of 1400 to 7000 Hz (Henry, Letowski, 2007), although, the level of amplification depends on some variables such as the direction and source of the incoming sound, when the source is directly in front of a person the incoming audio will be capture at its full level. The middle ear is a bony cavity and contains three little bones, which are called: the malleus or hammer, incus or anvil and stapes o stirrup, the first bone is attached to the eardrum

and the last one is connecting this mechanism to the oval window of inner ear, also acting as a protection for it. The main function of the middle ear is to convert the mechanical vibrations of the tympanic membrane into vibrations that the oval window can understand and transmit to the brain. The inner ear mechanism is where the semicircular canals, saccule, utricle and cochlea are located, being this last organ the end of the hearing process that vibrations go through. Finally, the cochlea is an organ in a form of a snail shell, it is divided into two canals called vestibule and tympani. The function of the cochlea is to help translating the sound waves coming into the ear into hearable sound that can be easily understood by the brain (Tyler, 2009). The structure of the inner ear can be seen in Fig 1.

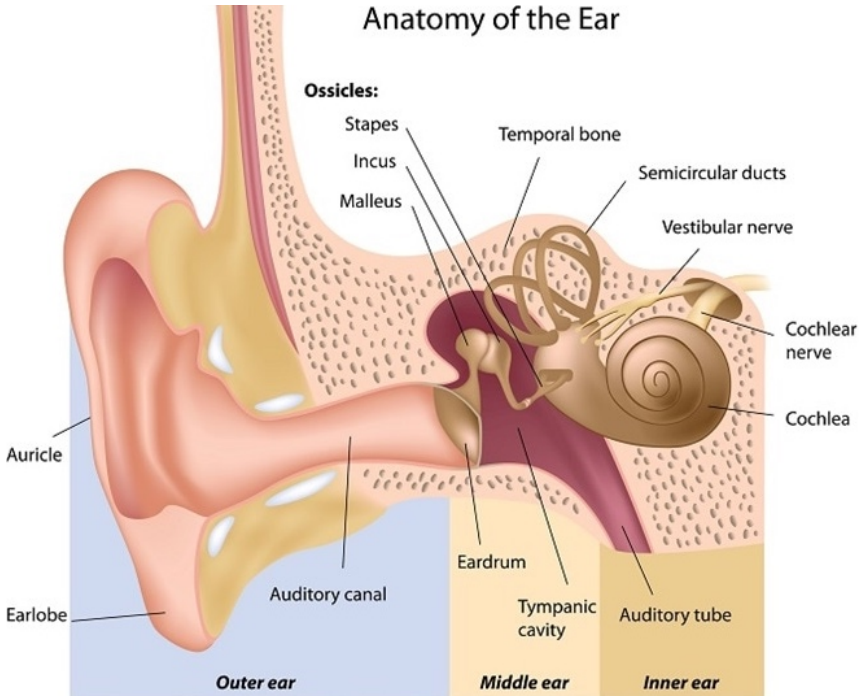

Figure 1. Structure of the inner ear (Khetrapal, 2018).

Many researches of the human skull and hearing by bone conduction have been already achieved, Chang, Kim and Stenfelt have directed a study and simulation of a bone-conducted sound transmission in a three-dimensional model of a human skull. In this paper, Chang and company investigated how BC could help people with hearing aids by considering a finite element analysis through sound wave vibrations coming from a source to the cochlea

measuring different transmission routes for BC. The transmission performance of the skull bones is affected by the anatomy, geometry and mechanical properties of the structures that compose the human skull and internal organs (Kim, et al., 2014).

Also, Stenfelt in his paper detailed, the differences between BC and AC, saying that BC and AC hearing thresholds are the fundamental measure of a person's hearing ability, although BC thresholds are mostly influenced by the vibrator transducer rather than a pathological hearing disorder, meaning AC thresholds are highly influenced by the outer and middle ear and the cochlea for both BC and AC. He mentions that the most used transducer by 2014 is the Radioear B71 which has limitations in his frequency (250 to 4000 Hz) and dynamic range, moreover, there is many other designs that are trying to overcome these current limitations, as this technology continue to grow. In another research found, this group talk about another problem with BC threshold testing, this involves the direct placement of the transducer over the skin, tissue and bone (Stenfelt, 2013). They have shown that there are two places in the skull for an optimal BC vibration transmission, which are: the frontal bone and the temporal bone. Although, the frontal bone could provide good vibrational transmission to the entire skull, there haven't been a proper way to place a transducer on the forehead making it viable to for people to use on a daily basis.

In order to conduct a BC study is necessary to know how the human head is shaped, it contains: the skull, cartilages, tissues and fluids. Where the skull itself consists of two distinguishable parts of bones which are: the cranium and the facial bones. The cranium protects the brain surrounding it with larger and solid pieces of bone, there are eight bones in the cranium: occipital, two temporals, two parietal, one sphenoid, one ethmoid and one frontal bone. The ears lay over the two temporal bones and these act as protectors for the inner ear from outside damage. Meanwhile the facial bones help supporting the face and mouth systems, consist of fourteen bones in the lower frontal part of the human head which are: the vomer, two

nasal conchae, two nasal bones, two maxillae, two zygomatic bones, two mandible, two lacrimal and two palatine bones. The structure of the human skill can be seen in Fig 2. Is important to say that mechanicals properties of soft tissue vary and depend on the person's gender, race and age (McBride, 2017).

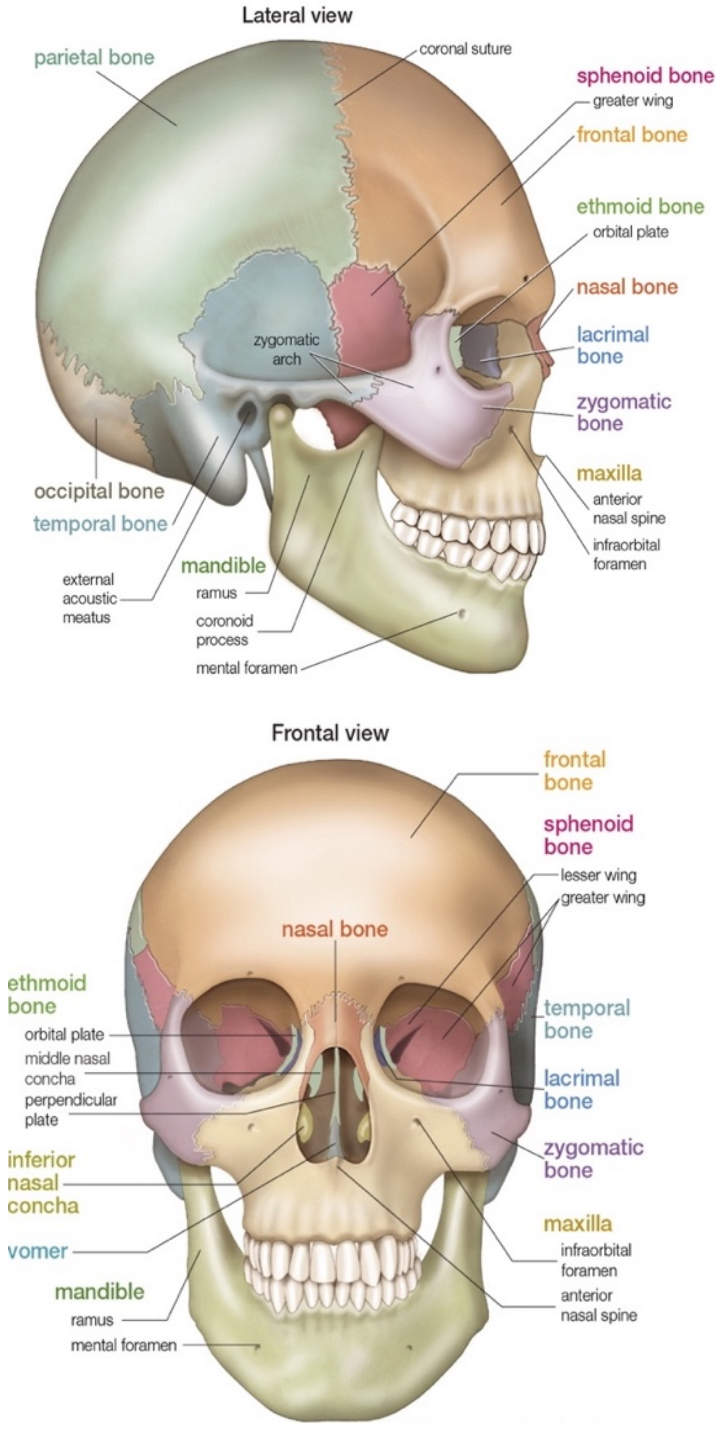

Figure 2. Structure of the human skull (Encyclopedia Britannica, 2011).

The cochlea and hearing organs could be stimulated by vibrations applied to any part of the human body. Moreover, the attenuation of sound by the body is relatively very high, with an exception for vibrations of low frequencies, considering 100 Hz or less. However, low frequency vibrations are received as haptic information if they vibrate at high intensities or if they are harmful vibrations, these sensations could not be perceived by the cochlea and probably will not activate it at all. So, low level tactile stimulation, range of 20–100 Hz, is not harmful for the body, it can disorientate bone conduction perception (Henry and Letowski 2007). The sensitivity of air conduction transmission stays in a range of 1000 to 3000 Hz, not able to hear low frequencies below 500Hz nor high frequencies above 5kHz (Silvian, White, 1933). On the other hand, BC transmission sensitivity is lower than the one for AC, although this is already discussed above.

As for the location of the transducer, device that produce vibrations in contact with the bone, there have been some studies regarding this matter. The selection of a location or the type of the vibrator or transducer will affect the spectral content transmitted to the bones and could compromise the level of effective signal. It is really important to take in consideration the level of the effective signal that is conducted to the bones, because the vibrator have a limited power. In theory, the closer the vibrator is located is to the cochlea, the better and stronger the response of the overall transmission is going to be. The closest bone that can achieve this purpose are the temporal bones, primarily because these are rigid bodies surrounding the cochlea, allowing a reception of frequencies near 4000Hz. The variability of sounds frequencies of 1 kHz or more is nearly the same at different placements location across the skull, it starts to vary when the frequencies are lower than that (Henry, Letowski, 2007). However, if the vibrator is placed on the temporal bones, just over the mastoid bone, the thresholds will be lower compared to any other bone in the human skull, being this area more sensitive to bone conduction transmission. Also, the temporal bones are used for bone

conduction for convenience and availability of headbands to hold the vibrators on place thank to the external ear auricle. The audible frequency range for bone conducted sounds have been reported to be 125 to 8000 Hz frequencies. (McBride, Letowsky and Tran, 2005).

The temporal bone is the main bone that is studied, as it was stated in the text above, it contains and protects the middle and inner parts of the ear and it is located on the lower lateral walls of the human skull. This bone is comprised of five parts, the zygomatic, styloid, tympanic, petromastoid and squamous, each of these parts connect and protect different parts of the human head. The squamous is the largest part of the temporal bone, connecting with the parietal bone, it is flat and has a slight convex shape. The petromastoid is located in the posterior side and it contains two items, the mastoid and the petrous. The mastoid comprises the mastoid air cells, these cells act as a reservoir of air, they equalize the pressure within the middle ear. The petrous part contains and protect the inner ear, it has a pyramidal shape (Jones, 2018). The temporal bone has four borders, these borders are holding the temporal bone to the skull, and are called sutures, as seen in the figure 3, which are the occipitomastoid suture that connects to the occipital bone, the squamosal suture connecting to the parietal bone, the sphenosquamosal suture that connects to the sphenoid bone and finally the zygomaticotemporal suture connecting to the zygomatic bone (Jones, 2018). The sutures are fibrous joints consisting mainly of collagen, and in the skull the bones are hold together by Sharpey's fibers, having a very limited or no movement under normal condition, this type of joints is called synarthrosis joints (Tomco, 2013).

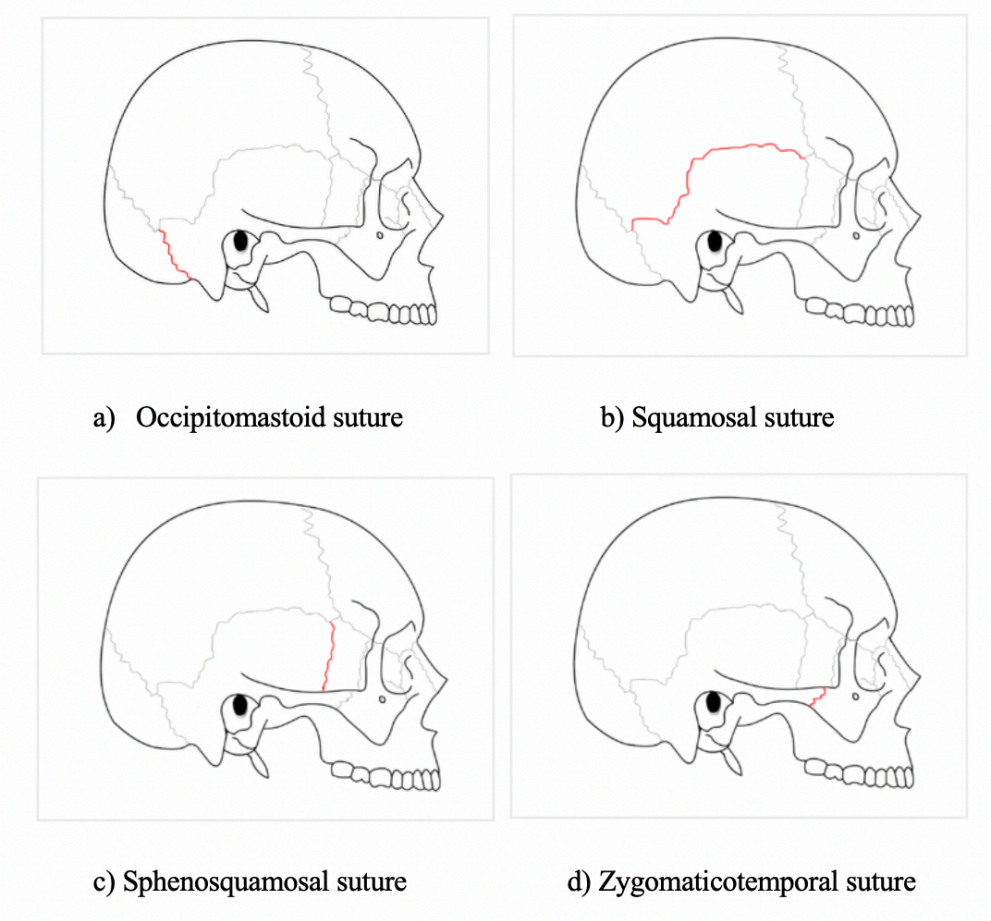

Figure 3. Borders of the temporal bone (Jones, 2018).

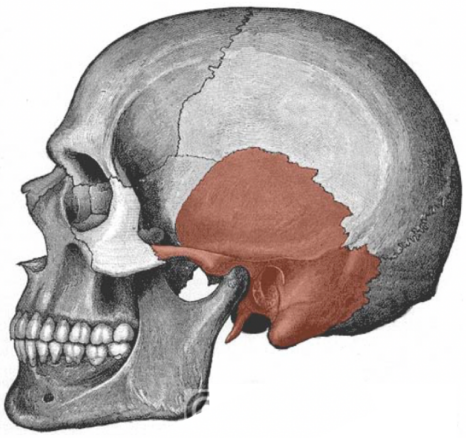

Figure 4. Lateral view of the human skull, the temporal bone is shown in a red color (Jones, 2018).

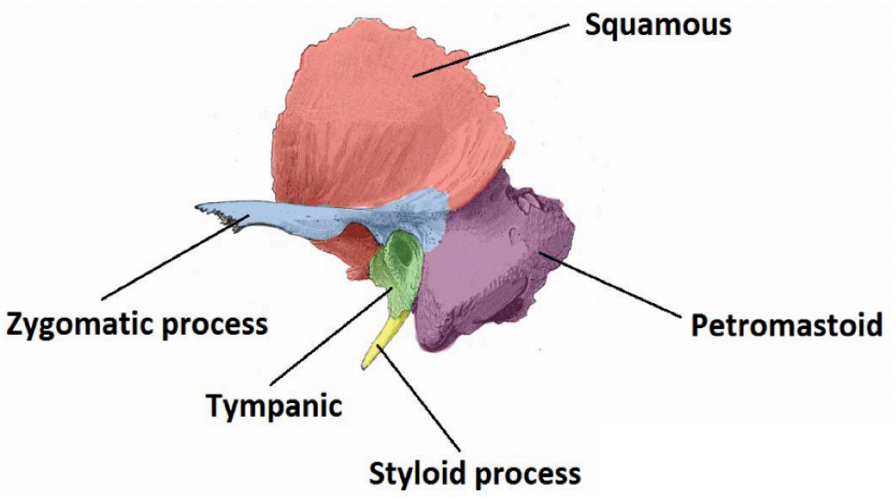

Figure 5. Parts of the temporal bone (Jones, 2018).

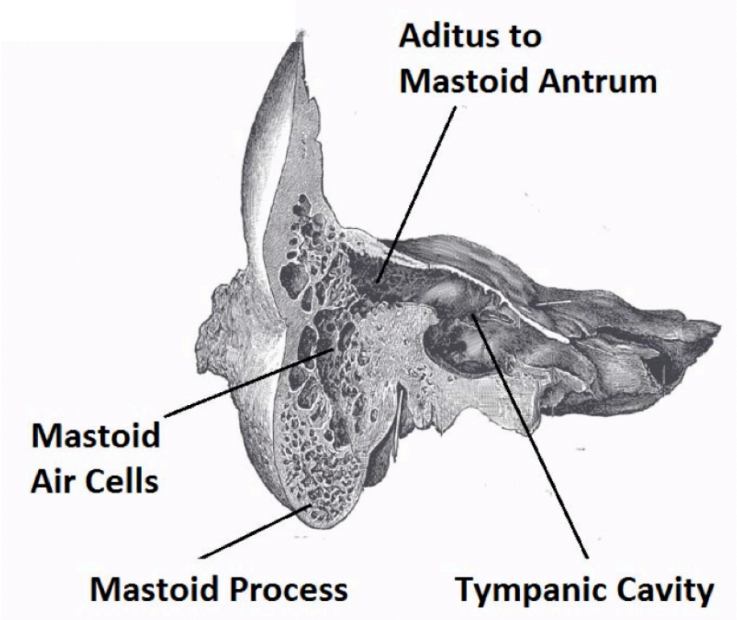

Figure 6. Coronal section of the temporal bone (Jones, 2018)

Choosing the right values for the mechanical properties of the cranial and temporal is important, as the temporal bone has the largest variation in properties of the whole skull, for example the zygomatic area has the largest Elastic module for all the cranial bones, and all this differences found correspond to the functional portions of the bone itself. In the following tables is shown the values for the different portions of the temporal bone: T1, T2 and T4 for

the squamous portion and T3 for the mastoid portion. Having high values of stiffness for the temporal bone gives it the greatest anisotropy of the human skull (Peterson, Dechow, 2003).

Table 1. Table of densities for different cranial bones (Peterson, Dechow, 2003).

Bone	Site	Density		Thickness	
		Mean	SD	Mean	SD
Parietal	1	1.877	.092	2.8	0.9
	2	1.845	.122	2.6	0.7
	3	1.795	.153	2.7	0.6
	4	1.803	.098	2.9	0.7
	5	1.772	.128	2.8	0.7
	6	1.766	.119	2.5	0.6
	7	1.825	.111	2.8	0.6
	8	1.773	.086	2.4	0.7
	9	1.807	.098	2.4	0.6
	10	1.779	.129	2.5	0.5
	11	1.813	.148	2.5	0.7
	12	1.824	.173	2.4	0.6
	13	1.859	.136	2.4	0.6
	14	1.841	.164	2.2	0.7
Grand mean		1.812	.127	2.5	0.7
Frontal	1	1.780	.095	2.5	0.4
	2	1.788	.117	2.6	0.3
	3	1.828	.128	2.4	0.7
	4	1.784	.128	2.4	0.5
	5	1.771	.116	2.7	0.6
	6	1.818	.126	2.4	0.5
	7	1.744	.131	2.4	0.5
	8	1.760	.153	2.6	0.8
	9	1.767	.153	2.6	0.6
Grand mean		1.783	.128	2.5	0.5
Occipital	1	1.786	.139	3.1	0.4
	2	1.816	.170	3.3	1.1
	3	1.911	.091	2.9	1.4
	4	1.878	.104	2.7	0.6
	5	1.907	.117	3.0	0.9
Grand mean		1.860	.133	3.0	0.9
Temporal	1	1.803	.190	1.8	0.4
	2	1.859	.158	1.8	0.4
	3	1.922	.098	3.1	1.0
	4	1.899	.111	2.4	0.4
Grand mean		1.868	.149	2.3	0.8
Zygoma	1	1.686	.216	2.1	0.5
	2	1.758	.192	2.3	0.5
	3	1.615	.165	2.2	0.4
	4	1.654	.200	2.0	0.6

Table 2. Table for the elastic moduli for different cranial bones (Peterson, Dechow, 2003).

Bone	Site	E_1		E_2		E_3		E_2/E_3	
		Mean	SD	Mean	SD	Mean	SD	Mean	SD
Parietal	1	14.8	2.3	15.7	2.6	20.9	3.5	0.76	0.13
	2	13.9	2.5	15.4	3.8	20.0	3.9	0.78	0.17
	3	12.8	3.8	14.6	3.7	17.9	4.7	0.83	0.10
	4	13.4	2.4	15.2	3.1	18.7	4.1	0.83	0.14
	5	12.7	2.6	14.1	3.5	18.5	4.4	0.78	0.14
	6	12.2	3.0	12.3	3.3	20.7	3.8	0.60	0.15
	7	13.3	2.8	14.3	3.7	19.1	4.7	0.77	0.15
	8	12.3	2.7	12.4	2.9	20.1	4.3	0.63	0.17
	9	12.8	2.5	13.7	4.0	19.9	4.6	0.72	0.23
	10	13.6	3.0	14.8	3.6	20.6	3.7	0.72	0.12
	11	13.9	2.7	15.0	3.1	23.5	4.3	0.65	0.13
	12	12.8	3.5	13.1	4.2	21.5	4.8	0.62	0.20
	13	13.1	2.6	14.2	3.4	20.5	4.7	0.71	0.17
	14	12.4	3.5	12.3	4.1	22.2	5.6	0.57	0.18
Grand mean		13.1	2.9	14.1	3.6	20.3	4.5	0.71	0.17
Frontal	1	12.5	2.4	13.4	3.4	20.2	4.3	0.68	0.18
	2	12.9	1.9	15.0	2.6	19.6	4.0	0.78	0.14
	3	12.9	2.4	15.0	3.2	20.6	3.5	0.74	0.16
	4	12.5	2.8	13.4	3.1	19.5	4.0	0.69	0.13
	5	12.4	2.1	15.8	2.6	19.4	3.4	0.81	0.12
	6	13.1	2.1	15.9	3.4	19.6	4.5	0.82	0.12
	7	12.3	2.5	14.1	3.6	18.6	3.5	0.76	0.17
	8	12.0	3.1	13.7	3.8	19.5	5.3	0.73	0.19
	9	11.8	3.2	12.6	4.4	17.6	5.0	0.71	0.14
Grand mean		12.5	2.5	14.3	3.5	19.4	4.2	0.75	0.16
Occipital	1	12.6	2.2	14.3	2.6	17.9	3.7	0.81	0.13
	2	13.5	2.8	16.8	3.9	20.9	4.6	0.81	0.13
	3	14.1	1.9	16.1	3.1	22.5	3.6	0.72	0.14
	4	13.7	2.4	16.0	3.4	20.6	5.0	0.79	0.15
	5	13.6	2.5	16.0	3.4	20.9	5.5	0.80	0.17
Grand mean		13.5	2.4	15.8	3.3	20.6	4.7	0.79	0.15
Temporal	1	11.7	3.7	12.2	4.1	20.4	5.3	0.61	0.19
	2	12.8	3.6	12.8	4.8	24.1	3.7	0.54	0.20
	3	15.0	1.9	17.7	2.4	21.8	1.9	0.81	0.09
	4	14.1	2.3	13.3	2.2	27.3	6.0	0.51	0.16
Grand mean		13.4	3.2	14.0	4.1	23.4	5.1	0.62	0.20
Zygoma	1	10.2	2.3	12.1	3.1	19.2	5.9	0.67	0.20
	2	11.0	3.5	12.5	3.7	20.5	6.1	0.63	0.18
	3	10.4	3.2	11.7	3.7	19.1	3.4	0.62	0.20
	4	9.7	2.1	10.5	3.8	19.7	6.2	0.56	0.21

Table 3. Table for Poisson's ratios for different cranial bones (Peterson, Dechow, 2003).

Bone	Site	V_{12}		V_{13}		V_{21}		V_{23}		V_{31}		V_{32}	
		Mean	SD	Mean	SD	Mean	SD	Mean	SD	Mean	SD	Mean	SD
Parietal	1	0.46	0.12	0.22	0.07	0.48	0.08	0.24	0.08	0.30	0.08	0.31	0.06
	2	0.44	0.16	0.25	0.09	0.46	0.11	0.23	0.07	0.35	0.11	0.30	0.05
	3	0.43	0.08	0.25	0.07	0.48	0.07	0.27	0.07	0.34	0.08	0.32	0.06
	4	0.40	0.10	0.26	0.08	0.45	0.08	0.25	0.07	0.36	0.08	0.30	0.06
	5	0.42	0.09	0.26	0.08	0.46	0.09	0.27	0.08	0.37	0.06	0.34	0.07
	6	0.53	0.14	0.19	0.07	0.51	0.08	0.20	0.05	0.31	0.08	0.34	0.06
	7	0.43	0.12	0.26	0.07	0.45	0.08	0.26	0.07	0.37	0.08	0.34	0.05
	8	0.54	0.15	0.18	0.08	0.54	0.10	0.21	0.08	0.28	0.08	0.32	0.06
	9	0.50	0.22	0.21	0.11	0.49	0.11	0.24	0.09	0.31	0.14	0.34	0.08
	10	0.45	0.09	0.22	0.04	0.48	0.08	0.22	0.05	0.33	0.05	0.30	0.05
	11	0.48	0.13	0.19	0.07	0.52	0.09	0.18	0.06	0.31	0.08	0.27	0.05
	12	0.52	0.24	0.21	0.12	0.48	0.11	0.22	0.07	0.31	0.18	0.39	0.13
	13	0.44	0.16	0.25	0.09	0.45	0.07	0.25	0.06	0.37	0.11	0.35	0.06
	14	0.60	0.23	0.18	0.08	0.55	0.07	0.19	0.05	0.30	0.12	0.38	0.20
Grand mean		0.47	0.16	0.22	0.08	0.48	0.09	0.23	0.08	0.33	0.10	0.33	0.09
Frontal	1	0.49	0.16	0.19	0.10	0.50	0.10	0.22	0.12	0.30	0.14	0.31	0.11
	2	0.38	0.11	0.26	0.08	0.42	0.10	0.24	0.06	0.38	0.09	0.30	0.06
	3	0.42	0.15	0.24	0.08	0.46	0.11	0.22	0.07	0.37	0.08	0.30	0.07
	4	0.47	0.10	0.21	0.08	0.51	0.12	0.24	0.06	0.32	0.12	0.35	0.11
	5	0.36	0.08	0.26	0.05	0.45	0.08	0.24	0.06	0.41	0.05	0.30	0.04
	6	0.40	0.09	0.24	0.05	0.48	0.07	0.24	0.06	0.36	0.06	0.29	0.06
	7	0.43	0.15	0.21	0.08	0.47	0.12	0.23	0.07	0.32	0.12	0.30	0.06
	8	0.46	0.14	0.22	0.10	0.51	0.12	0.22	0.09	0.34	0.12	0.29	0.07
	9	0.47	0.16	0.20	0.11	0.49	0.13	0.26	0.08	0.30	0.17	0.38	0.12
Grand mean		0.43	0.14	0.23	0.09	0.48	0.11	0.24	0.10	0.34	0.11	0.31	0.08
Occipital	1	0.38	0.10	0.28	0.09	0.43	0.11	0.28	0.08	0.39	0.10	0.34	0.08
	2	0.35	0.10	0.26	0.07	0.41	0.10	0.26	0.06	0.35	0.09	0.31	0.05
	3	0.40	0.12	0.24	0.08	0.44	0.09	0.22	0.07	0.37	0.09	0.30	0.05
	4	0.45	0.11	0.20	0.08	0.50	0.06	0.24	0.11	0.30	0.12	0.30	0.11
	5	0.39	0.13	0.24	0.10	0.44	0.10	0.28	0.10	0.33	0.13	0.34	0.08
Grand mean		0.40	0.12	0.24	0.09	0.45	0.09	0.26	0.10	0.35	0.11	0.32	0.08
Temporal	1	0.57	0.18	0.18	0.09	0.54	0.11	0.21	0.09	0.29	0.12	0.36	0.09
	2	0.62	0.21	0.14	0.09	0.57	0.12	0.16	0.06	0.24	0.12	0.30	0.06
	3	0.35	0.06	0.27	0.05	0.41	0.08	0.26	0.05	0.38	0.06	0.32	0.04
	4	0.52	0.15	0.16	0.11	0.48	0.12	0.17	0.10	0.27	0.11	0.31	0.09
Grand mean		0.52	0.19	0.19	0.09	0.50	0.12	0.20	0.09	0.30	0.11	0.32	0.07
Zygoma	1	0.44	0.22	0.21	0.11	0.48	0.16	0.22	0.10	0.36	0.19	0.32	0.10
	2	0.44	0.16	0.21	0.09	0.50	0.16	0.22	0.10	0.38	0.14	0.34	0.11
	3	0.46	0.20	0.20	0.09	0.47	0.12	0.19	0.06	0.34	0.18	0.31	0.09
	4	0.56	0.16	0.16	0.10	0.56	0.09	0.17	0.09	0.29	0.15	0.31	0.10

Table 4. Table for direction of the greatest stiffness for different cranial bones (Peterson, Dechow, 2003).

Bone	Site	Mean vector	Circular CI	Rayleigh's test of uniformity[a]
		Mean °	95% CI	*P* value
Parietal	5	103	15	0.01
	6	79	18	0.01
	11	26	17	0.01
	12	5	18	0.01
	13	26	20	0.02
Frontal	1	76	20	0.02
	3	10	13	0.01
	9	38	21	0.04
Temporal	4	25	8	0.01

In a study performed by Kim, Chang and Stenfelt (2014) using the FEM they analyzed a whole dry human skull applying a vibrational signal from 1 Hz to 20 kHz, the aim of this paper was to find the mechanical skull response to a vibratory system, although the material used for this analysis is not bone, they use polyurethane instead, this is made to be able to compare results from a previously made study where a whole human head, including skin, muscular tissue and intercranial liquids was analyzed, the properties used are the following:

Table 5. Mechanical properties of polyurethane (Kim, 2014)

Elastic Modulus (MPa)	Density (kg/m3)	Poisson's ratio	Loss factor
1	997.40	0.33	0.1 at 20kHz

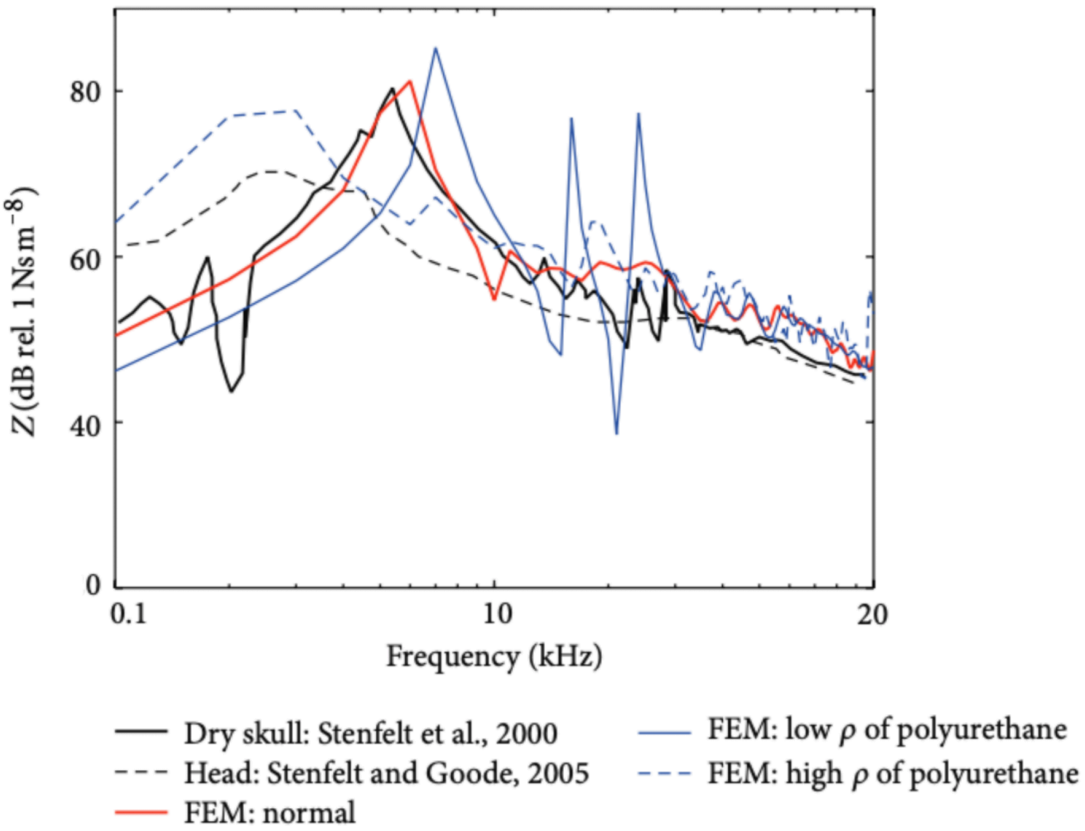

Figure 7. Displacement caused by a vibratory system in a dry skull using FEM (Kim, 2014)

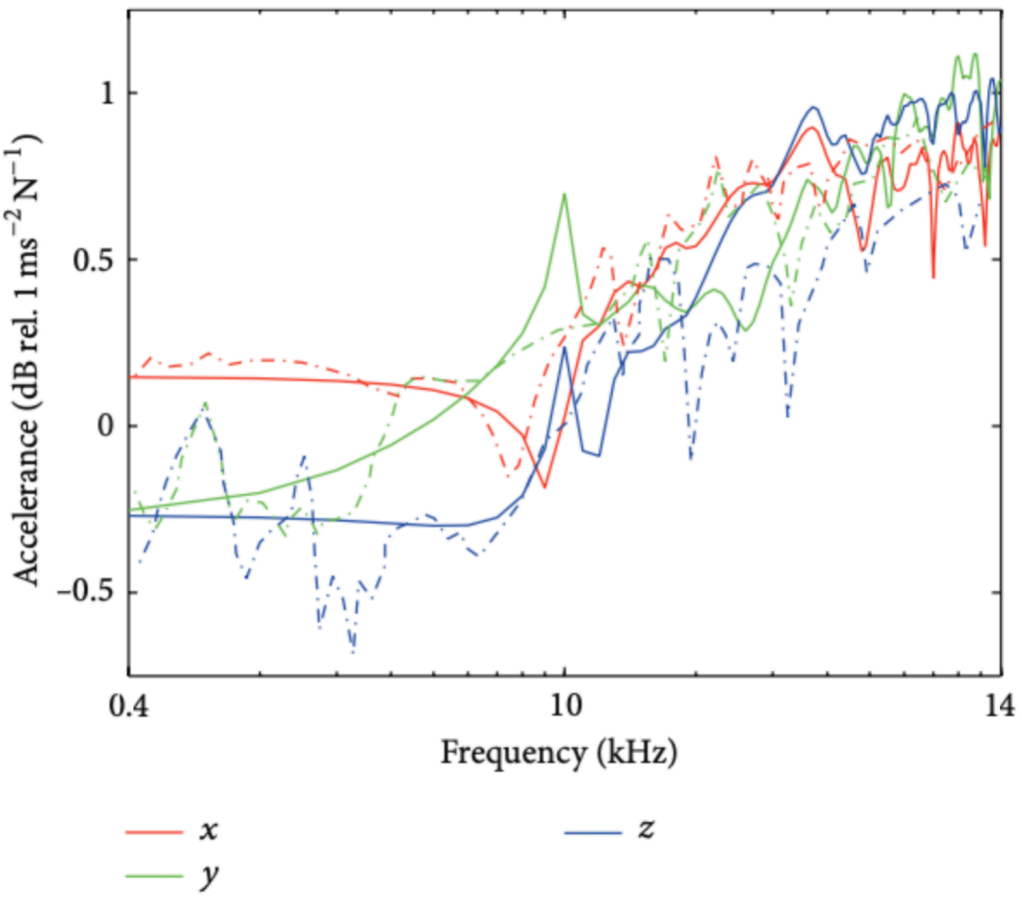

Figure 8. Acceleration caused by a vibratory system in a dry skull using FEM (Kim, 2014)

As seen in the following figures, the peaks generated from displacement occur approximately around 8 kHz and from 11 kHz to 16 kHz, this is showing where the system tend to produce a displacement in those frequency ranges. The unit shown to measure Z or displacement is in db., taking into consideration the original point where the displacement started. The results for this analysis also show the acceleration for the different axes, from 10 kHz to 14 kHz (Kim, et al., 2014).

Another study performed in 2011 shows a 3D model of the mastoid bone, which is part of the temporal bone, in this paper two finite element analysis were performed. The first one he discusses the natural vibration frequencies and vibration mode of the mastoid bone, in the second one he investigates the harmonic response and placement over the mastoid bone. The mastoid bone has the best vibrational response for audiometry testing, although the shape of

this bone doesn't allow to place a transducer over a plane surface, this bone shows rough protuberances (Jen-Fang, 2011). This work concludes with the results for the modal analysis of mastoid, the nine natural frequencies he worked with: 125 Hz, 250 Hz, 500 Hz, 750 Hz, 1 kHz, 2 kHz, 3 kHz, 4 kHz and 6 kHz, among the natural frequencies obtained from the vibration mode of the mastoid at 100 Hz to 10 kHz frequencies were similar to the pure-tone stimuli frequency for the clinical hearing test and for the placement and harmonic analysis, concluding by saying that the most optimal area to perform BC is when the transductor is placed at superior part rather than in the middle and inferior part. For his work, he also uses a smoothed model of the mastoid bone, keeping the same volume but changing the surface and points

Table 6. Temporal Bone structures differences (Jen-Fang, 2011)

	Surface area (mm^2)	Volume (mm^3)	Surfaces	Points	Differences
Original	4,532	10,682	95,266	47,635	1.00%
Simplified	3,953	10,585	1,000	502	0.91%
Smoothed	3,470	10,604	1,000	502	0.73%

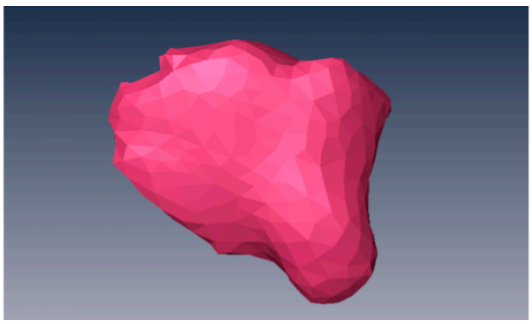

Figure 9. 3D image of the mastoid (Jen-Fang, 2011)

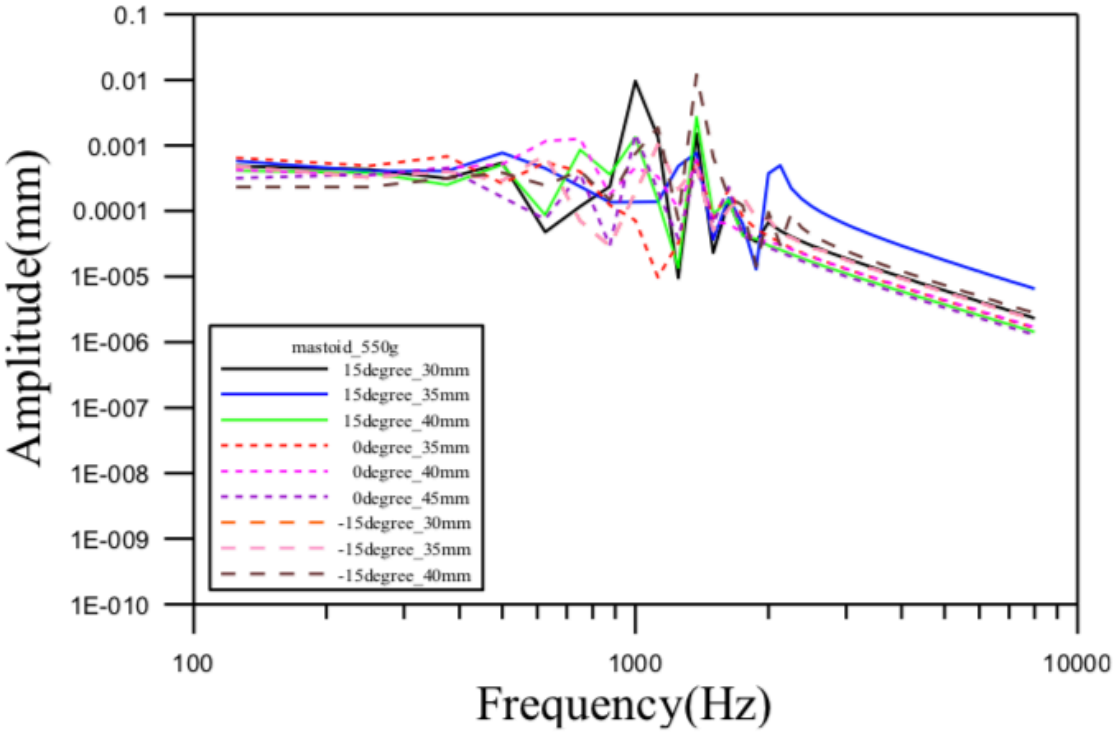

Figure 10. Frequency response on the surface of mastoid at 15 degrees, 0 degree and -15 degree (Jen-Fang, 2011)

Commercial bone conduction headphones and hearing by bone conduction have been the subject of many research studies over the last decade. Studies have shown that transporting sound through vibrations is achievable, and an alternative way to traditional speaker headphones (Ogiso, 2014). As technology continues to improve, it is important to develop new ways of hearing mechanisms, bone conduction is on an early stage, and has years to become a mainstream device to be used in a regular basis as the traditional headphones are. Thanks to FE analysis and the use of software, vibrational studies are able to be perform and studied. Since it is hard to come by a real bone and use it for testing because of ethical issues, FE analyses provide a theoretical analysis that can be used for testing and technologies development.

The purpose of this paper was to analyze the vibrational sound propagation that occurs at the temporal bone in the squamous area, when using bone conduction headphones found on the market in 2019. To achieve this goal a research on how sound transmission occurs inside the human skull and goes through the internal hearing organs, a computer simulation of a 3D temporal bone using finite element method have been done, also a vibrational test has been performed on a real temporal bone so the output signals of both tests could be compared. Materials and electronic components have been analyzed helping the propagation of the vibrations thought the bone.

2. METHODOLOGY

To accomplish a full analysis on a temporal bone when using BC headphones, a finite element analysis is made using Ansys 2017 Student Edition and a real test using a real temporal bone needs to be performed. In order to do so, this project dived into two parts, the first part or FEM simulation consist in 3 main steps, which are the following: development of the geometry of the temporal bone, conversion of the file to be used in Ansys, and FE analysis in Ansys. Alongside, for the second part or the vibrational testing using a real temporal bone, a base for the bone is needed, an accelerometer in conjunction with an array of National Instruments data acquisition equipment and LabView 2018 Student Edition software is also used. This project is divided in order to be able to compare both results, in this way a theorical and a real outcome will be seen, proper conclusions will be exclaimed after the comparison is made.

2.1. Finite Element Analysis

The temporal bone is composed of a complex structure which might be impossible to recreate using CAD software so as to get this geometry, a 3D scan needs to be made of a real bone. Using a Shining 3D EinScan Pro scanner and a real bone, a cloud point file was obtained as seen in figures 11 and 12. With MeshLab software, the point cloud file was converted into a stable, homogeneous STL file, which contains 81,062 triangles faces and 38,184 vertices, can be seen in figure 13 and 14. In MeshLab a tridimensional mesh is able to form from the multiple points gotten from the scan but also several modifications can be made such as selecting and erasing incorrect points or vertices, as well as interpolating to create new rough faces on the mesh, which be useful in order to maintain a uniform shape for the file that is being created, figure 15. Although for a simulation in Ansys this file was too large because of many faces and vertices, so in order to make the analysis is crucial to reduce some triangle faces of the mesh in order to make it simpler in areas that will not be to relevant for the present

study. The new file contains 30,334 faces and 15,253 vertices, this transformation can be seen in figure 16.

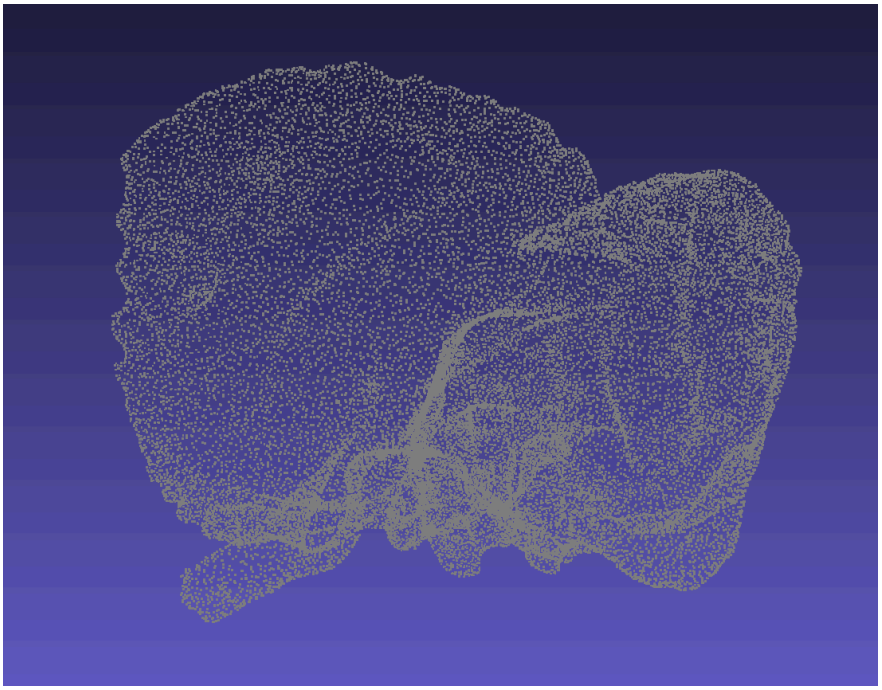

Figure 11. Point cloud file of a real temporal bone scanned using EinScan Pro

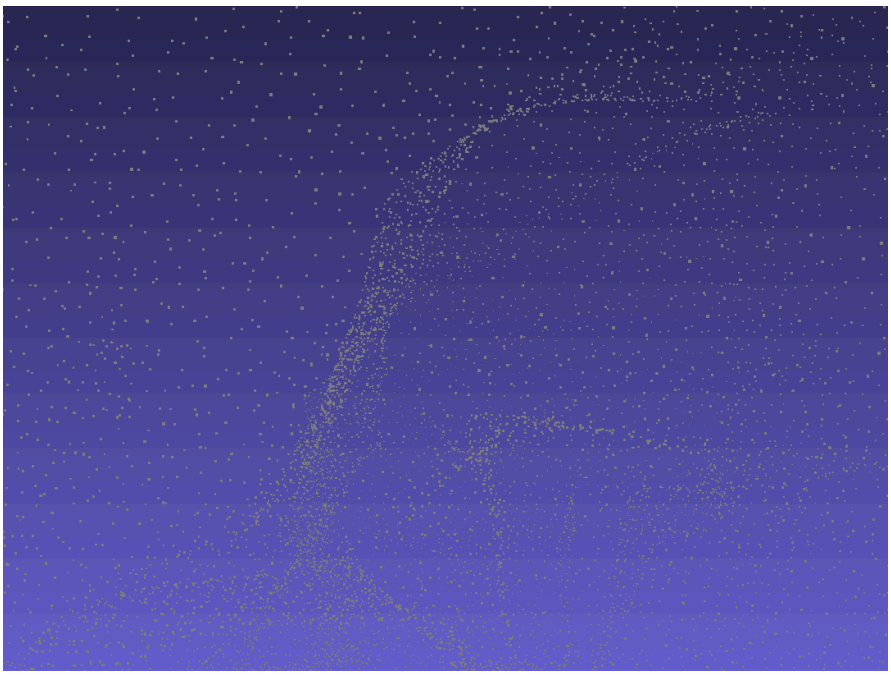

Figure 12. Point cloud file of a real temporal bone scanned using EinScan Pro zoomed

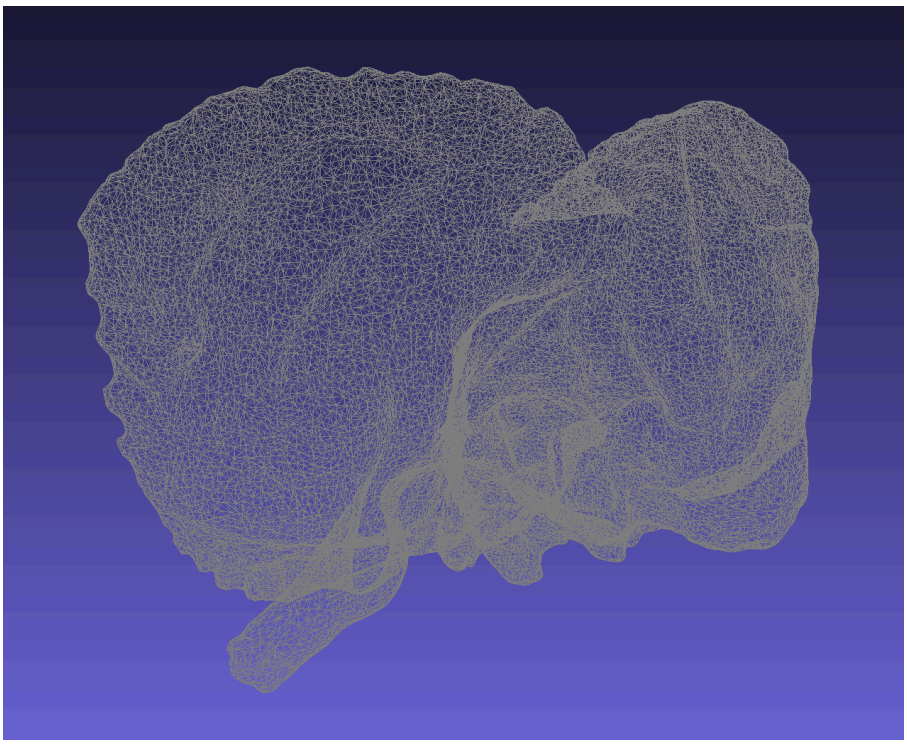

Figure 13. Mesh of the point cloud file of the temporal bone

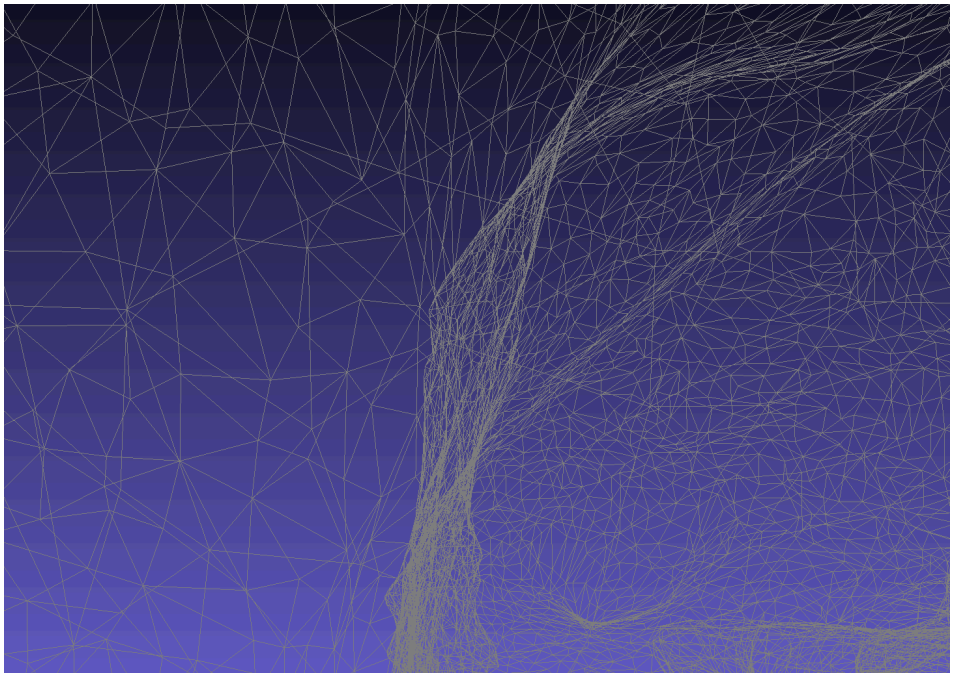

Figure 14. Mesh of the point cloud file of the temporal bone zoomed

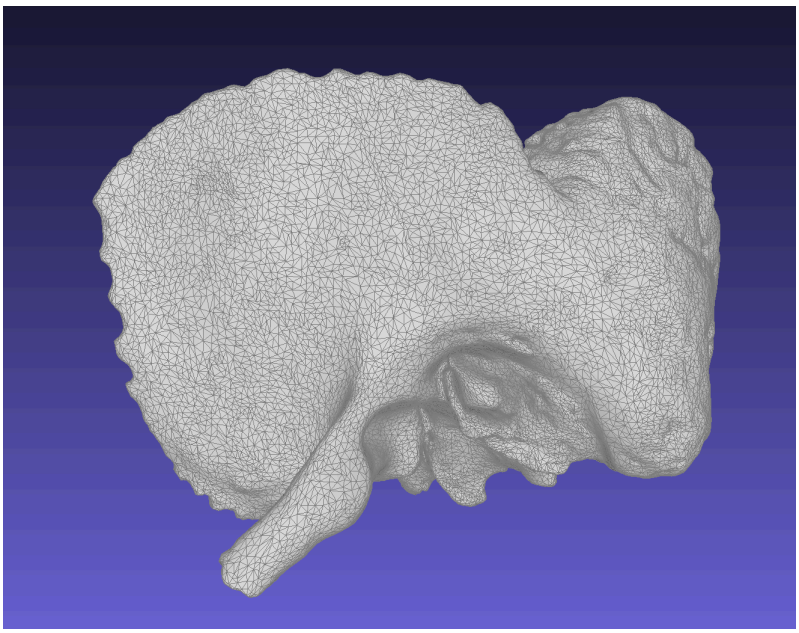

Figure 15. Final full mesh of the point cloud file of the temporal bone

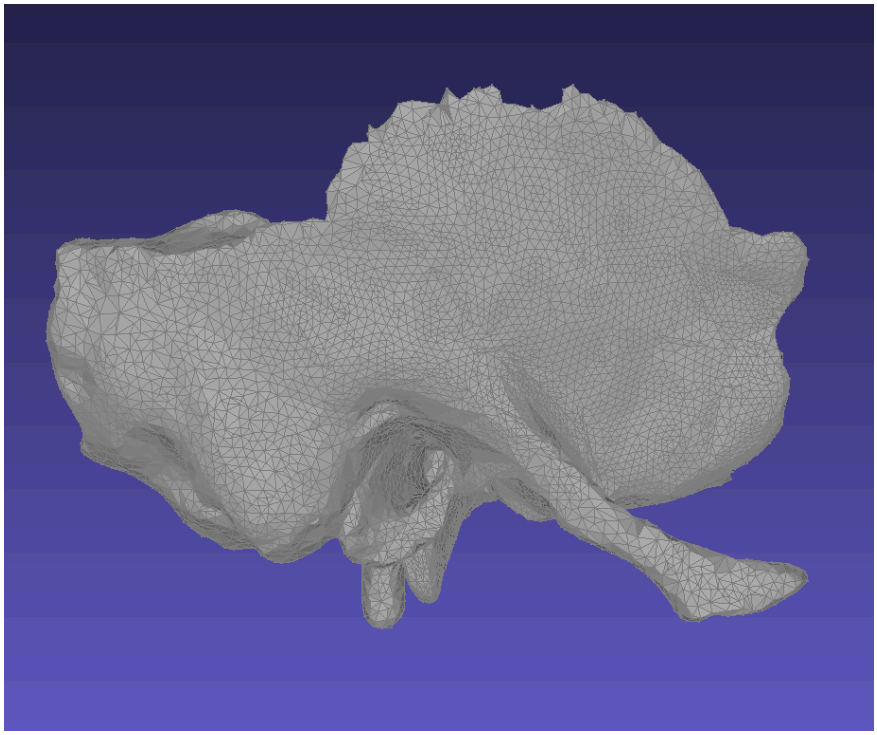

Figure 16. Final adaptive mesh of the temporal bone

For the mesh to be used in Ansys it needs to be converted into a STEP file, to do so, Fusion 360 do the conversion from Mesh to BRep, in other words it is converted into a solid, and it could be exported, this conversion is seen in figure 17.

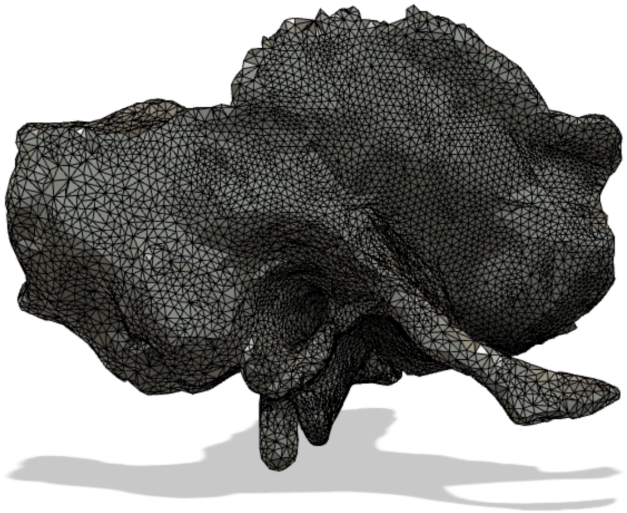

Figure 17. Temporal bone mesh converted into a BRep solid

Using Ansys 2018 simulation software, two modules are important for this project, the Modal and Harmonic Response module. Using Modal, the software is going to be able to extract natural modal frequencies in a set range. Loading the module into the Ansys Workbench to start the analysis programming will get the options as seen in figure 18. It is important to set the Engineering Data accordingly to the mechanical properties of the temporal bone previously stated in Introduction, figures 7, 8 and 9, where density and isotropic elasticity properties are written, figure 19, assuming the material of the bone has a isotropic elasticity with data from table 7.

Table 7. Temporal bone material properties

Density	$1860\ \frac{\mathrm{km}}{\mathrm{m}^3}$
Young's Modulus	$2{,}06\ \mathrm{e}^{10}$ Pa

Poisson's ratio	0,25
Constant damping ratio	0,005

In the Geometry section the STEP file is imported into Ansys and the Model is generated and the Multiple Systems - Mechanical window is opened, figure 20. In Mechanical, the Geometry is opened, and a Mesh can be generated as seen in figure 21. For this model a coarse mesh is applied, this coarse mesh is also selected in order to reduce simulation times, and RAM consumption, although Ansys can reduce the simulation time in comparison with other simulation programs, RAM usage and the temp files generated by the software during the simulation can cause problems and shut Ansys down.

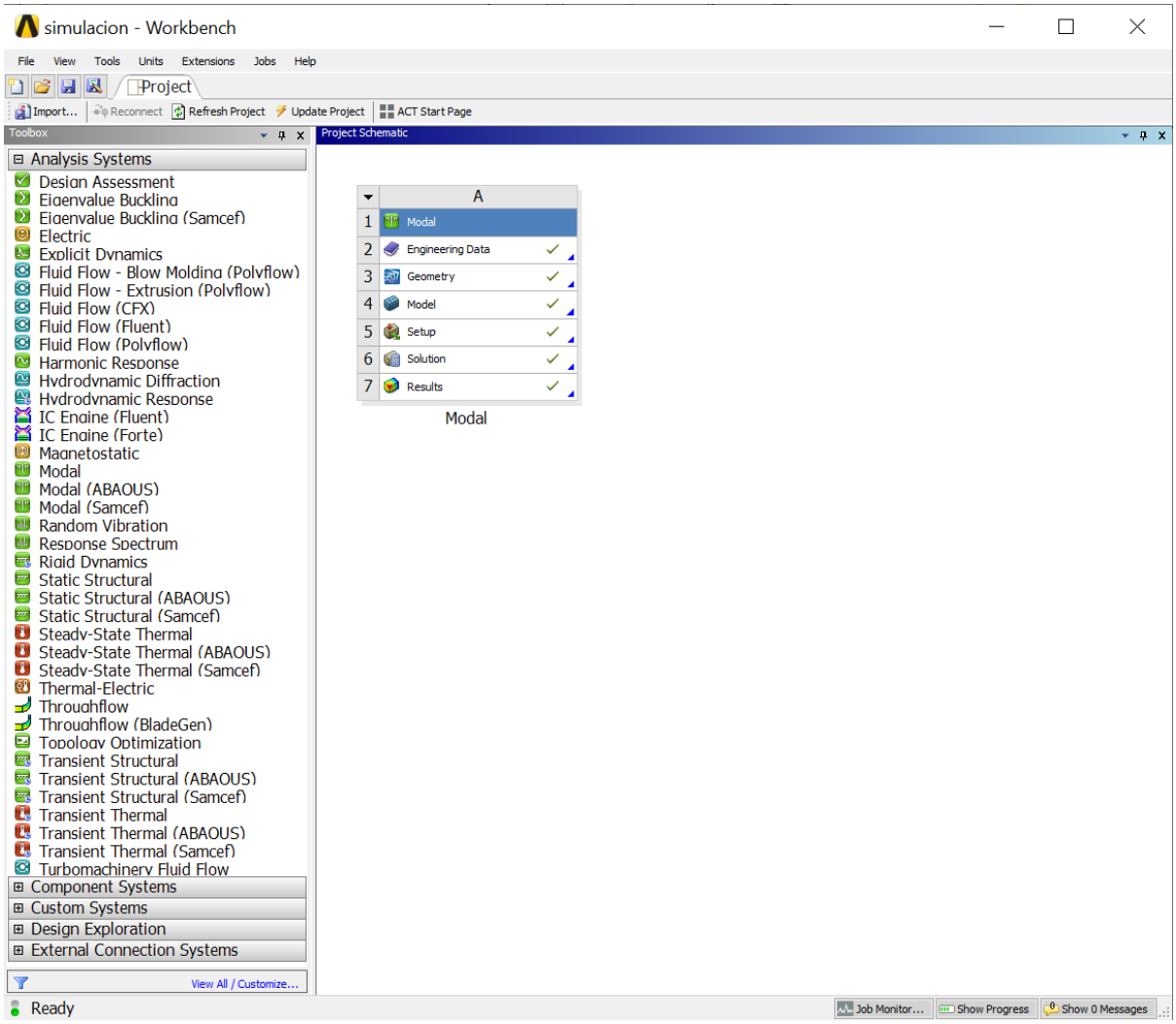

Figure 18. Ansys Workbench with Modal module

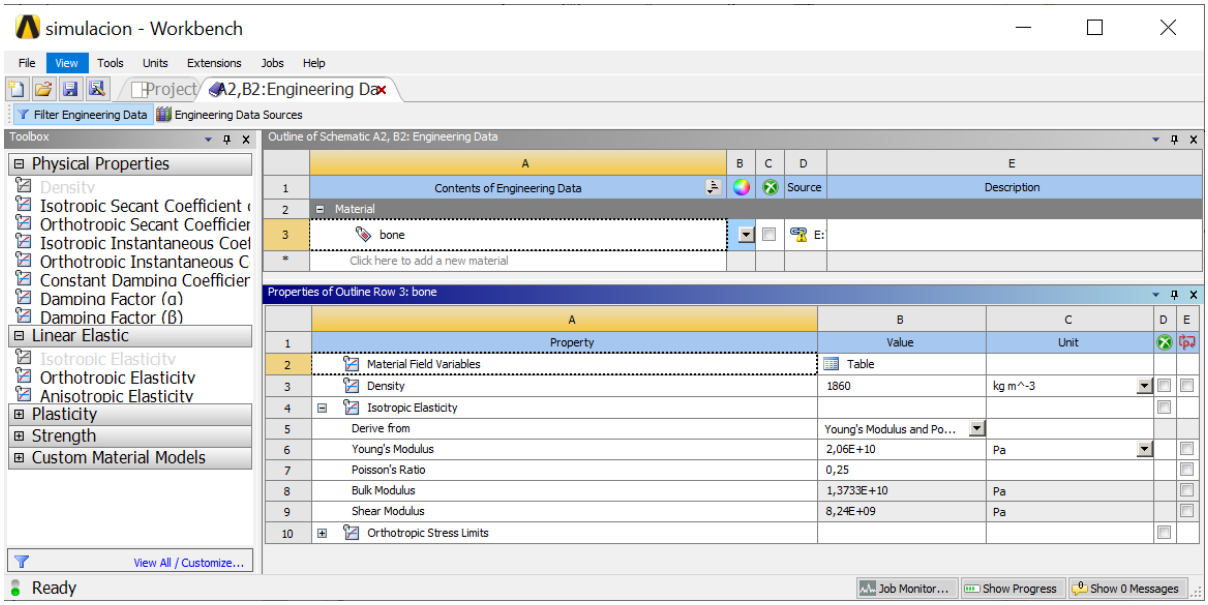

Figure 19. Engineering data for the mechanical properties of the temporal bone

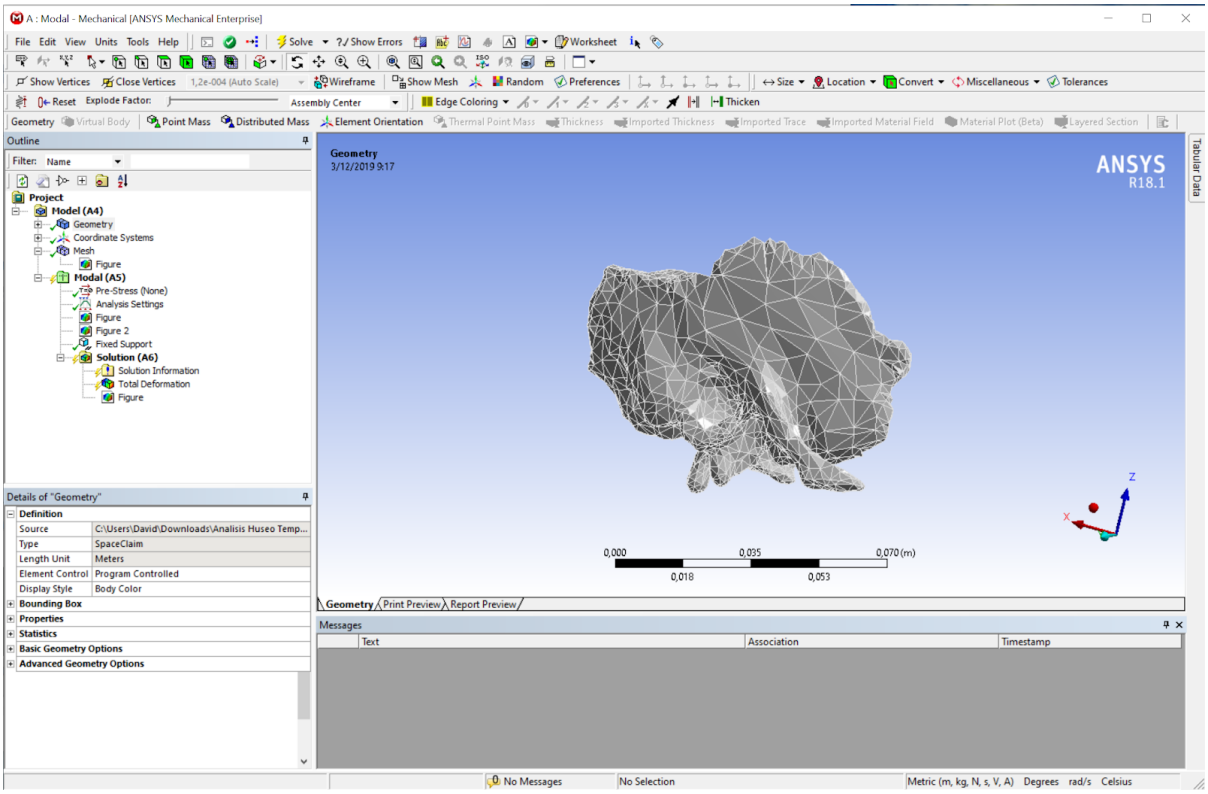

Figure 20. Ansys - Mechanical Geometry window

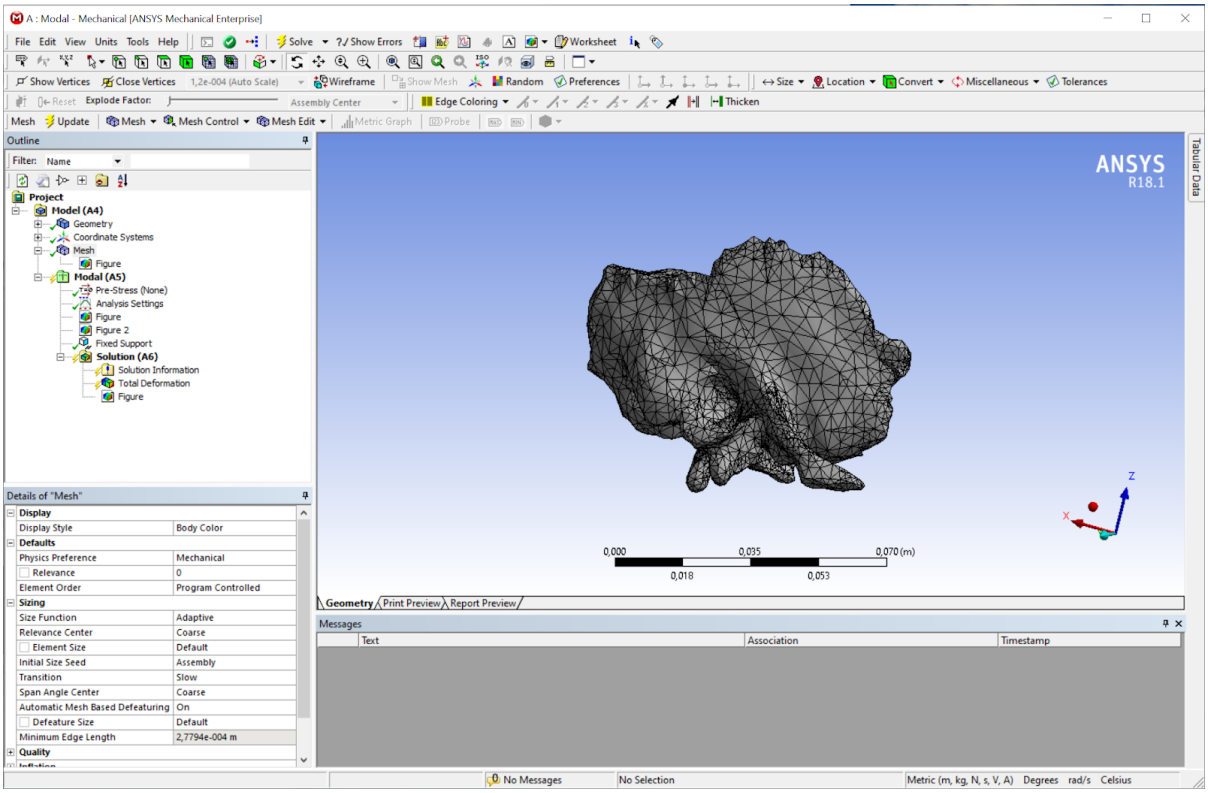

Figure 21. Ansys - Mechanical Temporal Bone mesh geometry and settings

For the Modal Analysis Settings, ten modes are set to find within a range of 0Hz and 20kHz, figure 20. In this module is important the set the fixed supports, as the temporal bone is attached to 4 bone borders sutures as stated previously in figure 3, which are: occipitomastoid, squamosal, sphenosquamosal and zygomaticotemporal sutures, as seen in the figures 23, 24, 25 and 26 below.

Details of "Analysis Settings"	
Options	
Max Modes to Find	10
Limit Search to Range	Yes
Range Minimum	0, Hz
Range Maximum	20000 Hz
Solver Controls	
Damped	No
Solver Type	Program Controlled
Rotordynamics Controls	
Output Controls	
Analysis Data Management	

Figure 22. Details and settings of the Modal Analysis in Ansys

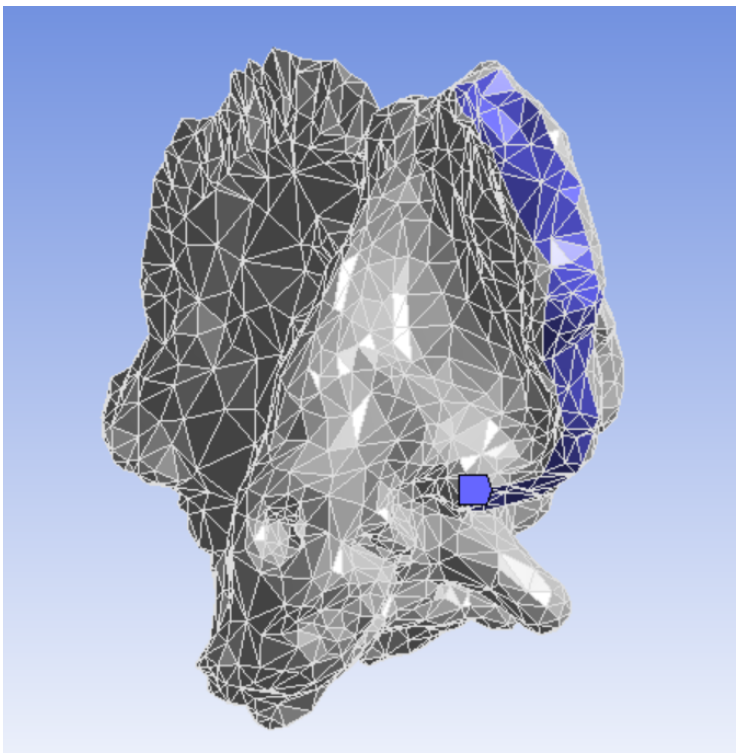

Figure 23. Zygomaticotemporal suture fixed support on the Modal module

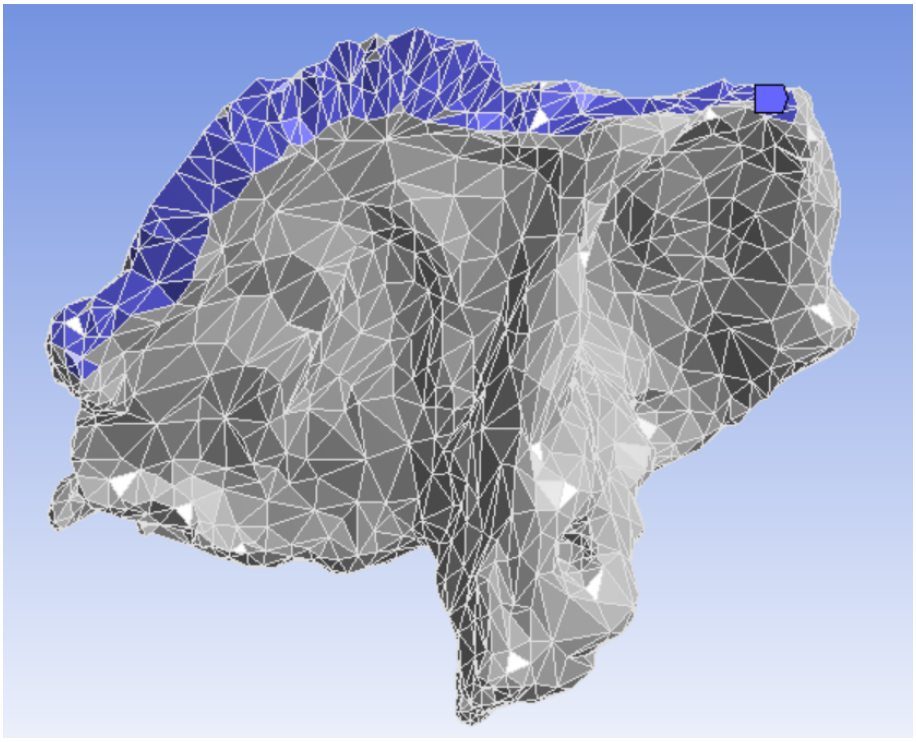

Figure 24. Squamosal suture fixed support on the Modal module

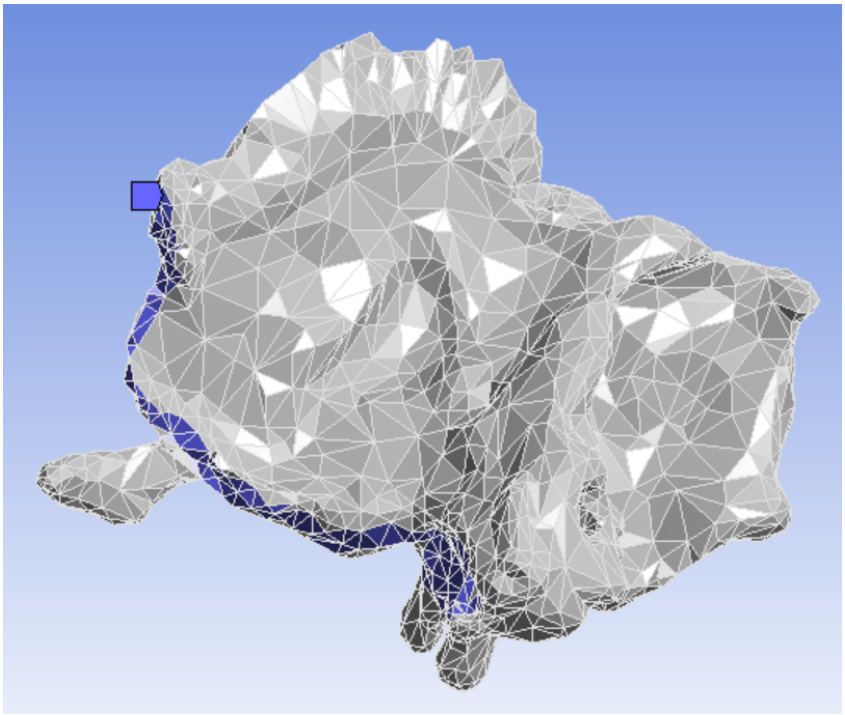

Figure 25. Sphenosquamosal suture fixed support on the Modal module

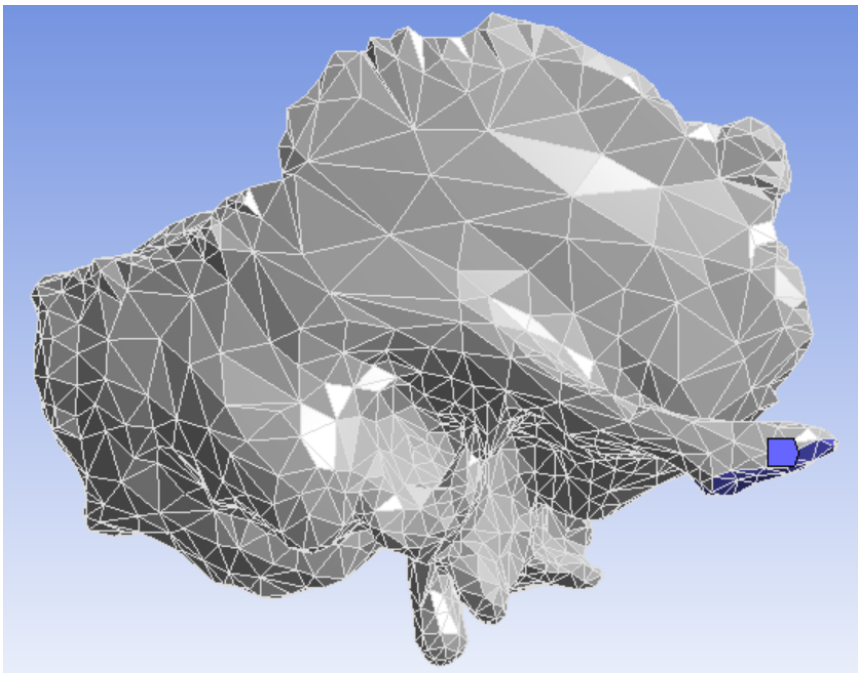

Figure 26. Zygomaticotemporal suture fixed support on the Modal module

For the Harmonic Response module, is important to connect in the Ansys Workbench the solution results to the Setup of this module, in this way, mechanical properties, fixtures and modal frequency extractions will be considered in this analysis as seen in figure 27 and 28. The

analysis settings for this module will be separated in two parts, the first one is analyzed in a frequency range of 1Hz to 10kHz and the second one in a range of 10kHz to 20kHz, this is done for RAM and computational power optimization for this FEM Analysis. Each Harmonic Response module is also plotting 250 points of displacement. In order to reproduce the effect BC headphones are causing over the temporal bone, a pressure force of 1,5 N in an area of 1,8 centimeters, or 88 Pa, is applied over the squamous section of the bone, figure 29. Finally, in order to obtain the desired results a nodal point probe is placed over the auditory canal region just over where the cochlea and semicircular canals are located, so Ansys can plot the desired displacement, as seen in figure 30.

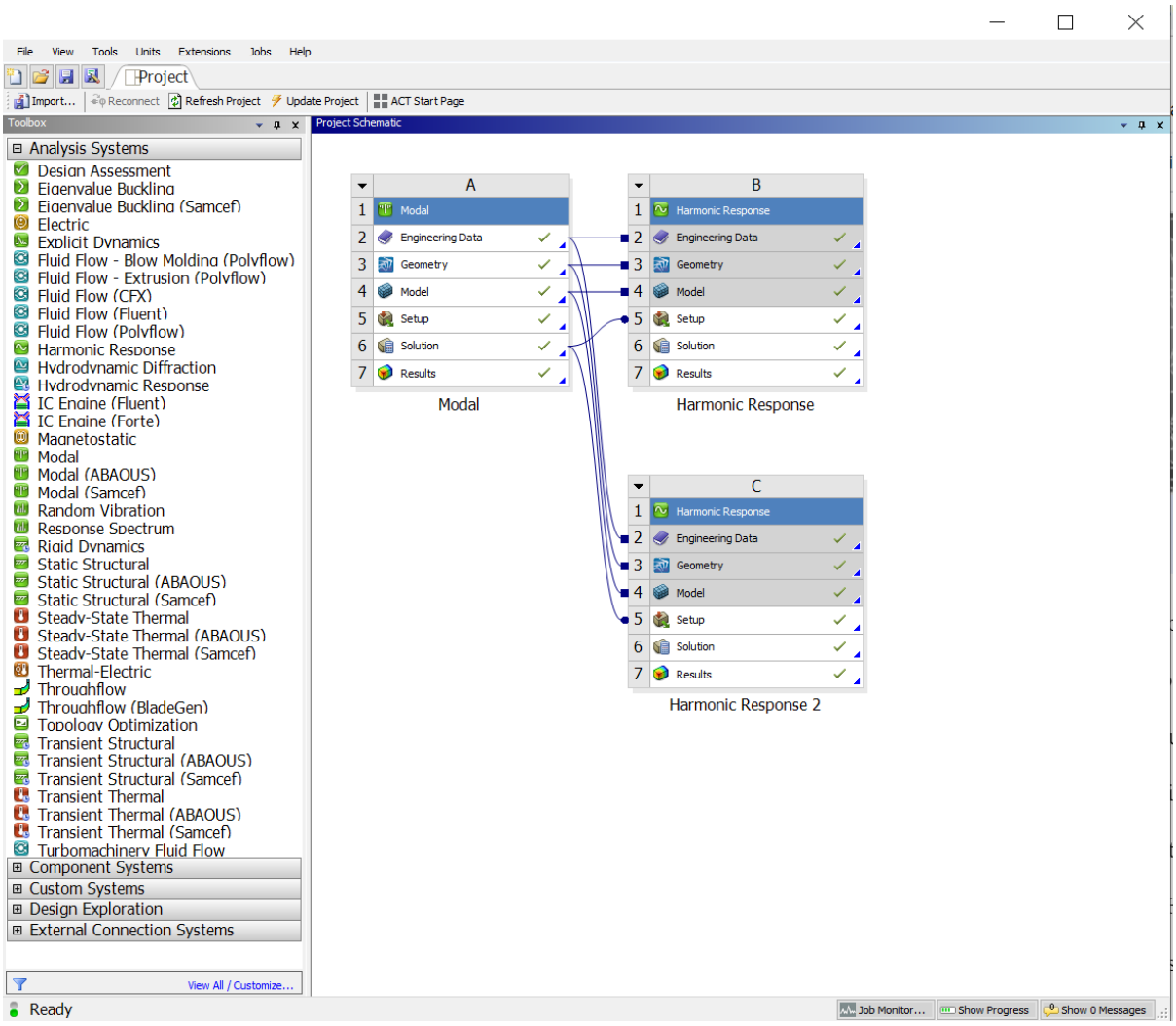

Figure 27. Harmonic Response modules connected to Modal module in Ansys Workbench

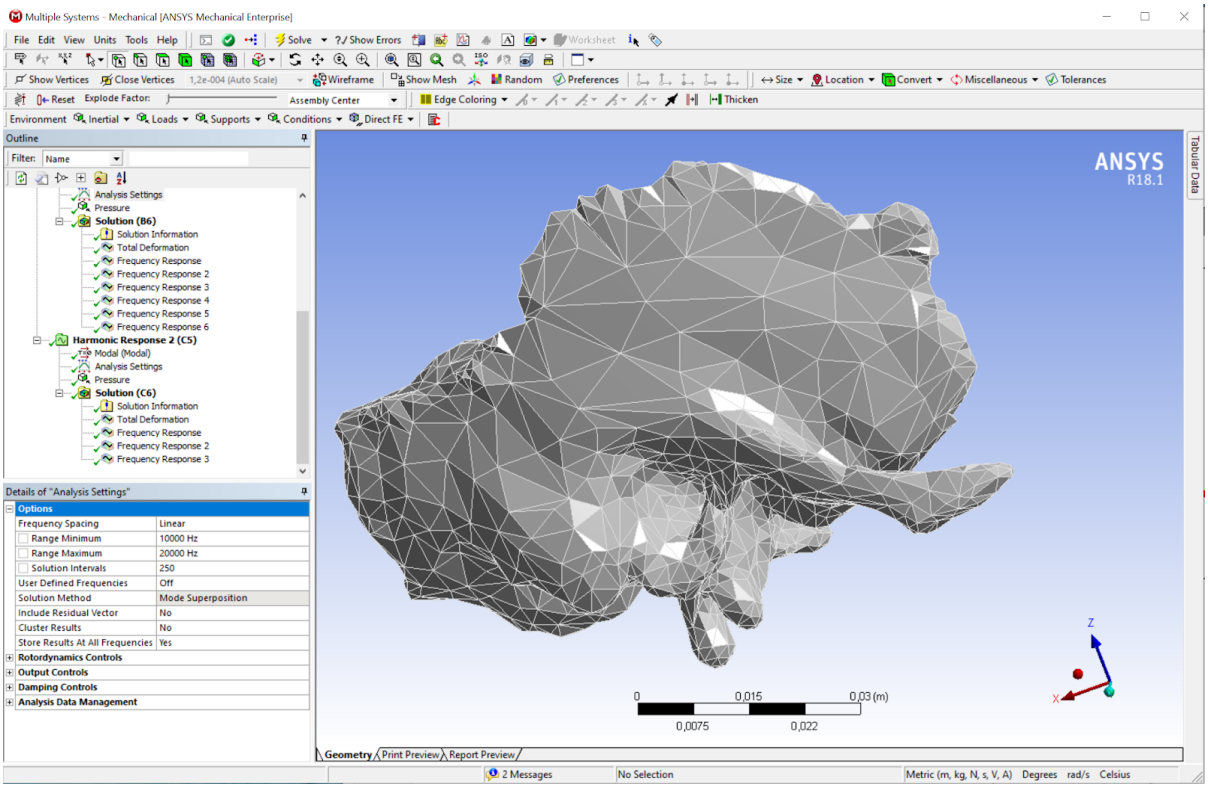

Figure 28. Harmonic Response module connected to Modal module in Ansys - Mechanical

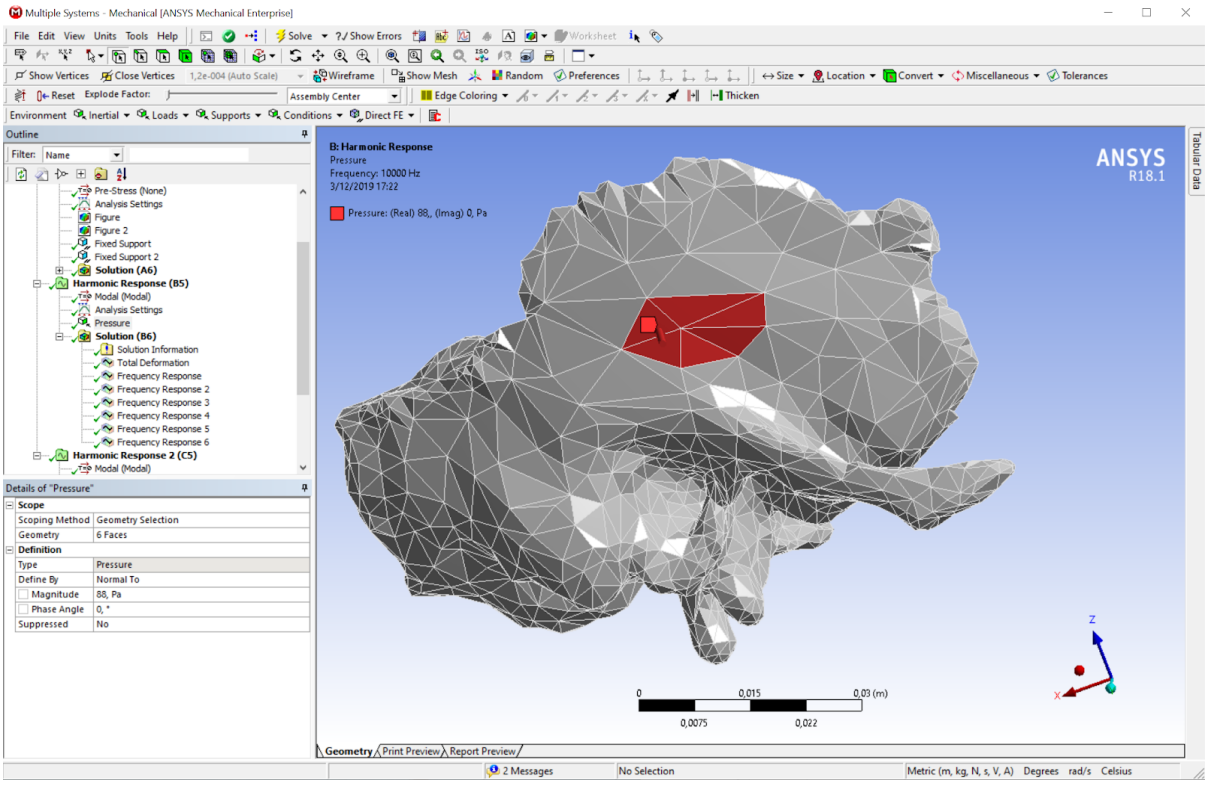

Figure 29. Pressure area over the temporal bone used in the Harmonic Response Module

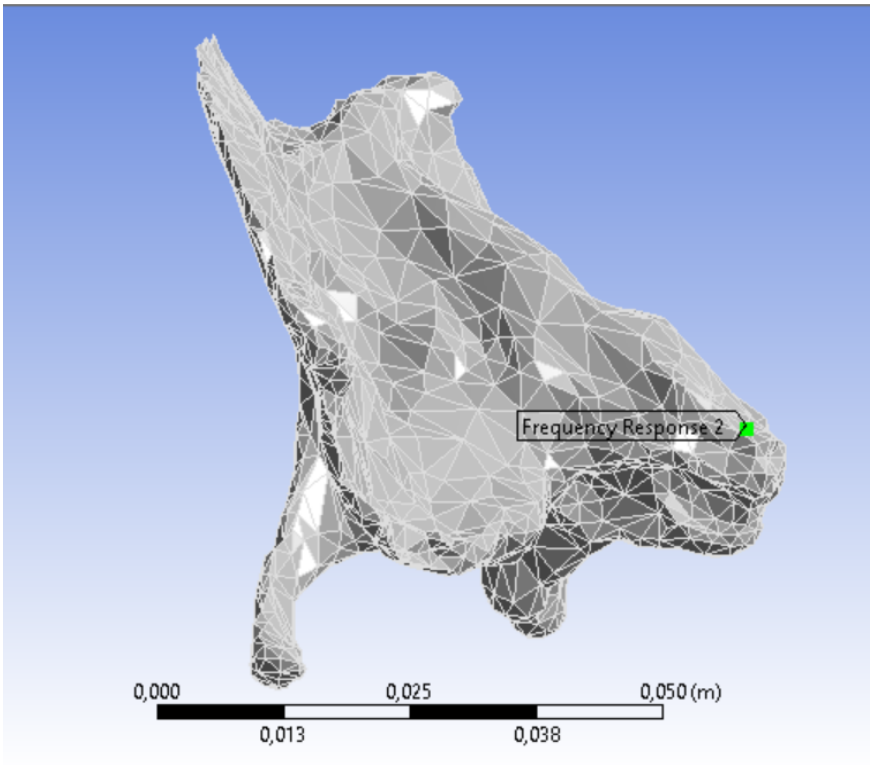

Figure 30. Nodal point tracking the displacement caused by the Harmonic Response Module

2.2. Real Bone Analysis

In order to get real data when using BC headphones on a dry bone a model of the adjacent bones which connect to the 4 sutures talked in the Introduction section, figure 3, was 3D printed, holding the real temporal bone in place. To get this analysis the following steps were made: Scanning the real bone to have a STL file to work with, obtain a skull from a 3D online source, adapt the two STL files so the real bone will fit on the 3D skull, build a stand for the 3D printed skull, using real BC headphones apply a sweep signal from 1 Hz to 10kHz and from 10kHz to 20kHz (Henry, Letowski, 2007) in the same area analyzed in FE, and process the results in LabView 2018 software using a accelerometer in two points of the real bone to track the movement caused by the signal applied by the BC headphones. Finally, in order to be able to compare the results obtained to the FE analysis, the acceleration raw signal needs to be filtered to reduce the noise caused by external factors, integrated twice to get displacement and perform a Fast Fourier Transformation (FFT) and plot all this using MATLAB 2016b.

As the real temporal bone was already scanned and used for the FE analysis, the STL file is need for cutting through a model a skull found in Grabcad.com which is a whole skull with independent bones. From this model the parietal, zygomatic, sphenoid and occipital bones are needed, figure 31.

Figure 31. Skull model with a parietal, zygomatic, sphenoid and occipital bones

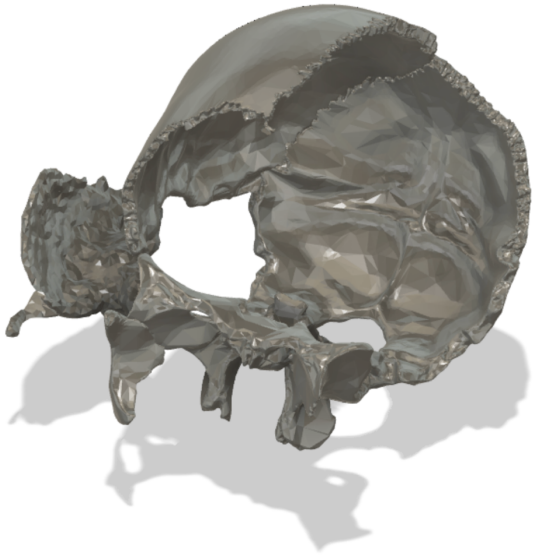

Figure 32. Skull cut with the real temporal bone scanned

Figure 33. 3D skull model with the cut for the real temporal bone

Is important to cut the skull using the real model of the temporal bone that is going to be used in the tests, this way, once printed the real bone will fit perfectly, as seen in figure 32 and 33. As the aim of this test is to simulate the real temporal bone in conjunction with the rest of the cranial bones as if it was in a complete skull, is important to make a proper set up.

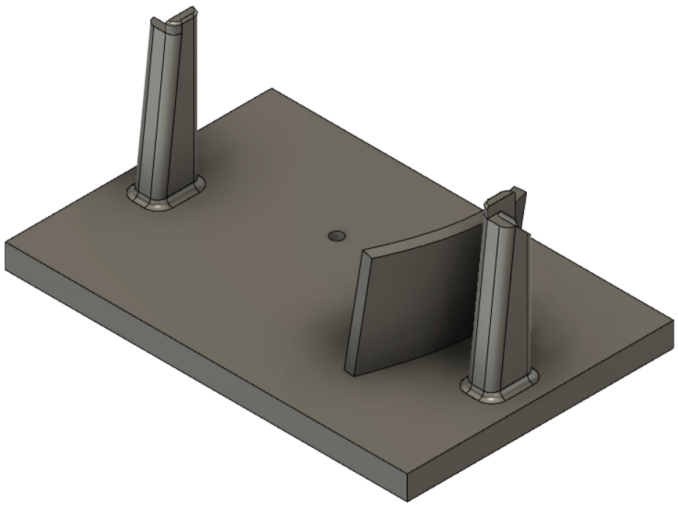

Figure 34. Stand base for the 3D printed skull and temporal bone isometric view

The base shown in figure 34, was also 3D printed in order to fix the skull and the temporal bone, the two columns on the sides will act as a support for the headphone bands and also will simulate the function that external ears will have when using BC headphones. This base was made taking in consideration dimensions of the 3D printed skull, as seen in figure 35, as well as where the transducer of the BC headphones will be placed on the temporal bone. Both pieces were 3D printed separately.

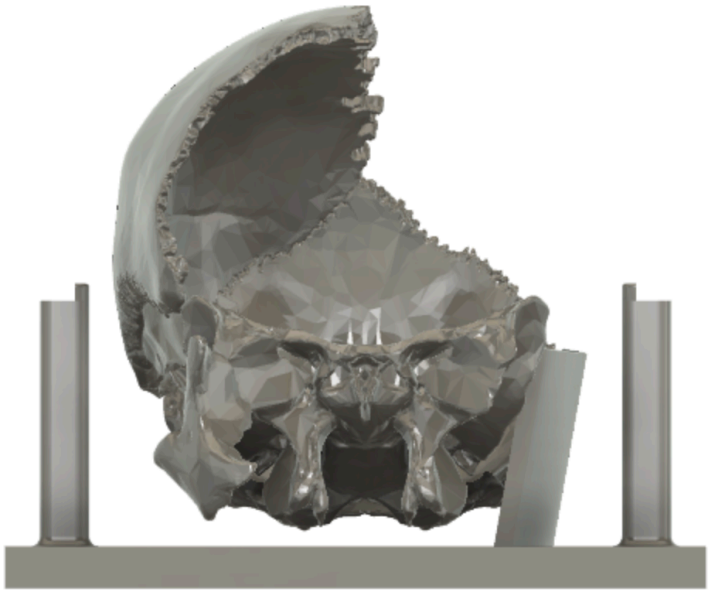

Figure 35. Base and skull for 3D printing

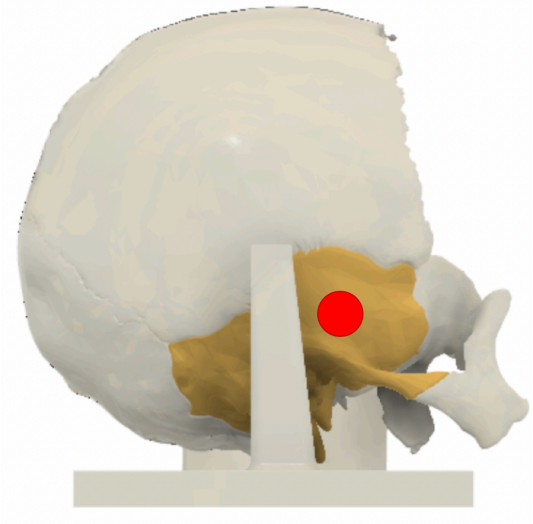

Figure 36. Location of the BC headphone right transducer.

In order to perform the test once the set-up is ready, the right BC headphone transducer is placed over the squamous area of the temporal bone as seen in the figure 36. The test includes one placement for the accelerometer that are show in the following figure 37, which is placed over the tympanic cavity where the internal ear organs and more importantly the cochlea are located. This placement is crucial in order to understand how the vibration caused by the transducer is traveling from the squamous area to the tympanic cavity area.

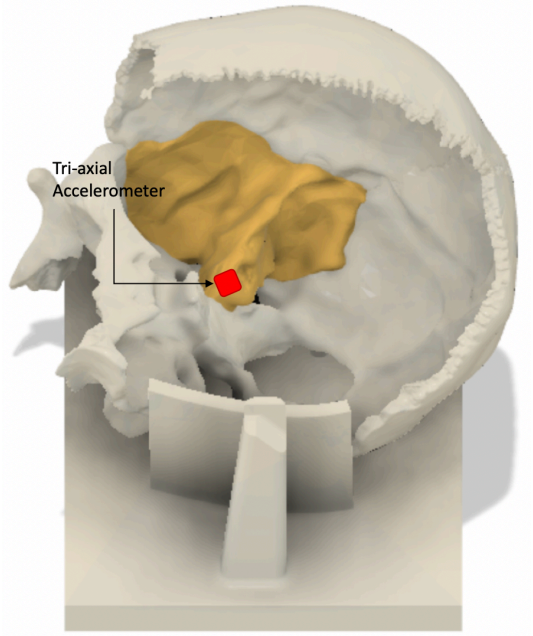

Figure 37. Location of the accelerometer on the temporal bone

To get the displacement of the bone caused by the BC transducer, a National Instrument DAQ, an acquisition data card in conjunction with a triaxial accelerometer are used, connected to a PC using LabView 2018 in the following order, figure 38.

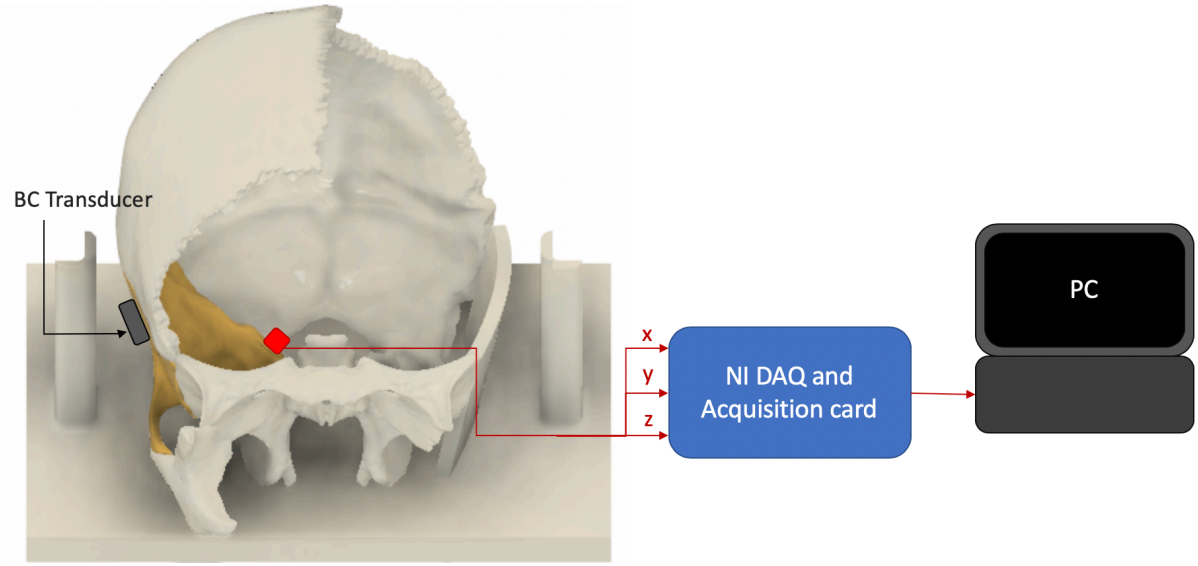

Figure 38. Final skull-temporal bone Set-up

Using LabView 2018 with DAQ Assistant 2018 plugin the following code is created in order to gather the data taken by the triaxial accelerometer. In this code, DAQ Assistant is acquiring and processing the data taken by the digital signal processing board dividing each axis of the accelerometer in individual inputs, by doing this, each axis has its own parameters of acceleration, figure 39. Each input needs to be configured in order to calibrate the sensitivity of each axis, this calibration specifications are set by the manufacturer, PCB Piezotronics, as seen in figures 40, 41 and 42. For the Timing Settings, the DAQ Assistant is taking N Samples which are 500k Samples under 10 seconds at a sampling rate of 40k Hz. As for the input signal going to the BC headphones a frequency generator is connected generating a chirp sine wave signal in a frequency range of 1Hz to 10kHz and in another instance from 10kHz to 20kHz, doing this the whole human audible spectrum is taken into consideration, but it is divided into two parts because of the software and computer capabilities. In the code, a plot of the raw data signal is being generated and also a power spectrum plot is being generated using the Spectral

Measurements module, figure 43, to get a rough idea of the frequencies involved, for its configuration a Power spectrum is selected as mentioned and a Linear Result, figure 44. Finally, the code is exporting the data to Excel 2016 using the Write to Measurement module.

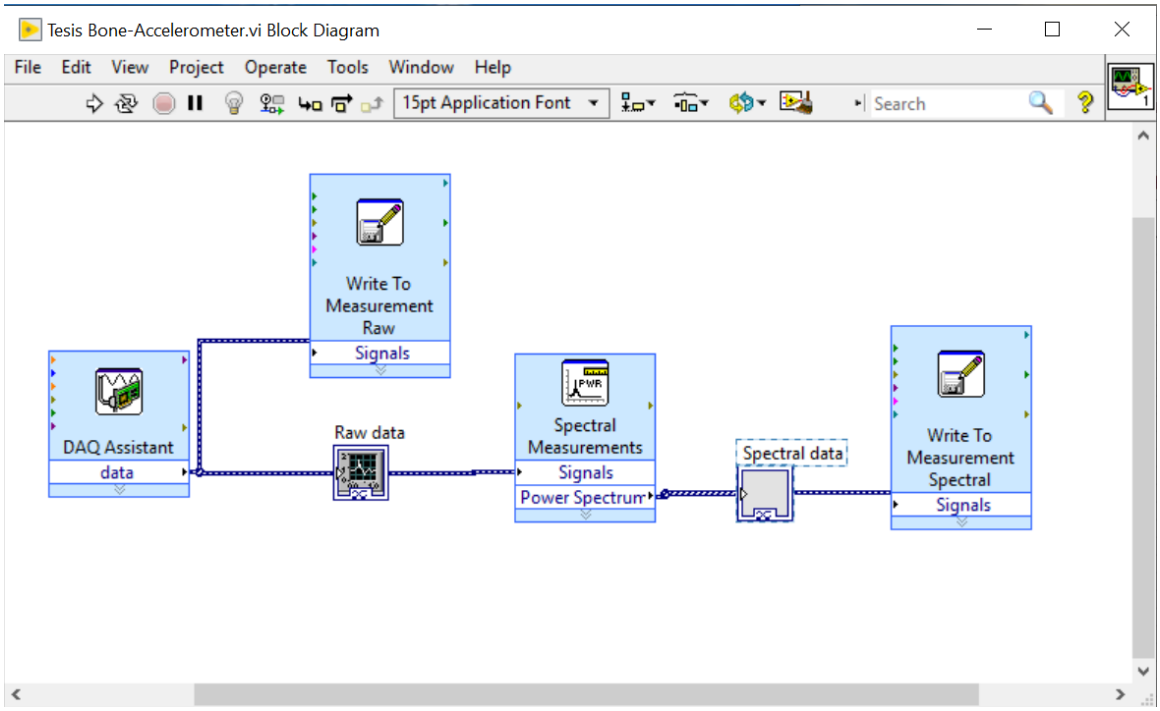

Figure 39. LabView 2018 code used in conjunction with DAQ Assistant

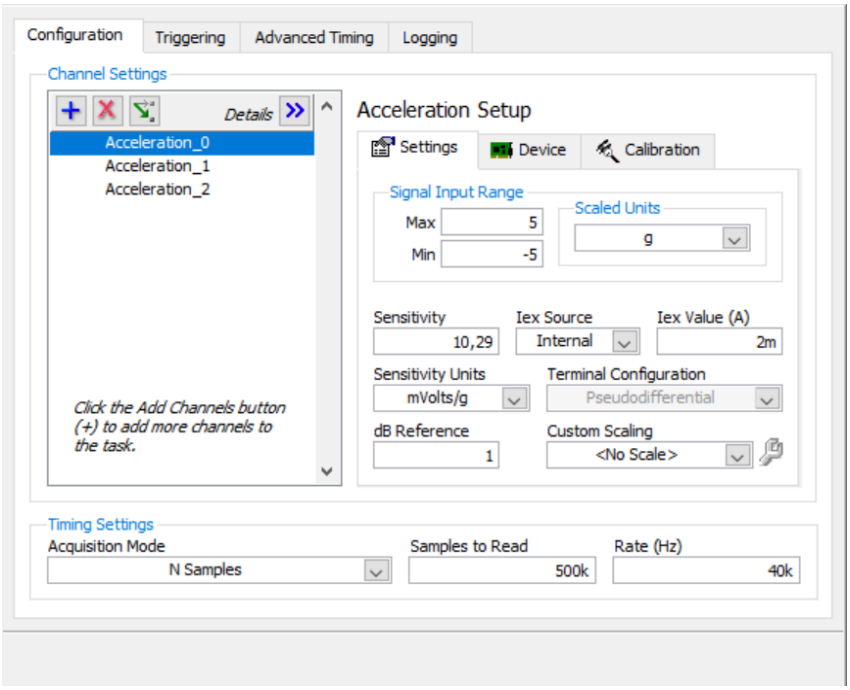

Figure 40. DAQ Assistant settings for X axis

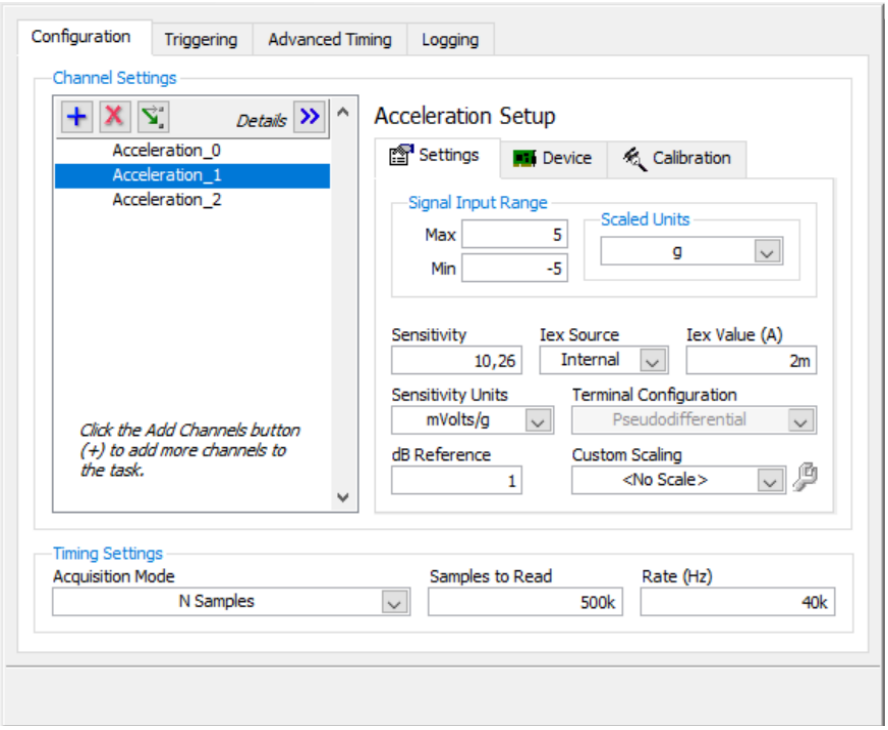

Figure 41. DAQ Assistant settings for Y axis

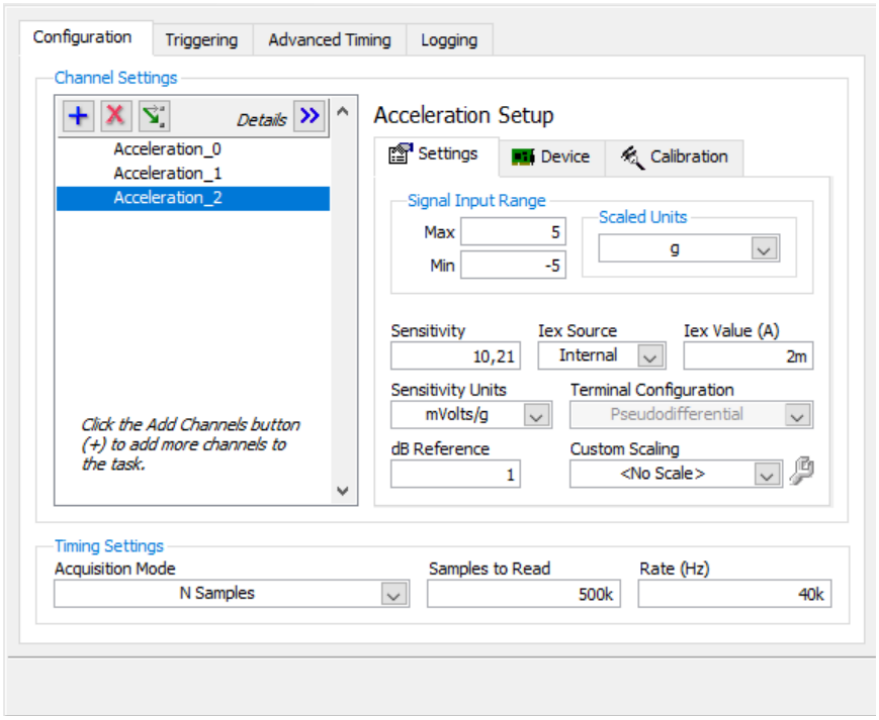

Figure 42. DAQ Assistant settings for Z axis

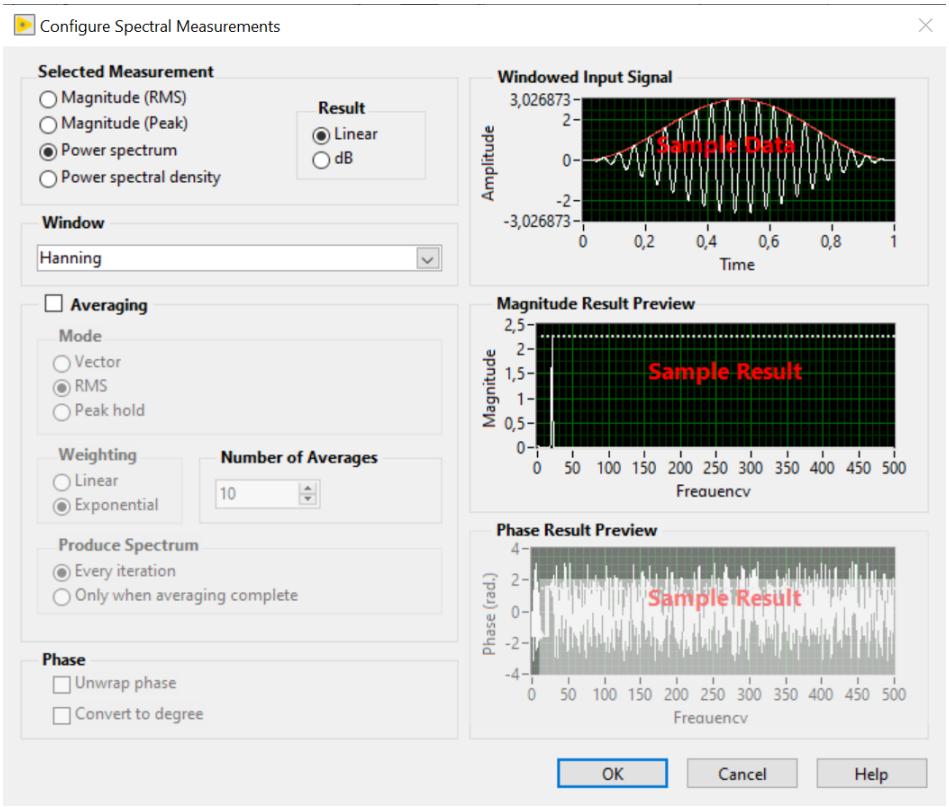

Figure 43. Spectral Measurement Set-up

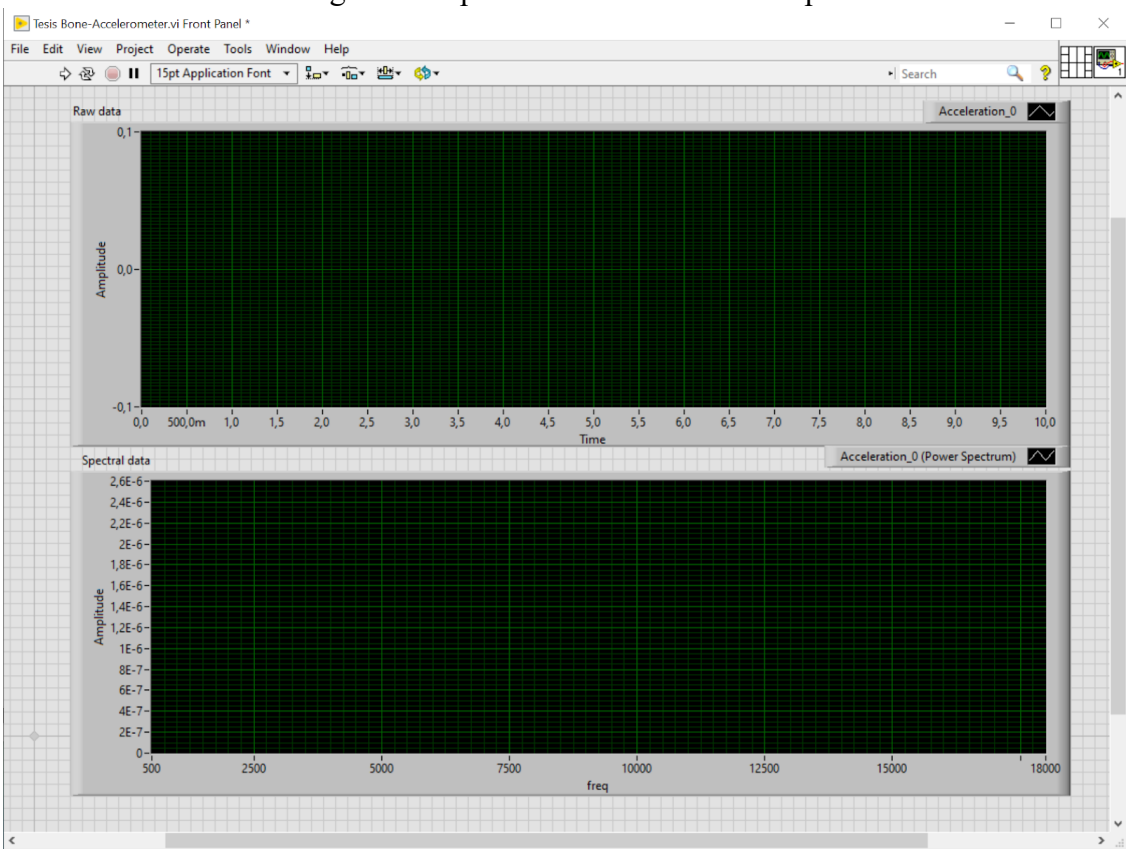

Figure 44. LabView Front Panel for the raw and spectral measurements plots

Once the data is obtained, it is important to filter the signal to reduce the noise that the triaxial accelerometer may have taken from any outside sources, for this purpose a bandpass filter was applied to the signal using MATLAB 2016b. The bandpass filter will pass the frequencies within a certain range and attenuate all the frequencies that are not included in that range, this way, all the frequencies that need to be shown in the signal that correspond to the applied ranges set 1, 1 Hz – 10 kHz and set 2, 10 kHz – 20 kHz will remain similar to the raw data, although the shape form of the signal will be smoothed cutting undesired frequencies. In order to do so a Butterworth filter order and cutoff frequency code should be used to pass the raw data:

$$[\mathrm{n}, \mathrm{Wn}] = \mathrm{buttord}(\mathrm{Wp}, \mathrm{Ws}, \mathrm{Rp}, \mathrm{Rs})$$

Where n will return the lowest order of the digital filter with no more than the value selected for the Passband ripple (Rp) in dB and at least an attenuation value selected for the stopband attenuation (Rs) also in dB. Wp is the passband or cutoff frequency for the whole bandpass and Ws is the stopband edge frequencies of the filter, which are normalized from 0 to 1, if the chosen value is 1 it will correspond to π rad/sample. Wn is the vector of corresponding cutoff frequencies (MathWorks documentation, 2019).

With the acceleration signal already filtered, a double integral could be made in order to obtain displacement. As the function for the filtered acceleration signal is unknown, using MATLAB and the Cumulative trapezoidal numerical integration, cumtrapz, the displacement could be easily obtained. Cumtrapz computes an approximate cumulative integral of a value using the trapezoidal method using a unit spacing:

$$\mathrm{Q} = \mathrm{cumtrapz}(\mathrm{X}, \mathrm{Y})$$

Where Y will be integrated to the coordinates specified by X. This process is repeated twice from the acceleration signal to be converted into velocity and finally into displacement (MathWorks documentation, 2019).

Finally, to obtain a plot amplitude in meters vs frequency in hertz an FFT should be made for the displacement data obtain after the integration, to do so, a fft and a code in MATLAB should be use, where fft(X) is computing a fast Fourier transform algorithm (MathWorks documentation, 2019):

$$Y = \text{fft}(X)$$

3. RESULTS AND DATA ANALYSIS

3.1. Finite Element Analysis

The following results correspond to the FE analysis of the temporal bone using Ansys 2017. For the Modal Module or natural frequency extraction, the software found 5 vibrational modes within a range of 1 Hz to 20 kHz, which correspond to the human audible frequency range. These modes correspond to the shape deformation that certain frequencies can induce on the temporal bone model, and they can be seen in the next figures:

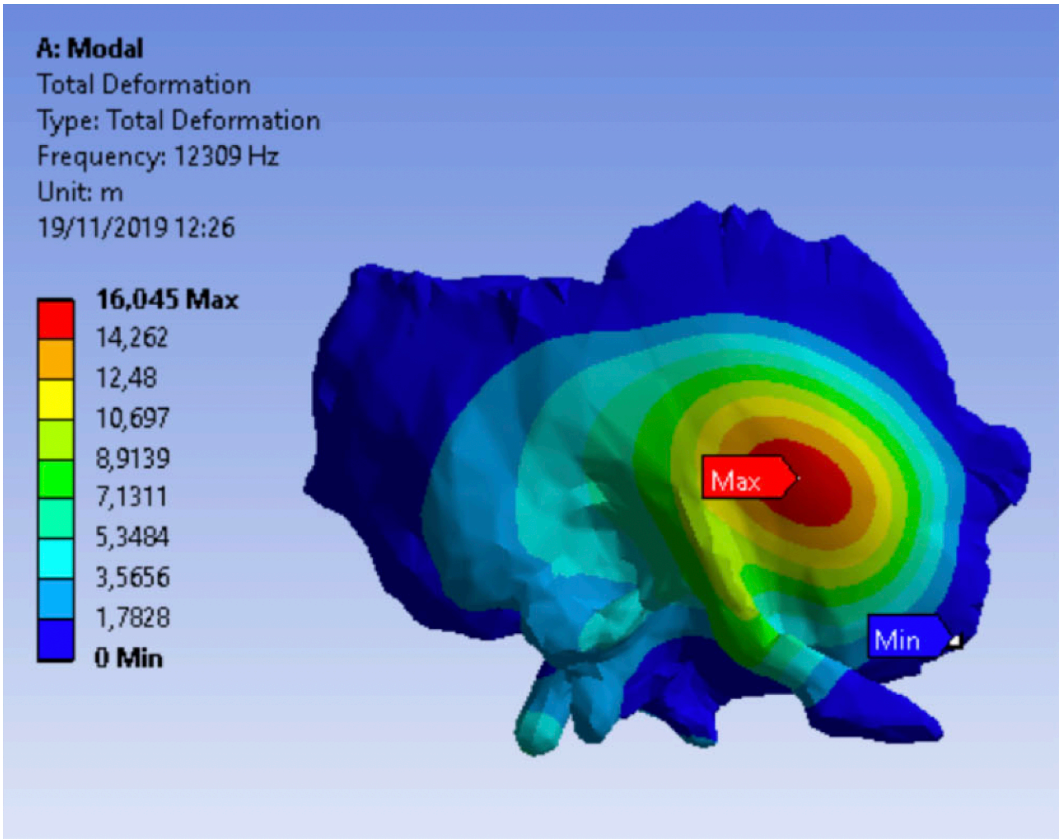

Figure 45. Ansys Modal Module, vibrational mode number 1, at 12309 Hz

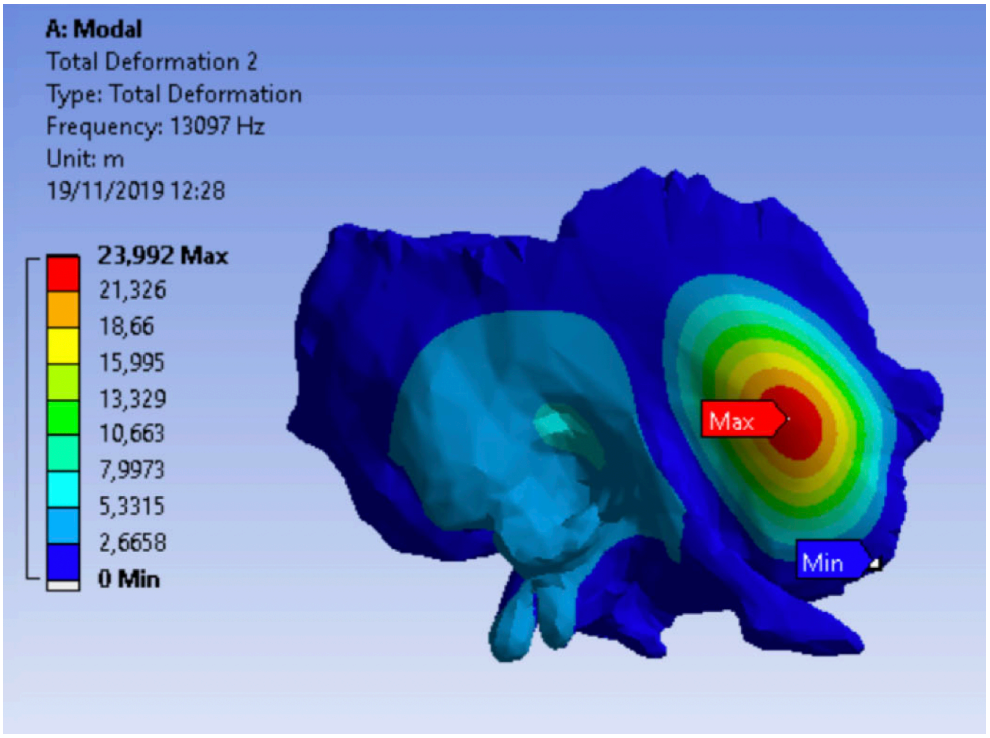

Figure 46. Ansys Modal Module, vibrational mode number 2, at 13097 Hz

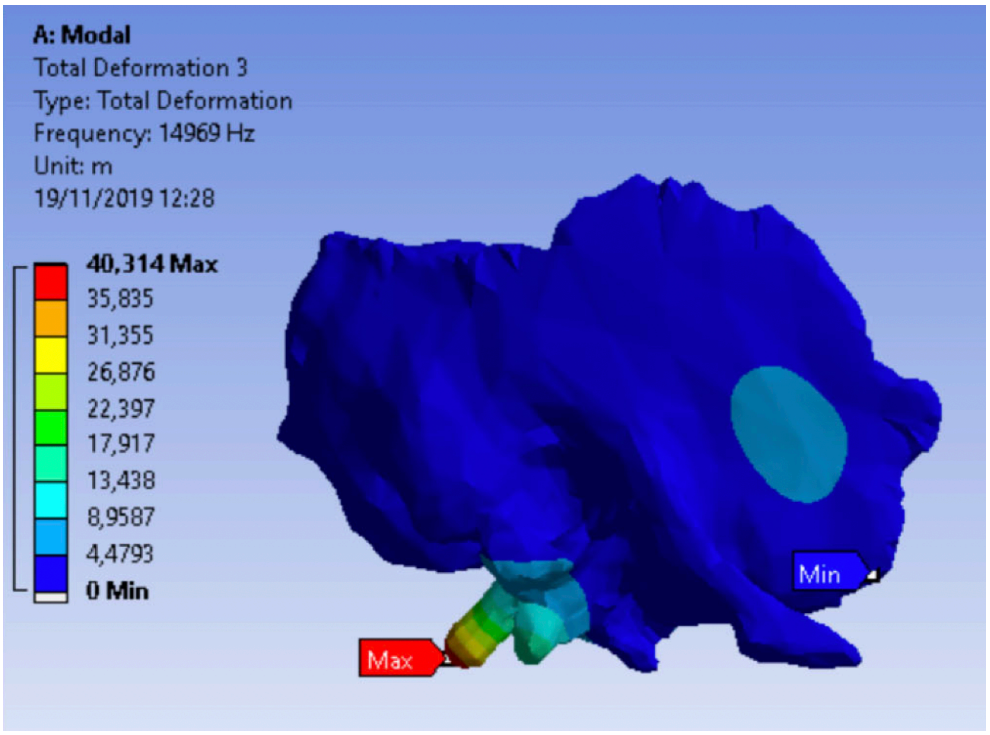

Figure 47. Ansys Modal Module, vibrational mode number 3, at 14969 Hz

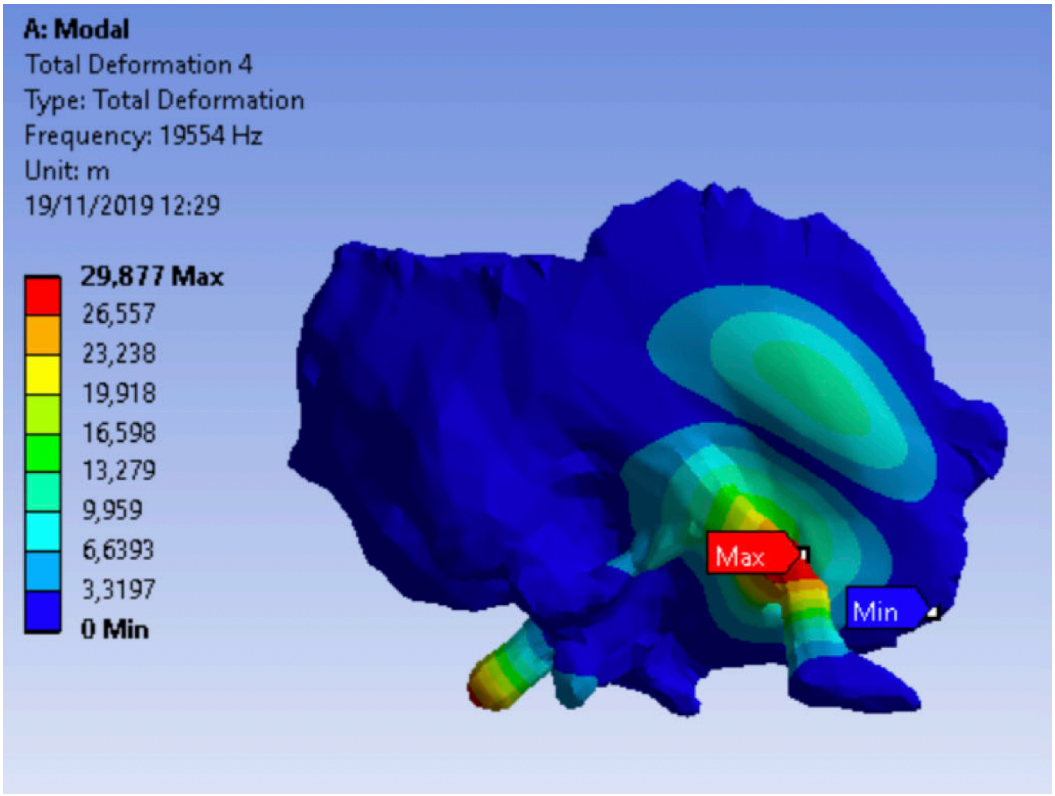

Figure 48. Ansys Modal Module, vibrational mode number 4, at 19554 Hz

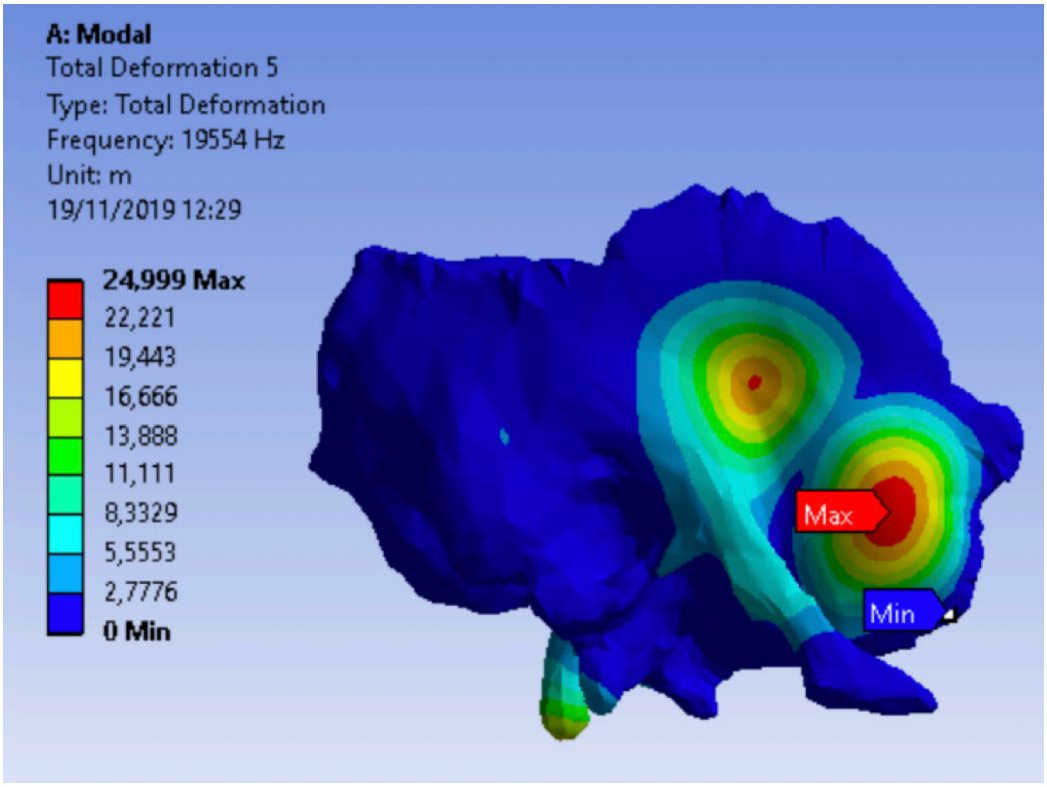

Figure 49. Ansys Modal Module, vibrational mode number 5, at 18686 Hz

From the modes found, number 1, 2 and 6 are the more important as these modes are reacting in a perpendicular motion to the pressure force that will be applied by the pressure force caused by the BC transducer. While the remaining modes have their reaction in other areas, as well as other motion which are not relevant for this study, as the main focus is to analyze the response of the squamous portion of the temporal bone when the BC headphones are used.

Harmonic Response module show the total deformation caused by the 1,5 Newton pressure force in an approximate area of 1,8 centimeters in the temporal bone, for two separately range sets: 1 Hz - 10 kHz and 10kHz to 20 kHz, figure x and figure x correspondingly. For the first set the maximum deformation value is 1,38e^{-9} meters, for the second set the value is 6,46e^{-9} meters. These values represent how a dry temporal bone is being affected by the applied pressure which is simulating the action BC headphones or transducer could have when vibrating within those ranges, figures 50 and 51.

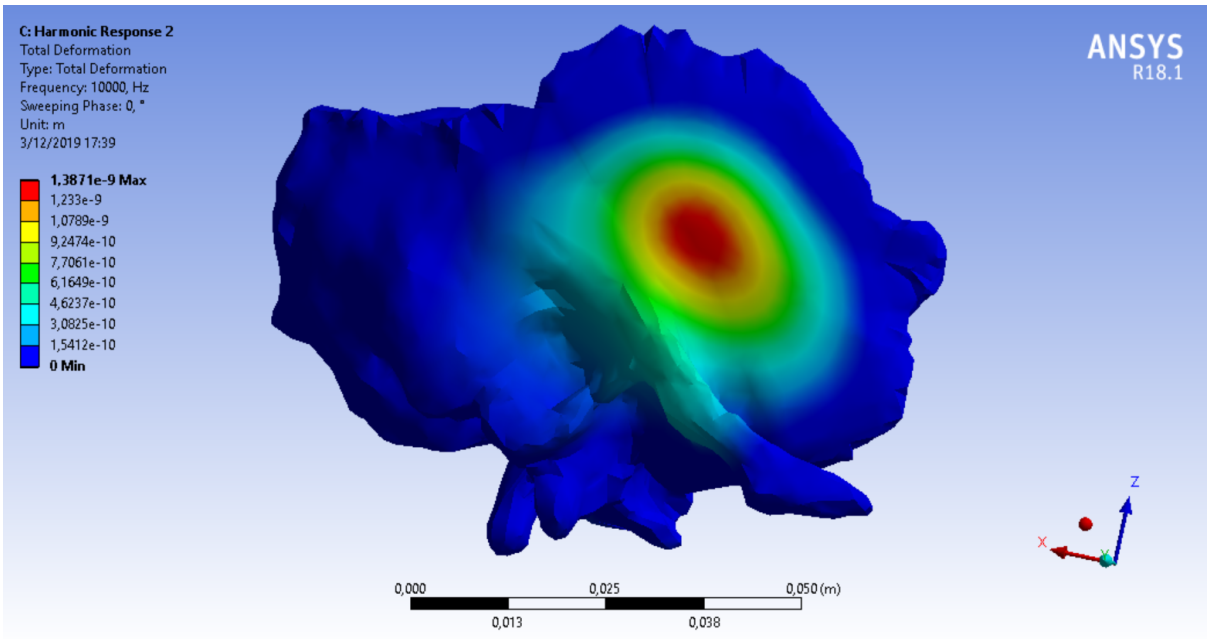

Figure 50. Total deformation for 1 Hz – 10 kHz in the Harmonic Response module

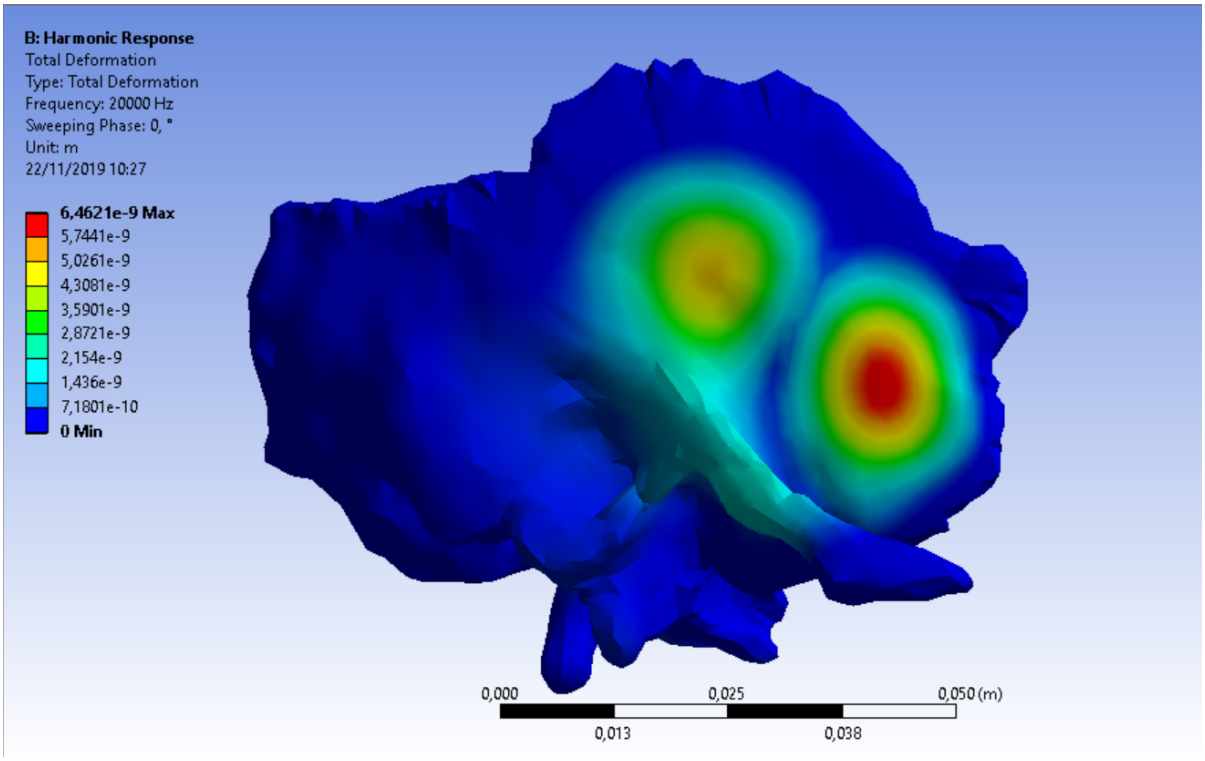

Figure 51. Total deformation for 10 kHz – 20 kHz in the Harmonic Response module

For the nodal point tracking the displacement caused by the Harmonic Response in the tympanic cavity where the cochlea would be located, plots for each axis X, Y and Z:

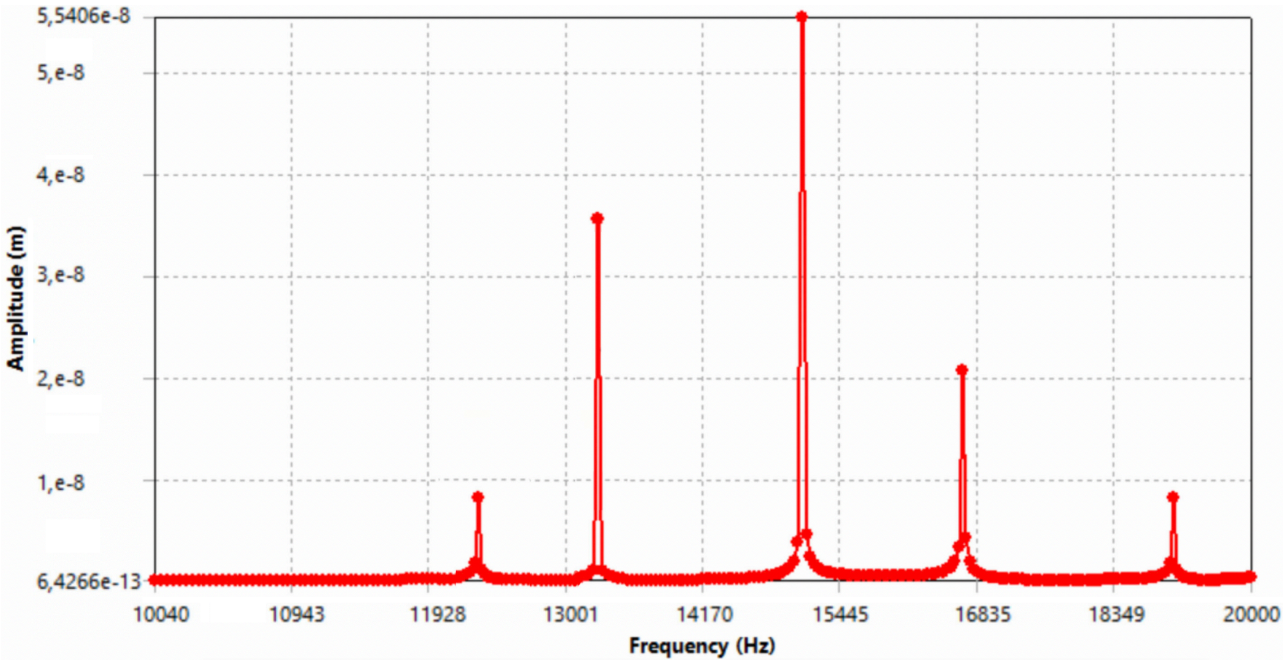

Figure 52. Y axis real displacement in the nodal tracking point caused by the Harmonic Response

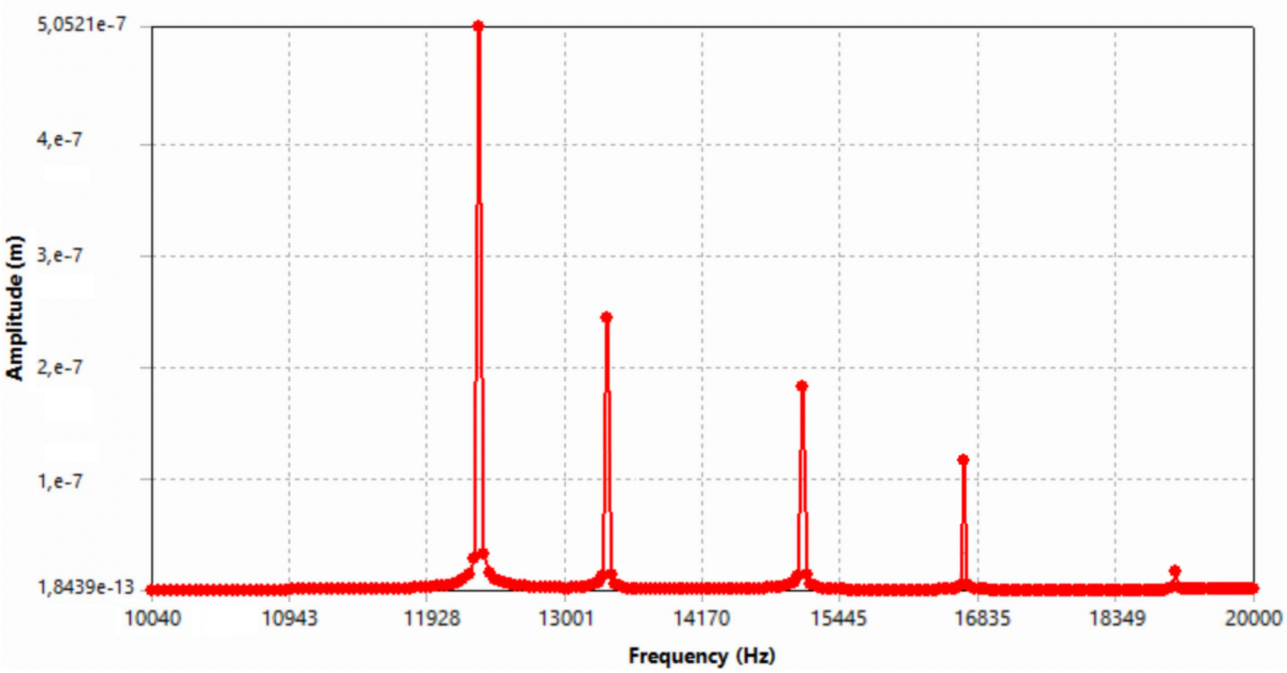

Figure 53. X axis real displacement in the nodal tracking point caused by the Harmonic Response

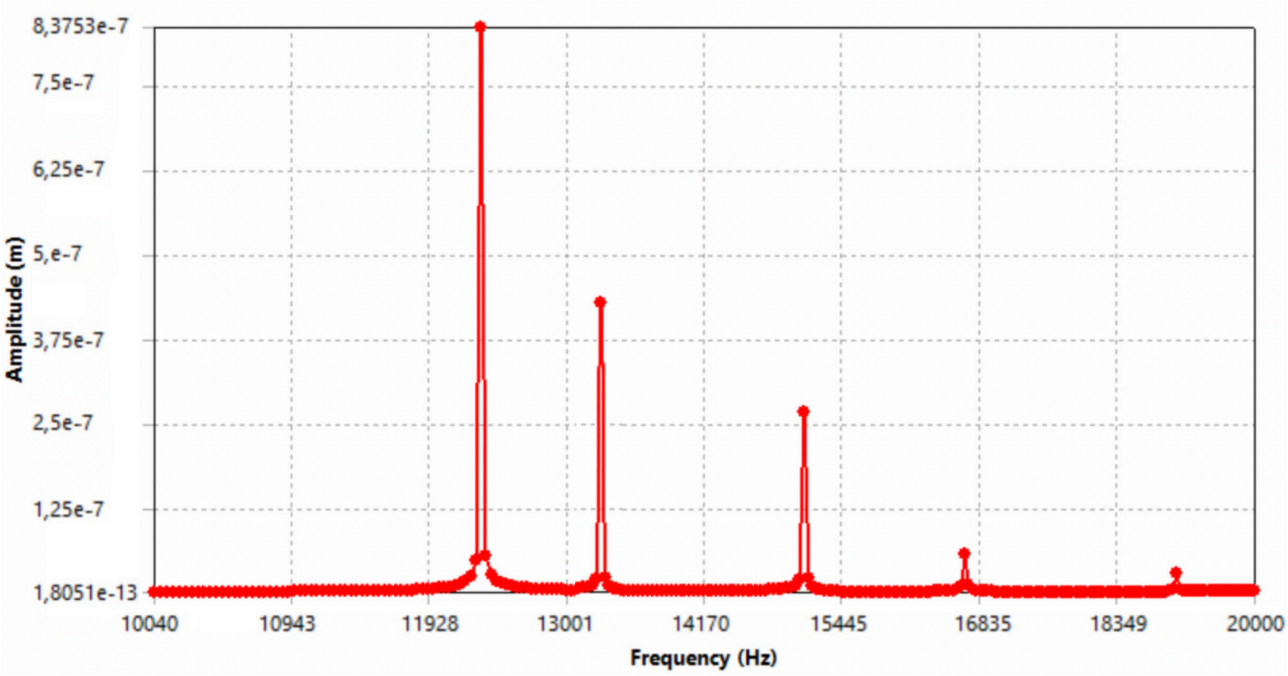

Figure 54. Z axis real displacement in the nodal tracking point caused by the Harmonic Response

3.2. Real Bone Analysis

Results obtained from the real temporal test using LabView 2018 shows two plots, the upper plot correspond to the raw data taken from the vibrational testing, amplitude vs time, while the bottom plot shows an FFT power spectral plot, amplitude vs frequency. For each set 10 measurements were taken. For the first set, 1 Hz to 10 kHz the data obtained is shown in the figures 55 - 64 and for the second set, 10 kHz to 20 kHz the data obtained is shown in the figures 65 - 74:

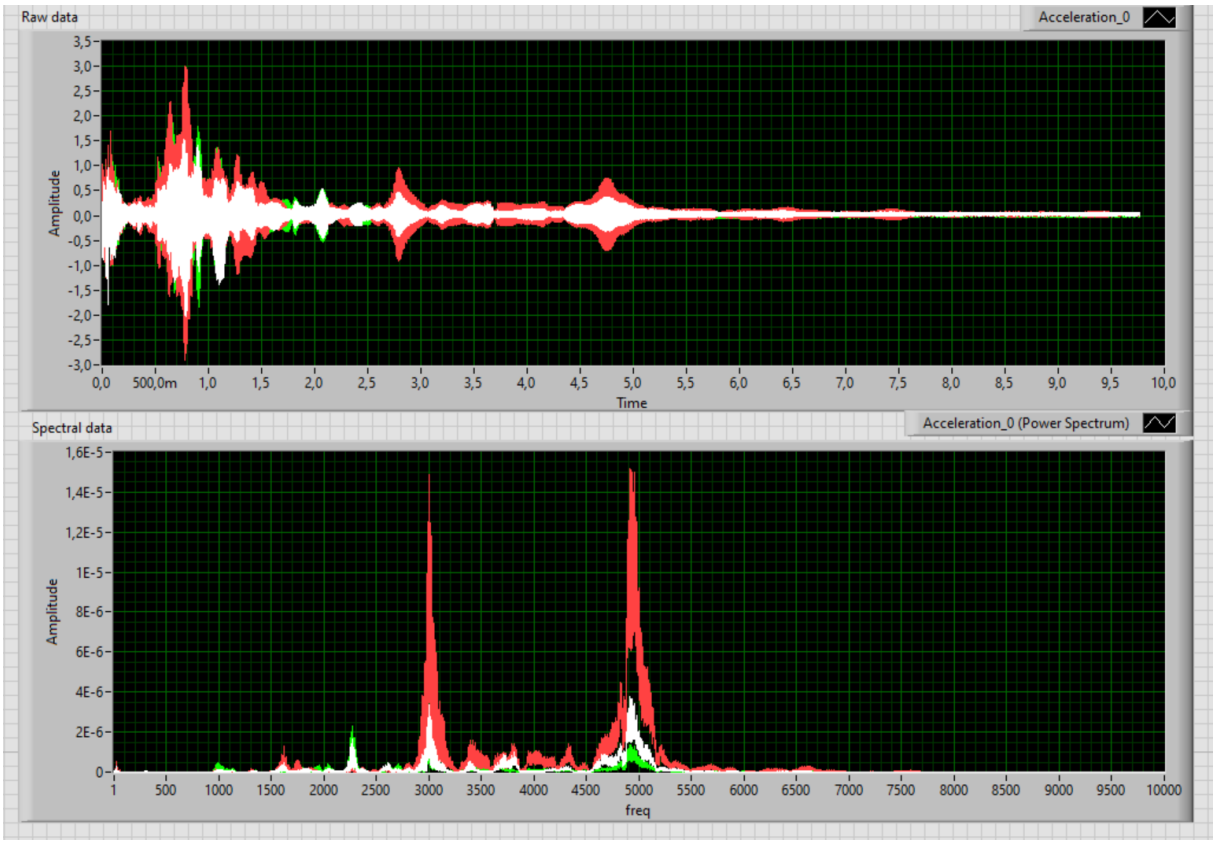

Figure 55. Raw and Spectral plot for the first set 1 Hz to 10 kHz from LabView number 1

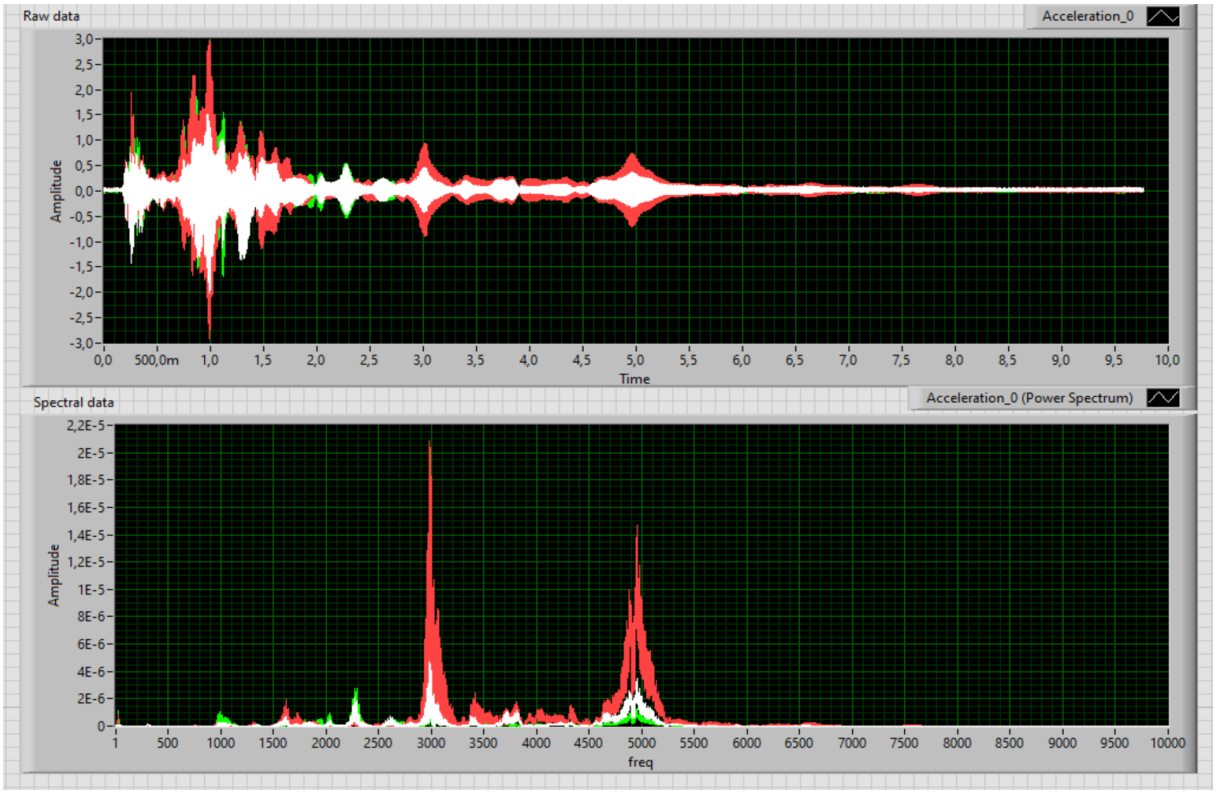

Figure 56. Raw and Spectral plot for the first set 1 Hz to 10 kHz from LabView number 2

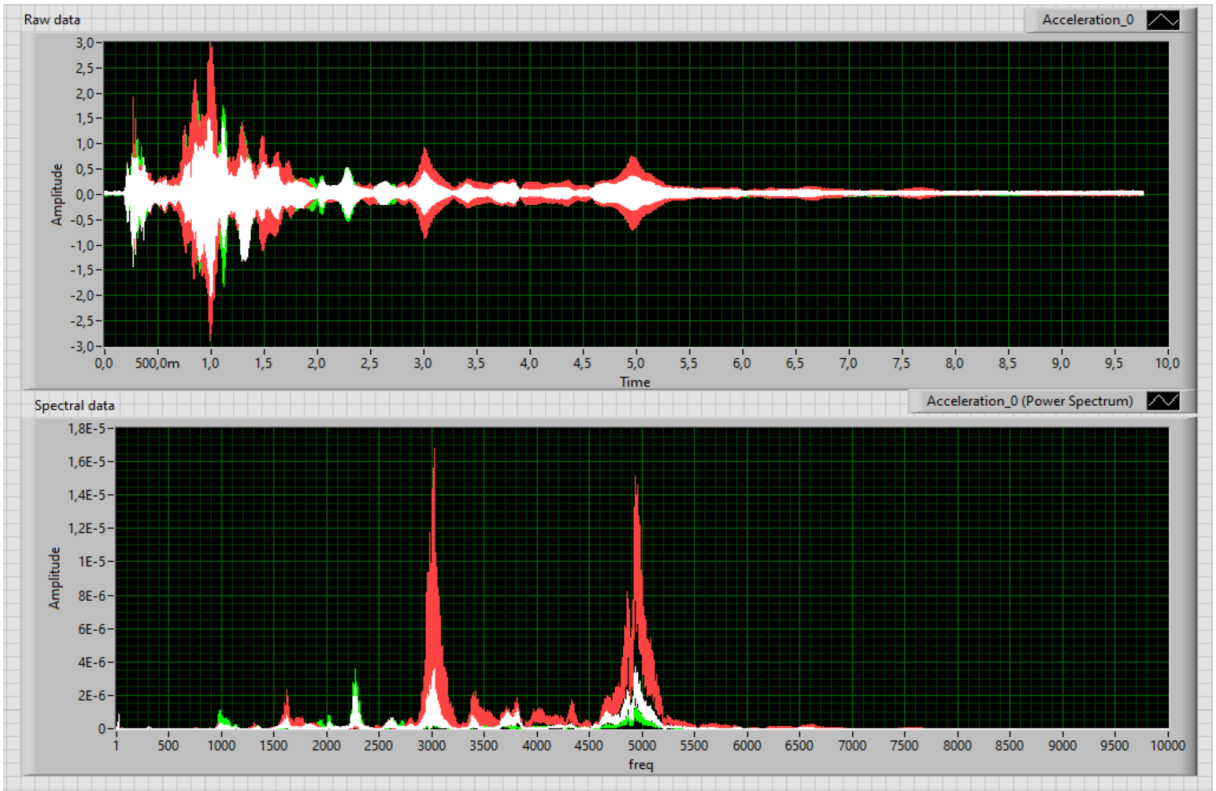

Figure 57. Raw and Spectral plot for the first set 1 Hz to 10 kHz from LabView number 3

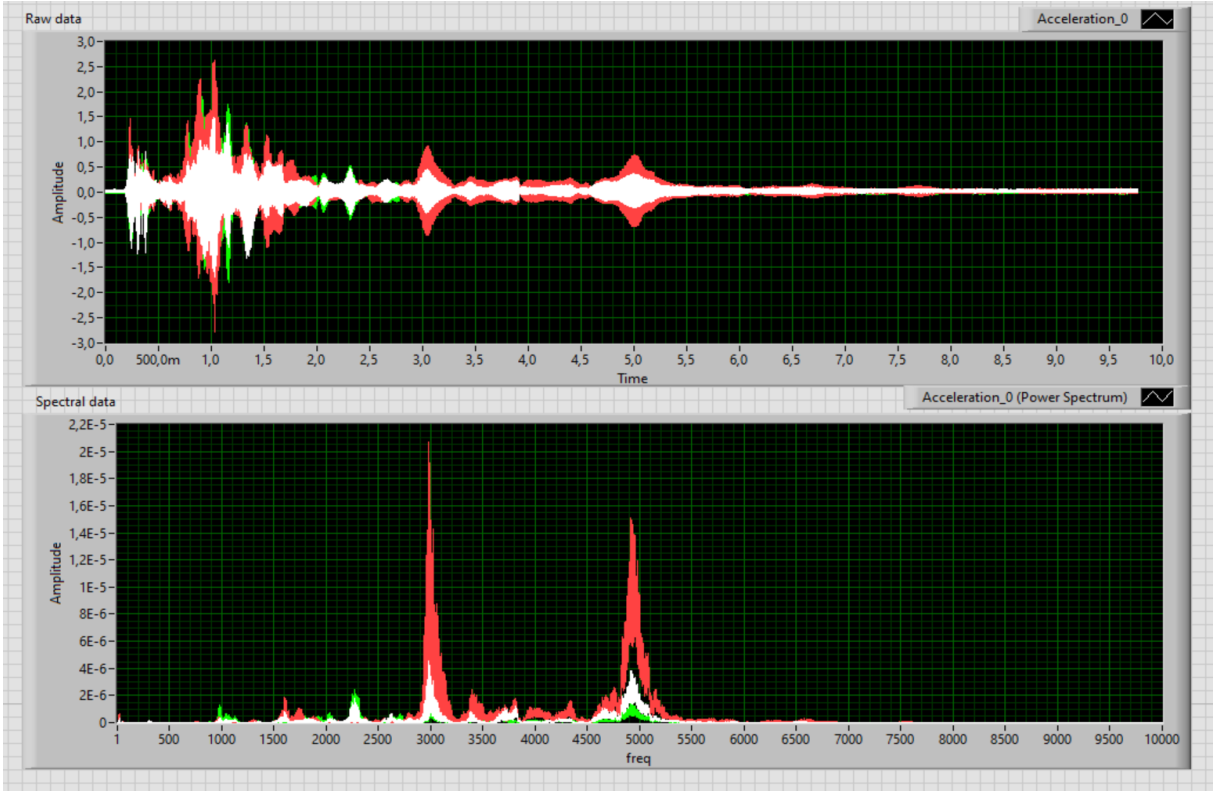

Figure 58. Raw and Spectral plot for the first set 1 Hz to 10 kHz from LabView number 4

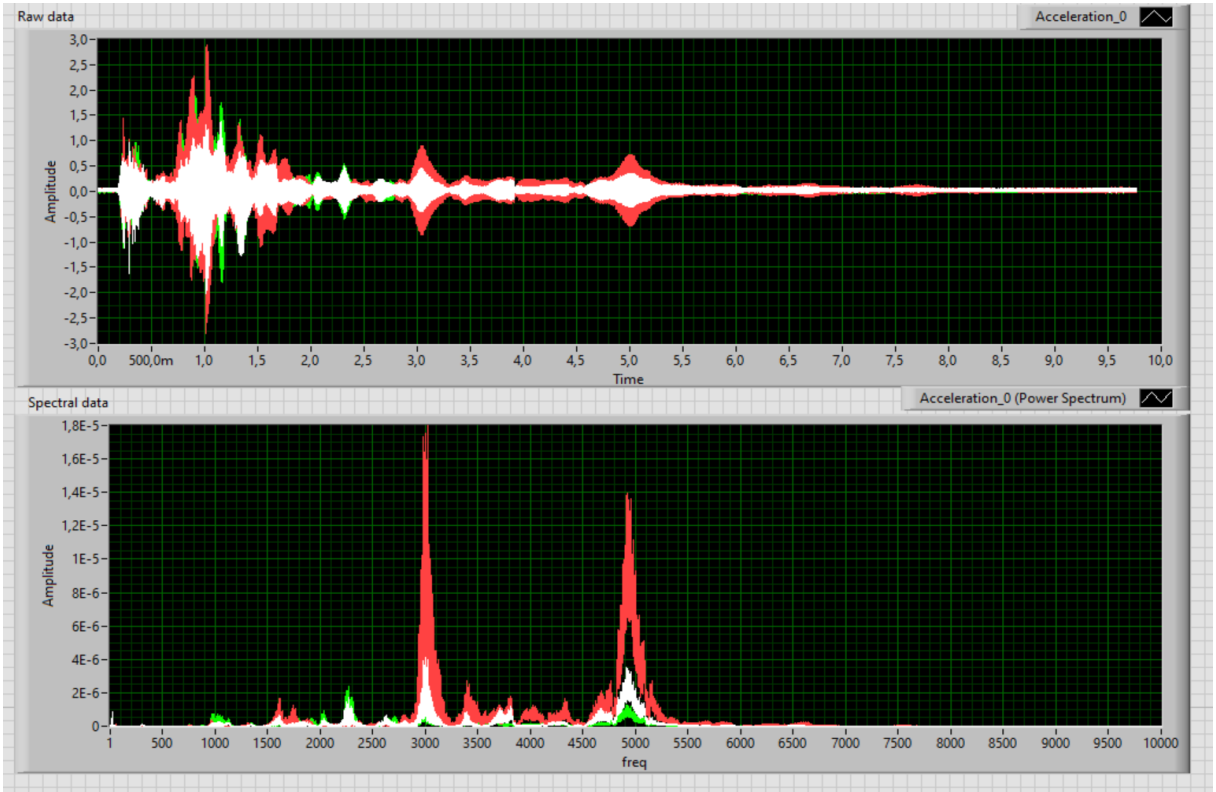

Figure 59. Raw and Spectral plot for the first set 1 Hz to 10 kHz from LabView number 5

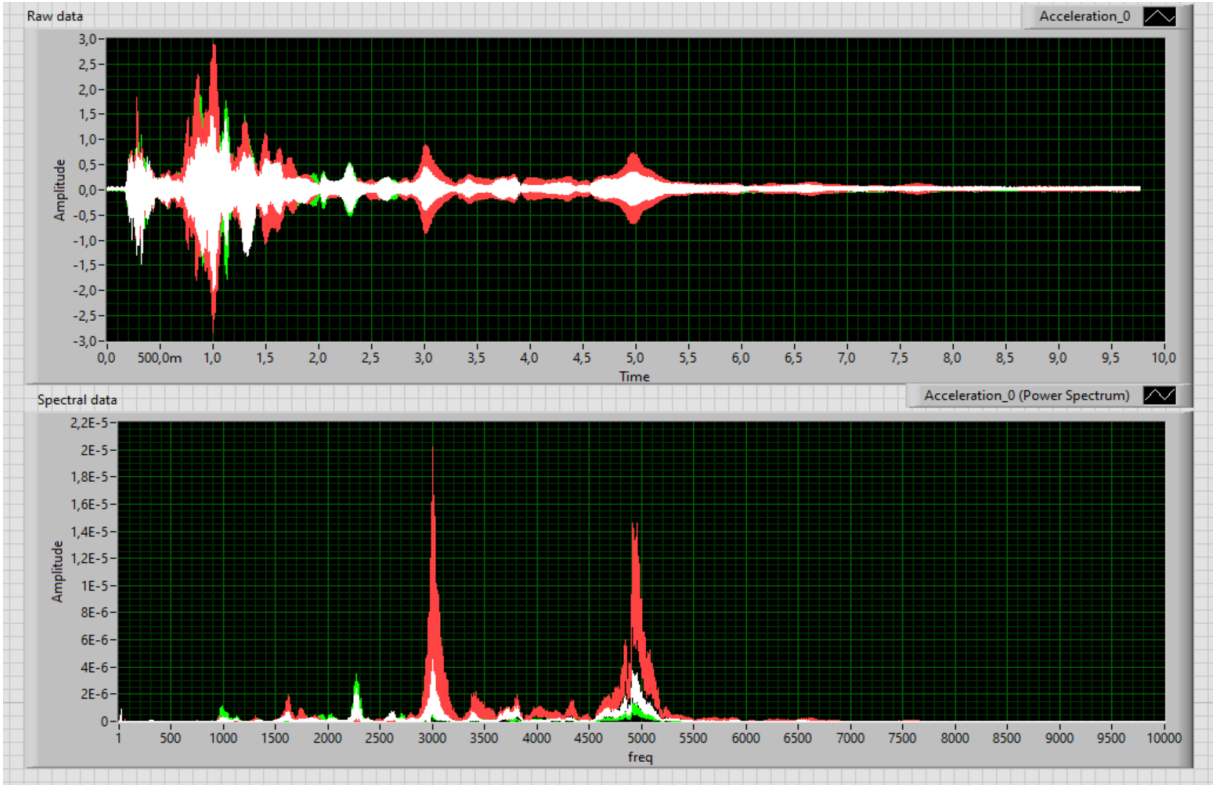

Figure 60. Raw and Spectral plot for the first set 1 Hz to 10 kHz from LabView number 6

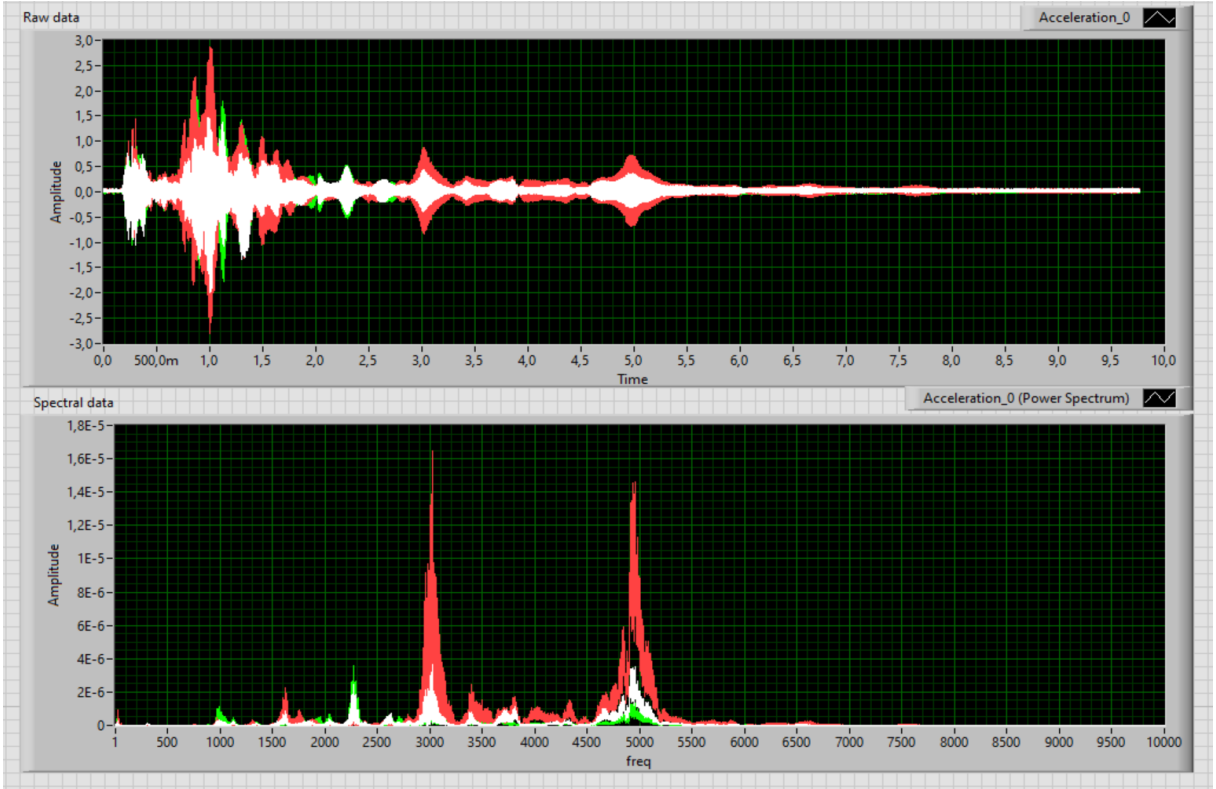

Figure 61. Raw and Spectral plot for the first set 1 Hz to 10 kHz from LabView number 7

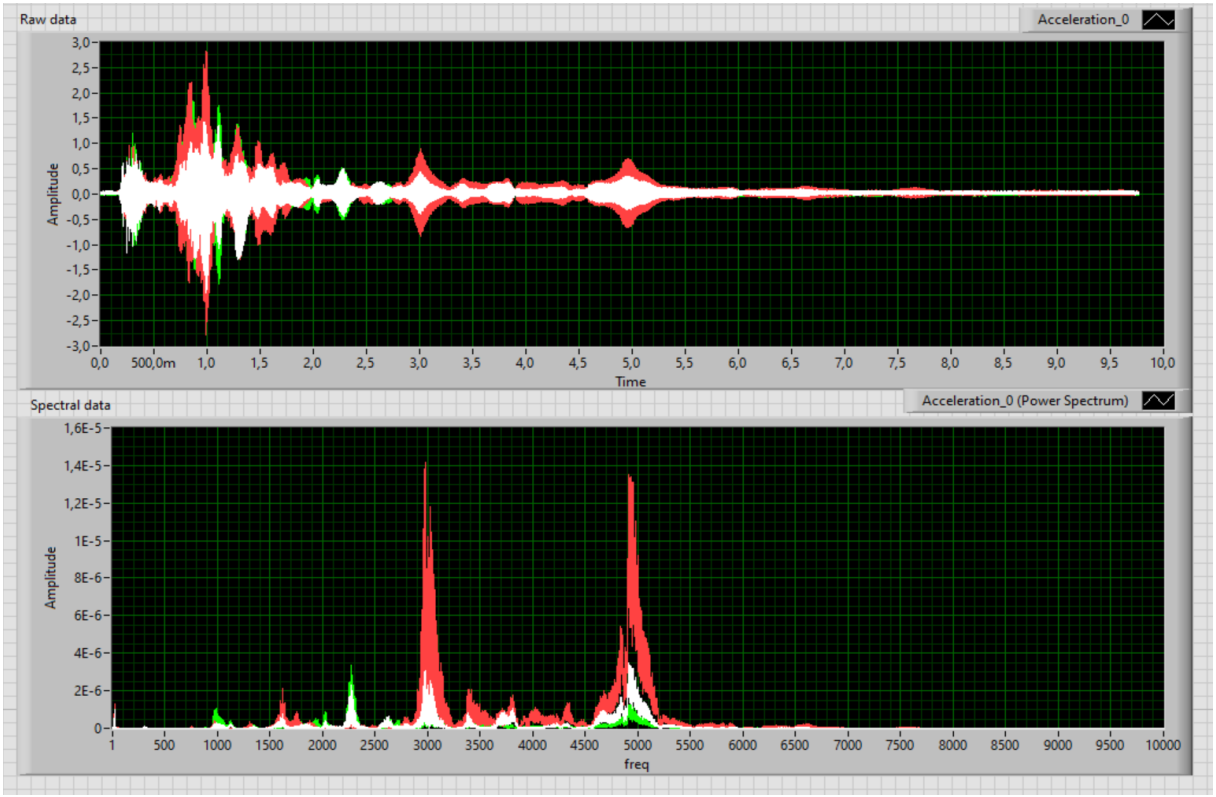

Figure 62. Raw and Spectral plot for the first set 1 Hz to 10 kHz from LabView number 8

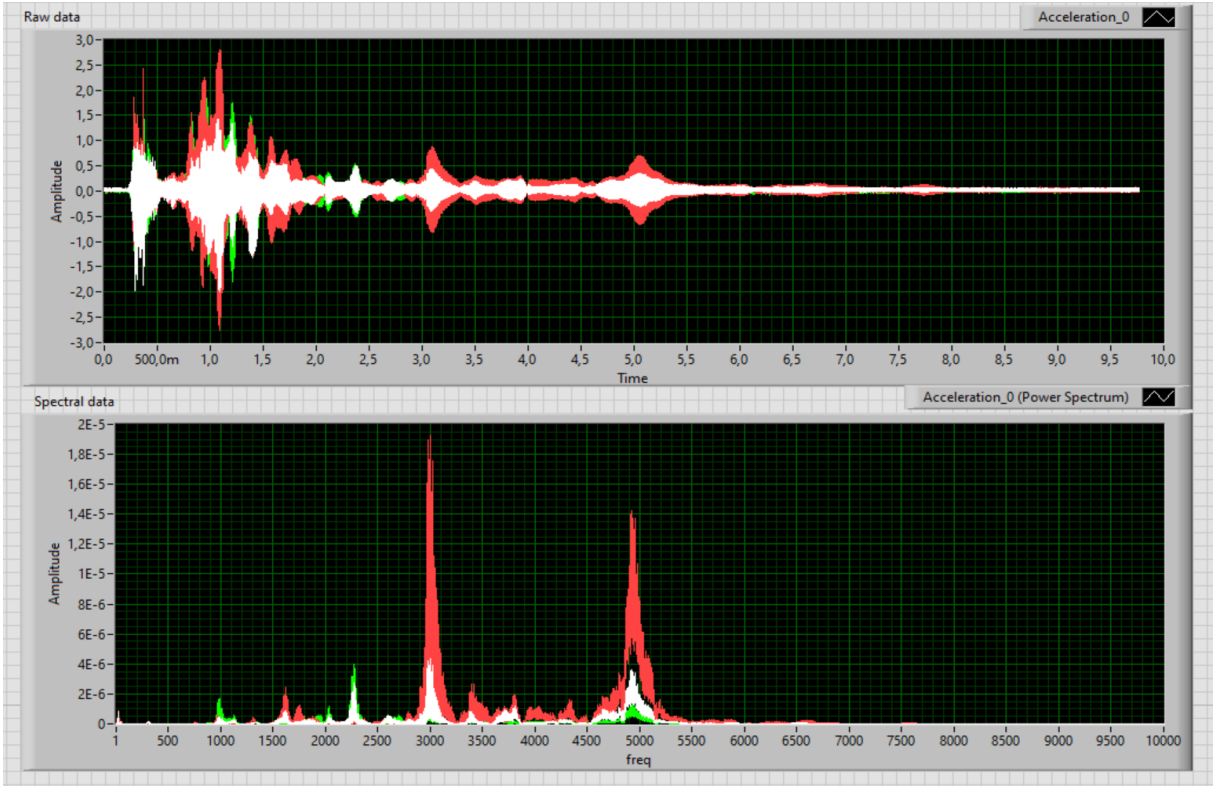

Figure 63. Raw and Spectral plot for the first set 1 Hz to 10 kHz from LabView number 9

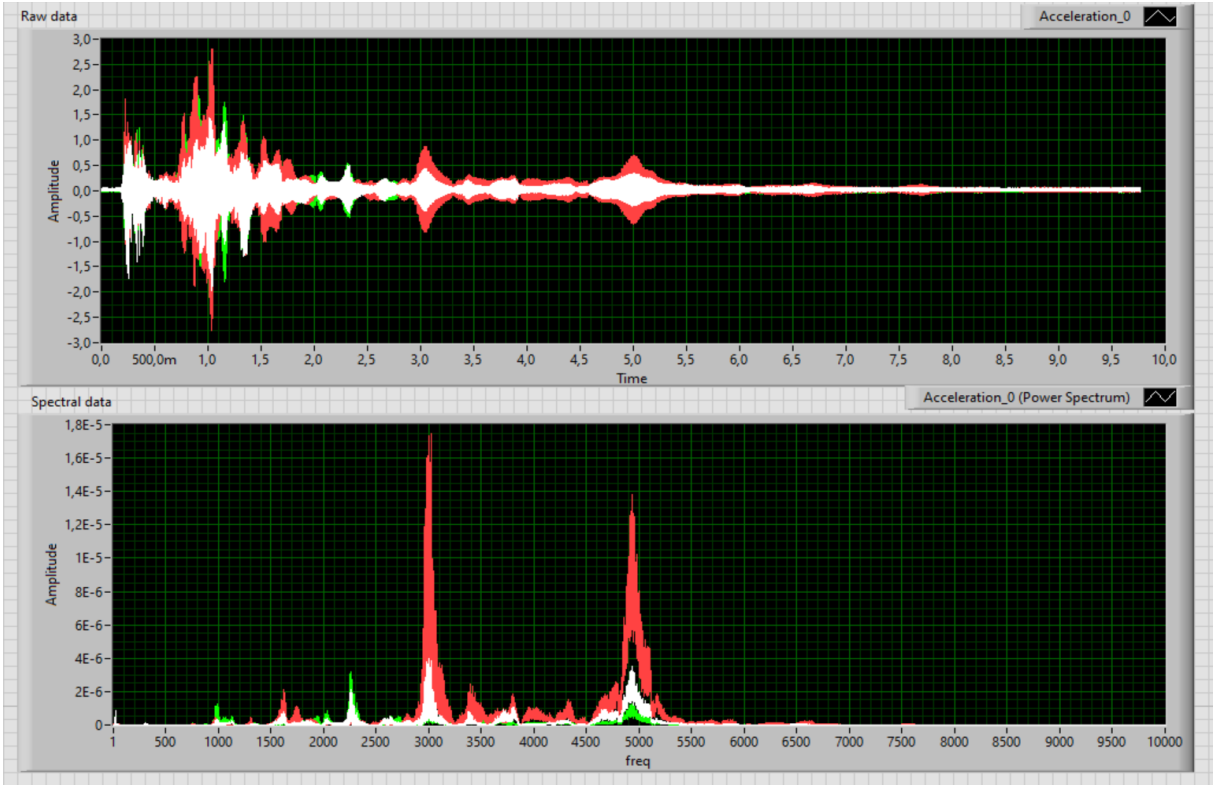

Figure 64. Raw and Spectral plot for the first set 1 Hz to 10 kHz from LabView number 10

Figure 65. Raw and Spectral plot for second set 20 kHz to 10 kHz from LabView number 1

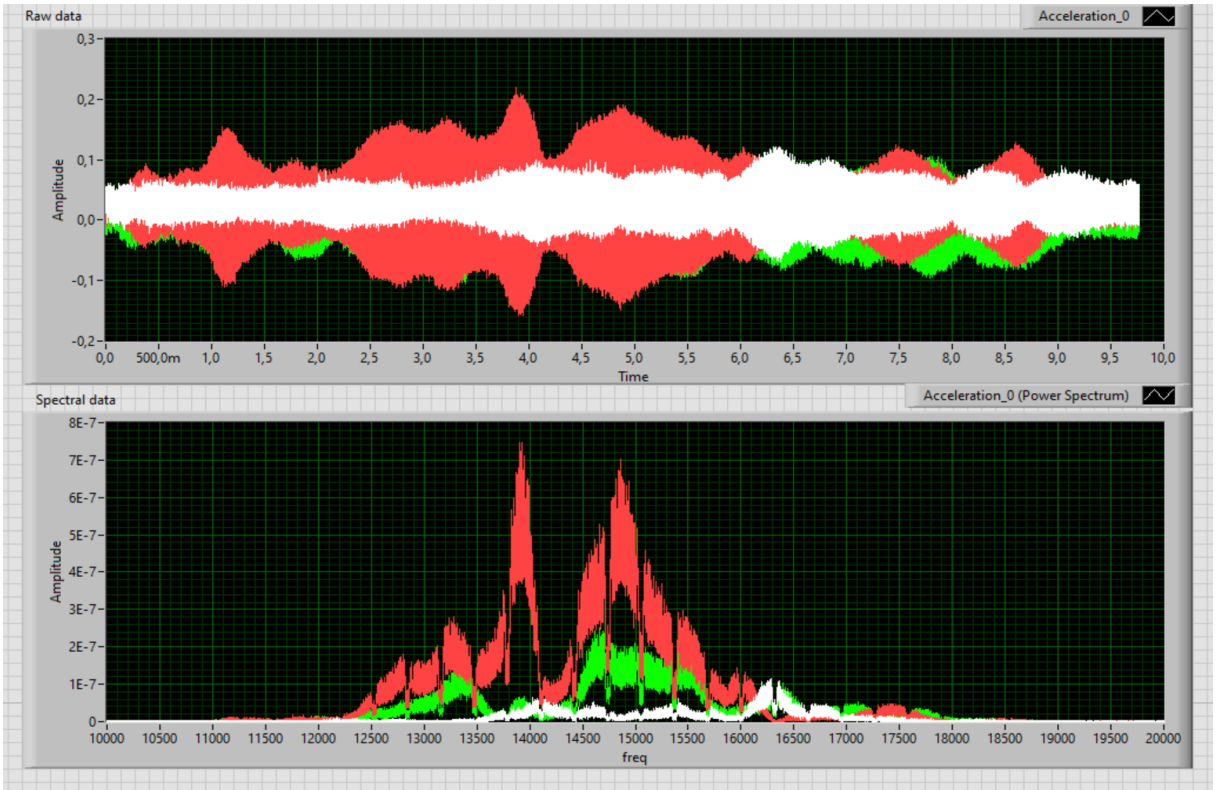

Figure 66. Raw and Spectral plot for second set 20 kHz to 10 kHz from LabView number 2

Figure 67. Raw and Spectral plot for second set 20 kHz to 10 kHz from LabView number 3

Figure 68. Raw and Spectral plot for second set 20 kHz to 10 kHz from LabView number 4

Figure 69. Raw and Spectral plot for second set 20 kHz to 10 kHz from LabView number 5

Figure 70. Raw and Spectral plot for second set 20 kHz to 10 kHz from LabView number 6

Figure 71. Raw and Spectral plot for second set 20 kHz to 10 kHz from LabView number 7

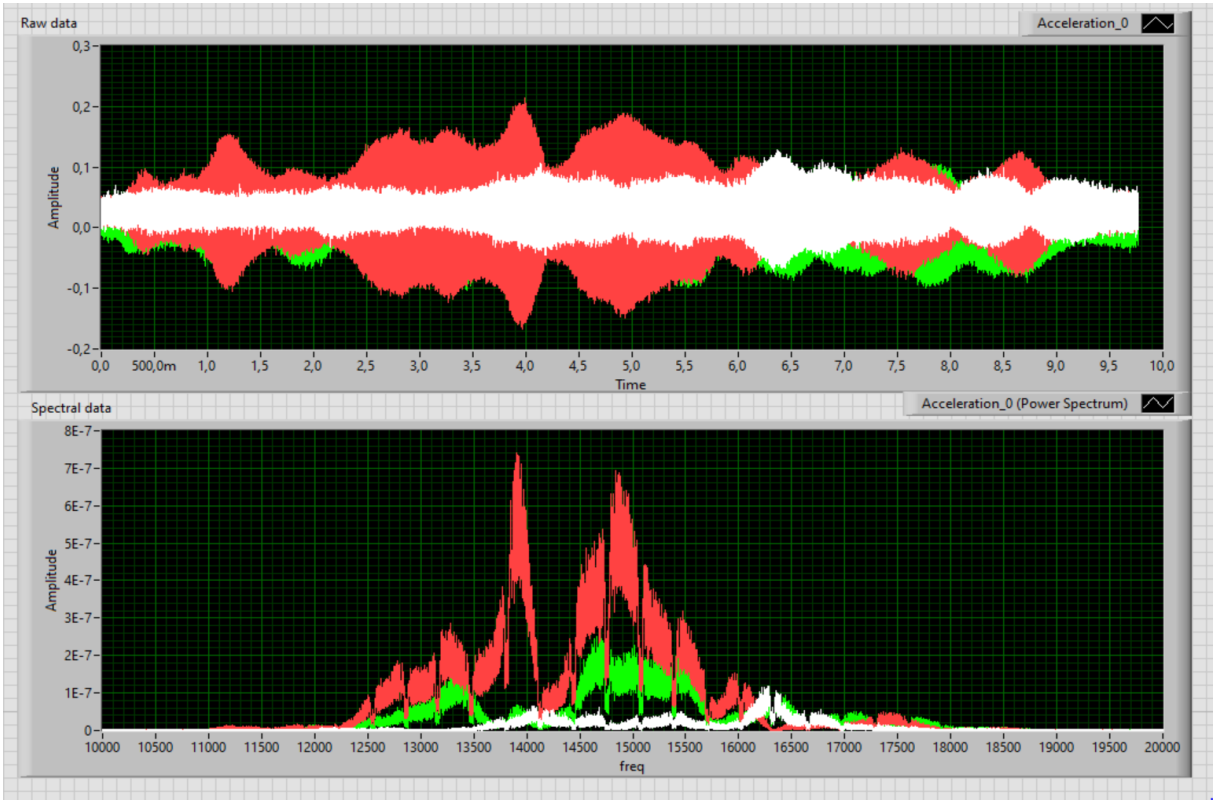

Figure 72. Raw and Spectral plot for second set 20 kHz to 10 kHz from LabView number 8

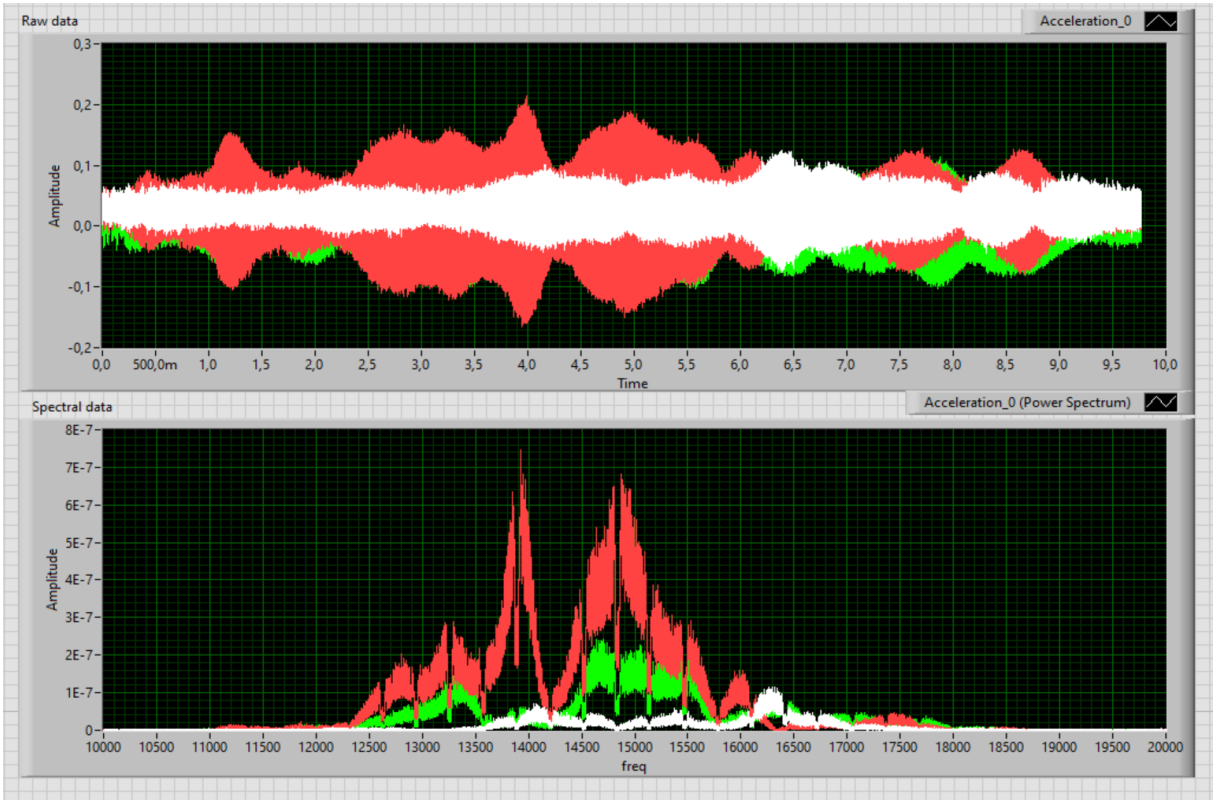

Figure 73. Raw and Spectral plot for second set 20 kHz to 10 kHz from LabView number 9

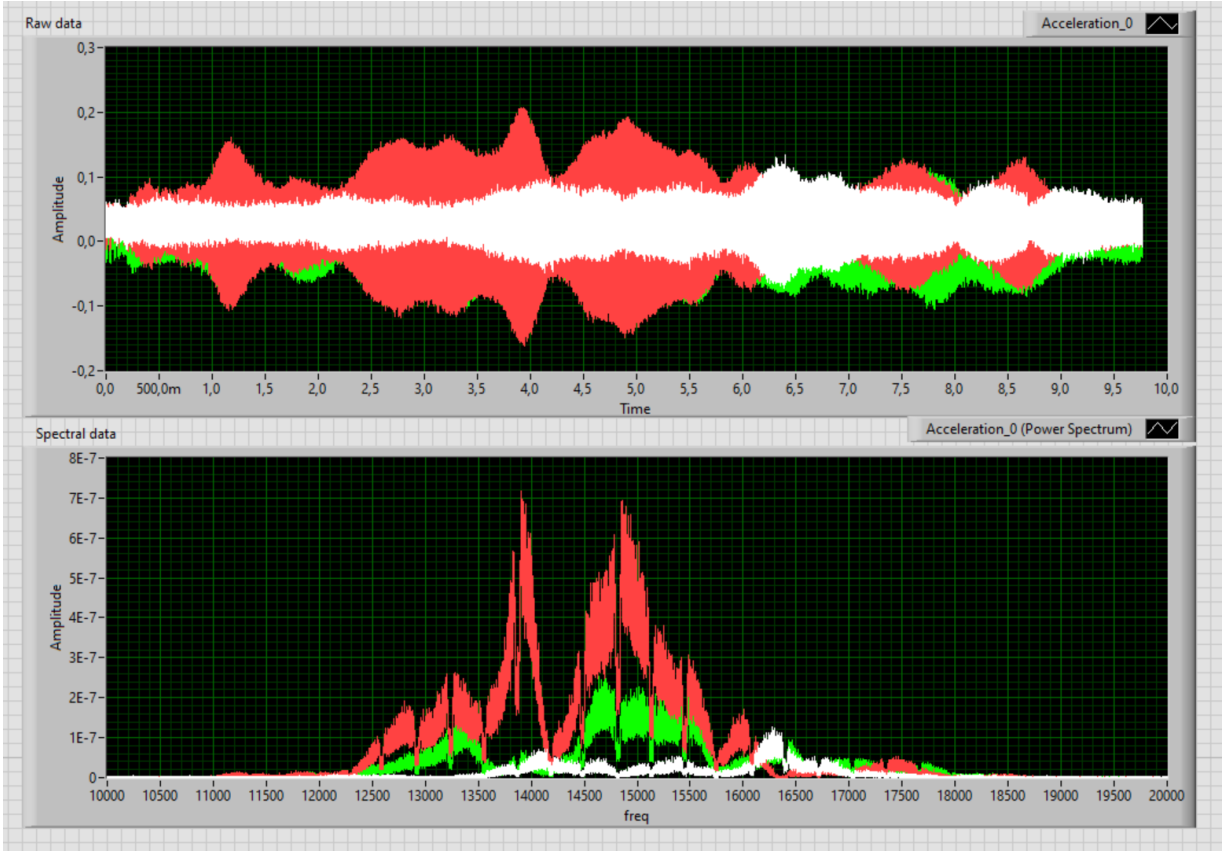

Figure 74. Raw and Spectral plot for second set 20 kHz to 10 kHz from LabView number 10

Data from the Raw signal number 8 is chosen to be analyzed and compared to the results obtained in Ansys 2017, although all signals are pretty similar, number 8 has the closest frequencies to a closed value, in this case to 14000 and 15000 Hz, the data taken from 1Hz to 10kHz is not taken into consideration as Ansys doesn't show any modes for this frequency ranges. In order to filter this signal chosen, the code found in the Annexed 6.3 is used. The plot for each acceleration axis with no filter can be seen in figure 75, and the filtered signal can be seen in the next figure 77. With the filtered signal, a double integration to obtain displacement is performed using the MATLAB code found in the Annexed 6.4, the plot for the displacement for each axis caused by the BC headphones is seen in figure 77. Finally, a plot amplitude vs frequency of the displacement using FFT for each axis is made using the same code, here it we observe the dominant frequencies within this range, figure 78.

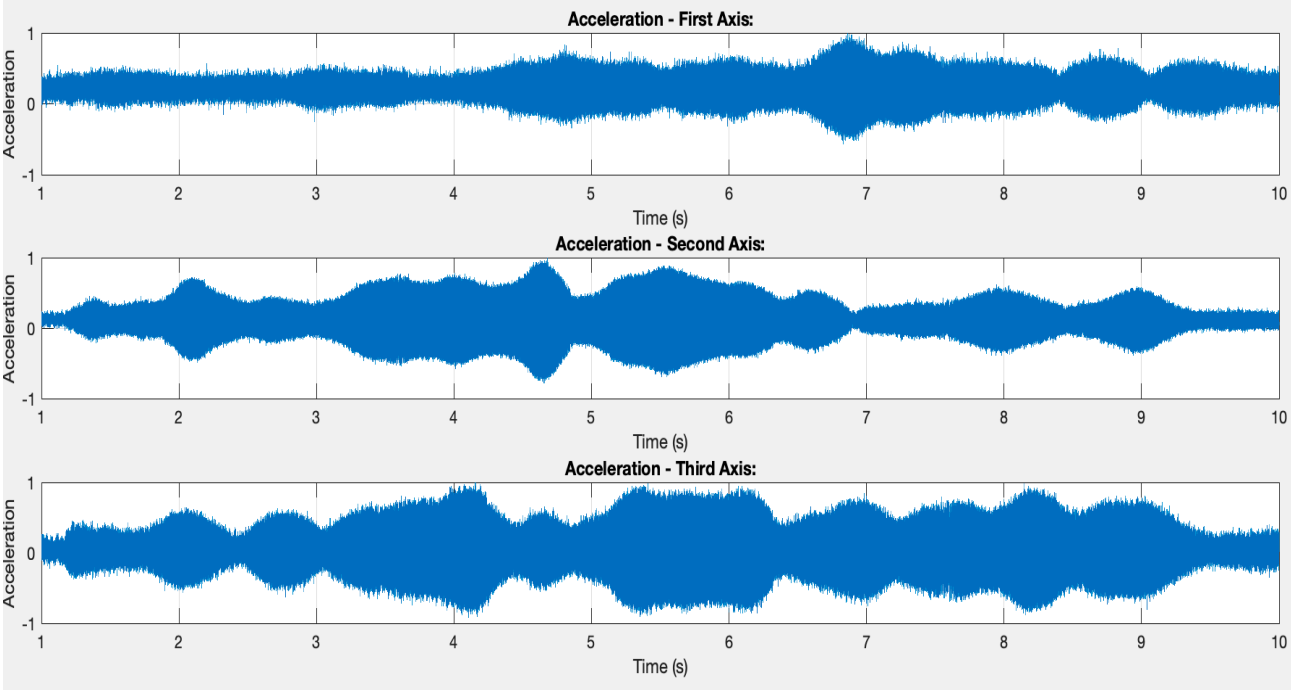

Figure 75. Raw acceleration signal for each axis plotted using MATLAB

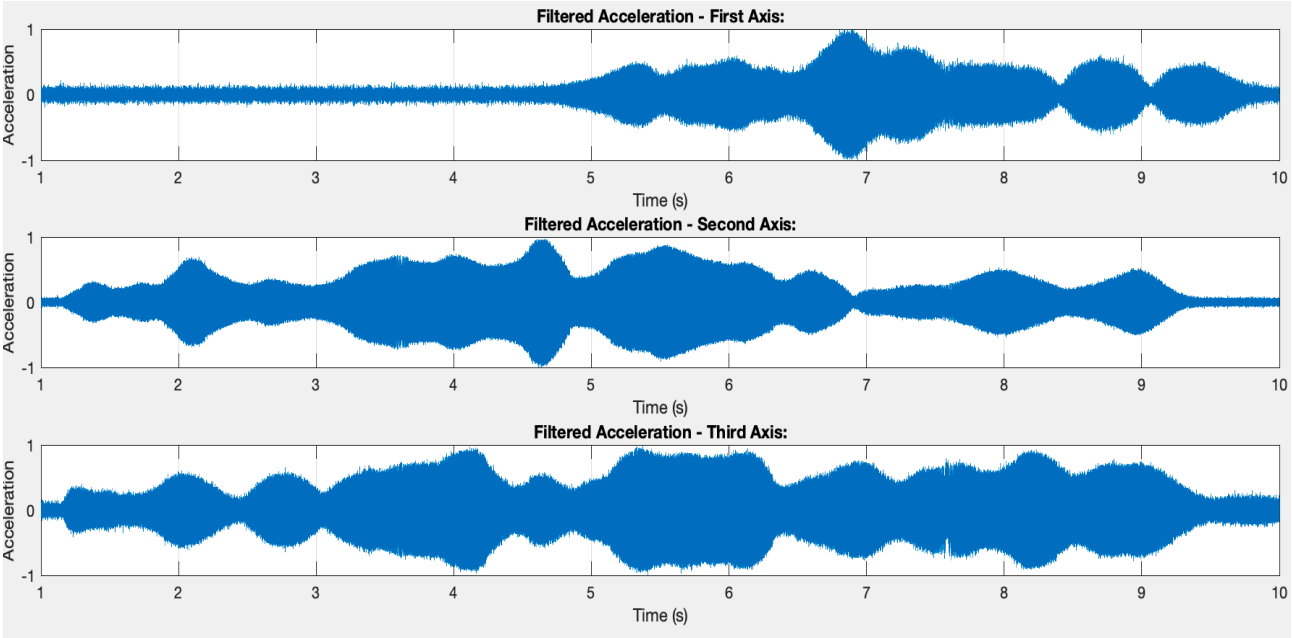

Figure 76. Filtered acceleration signal for each axis plotted using MATLAB

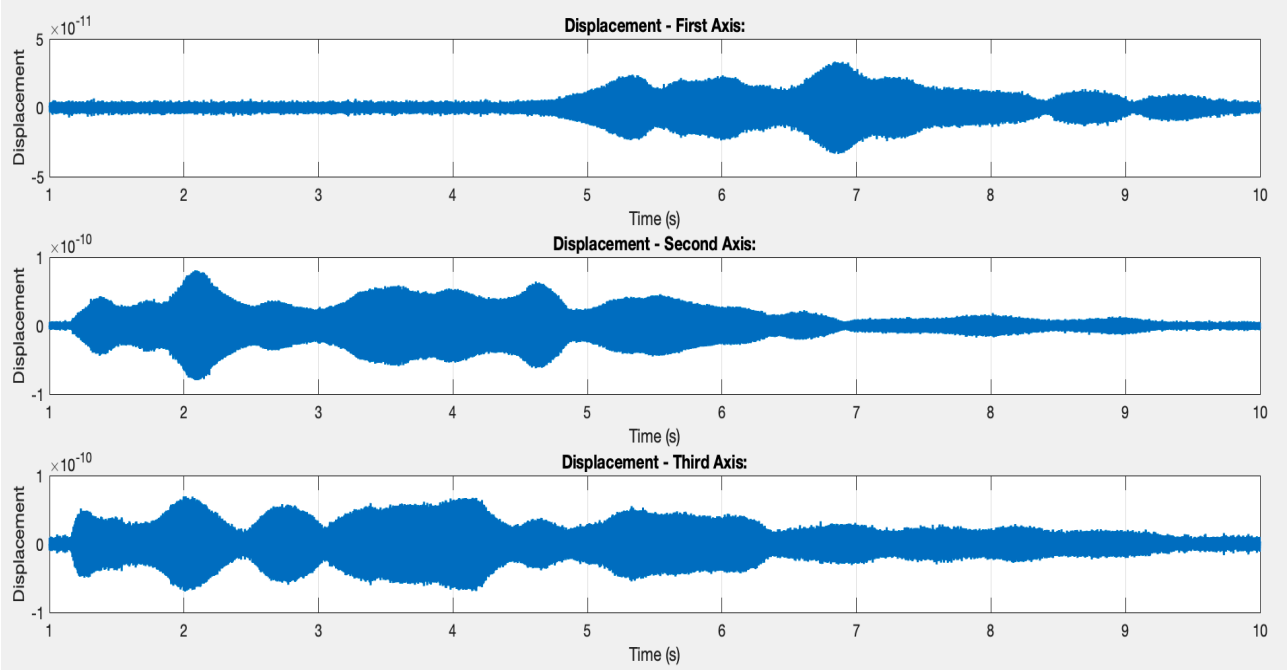

Figure 77. Displacement caused by the BC headphones for each axis plotted using MATLAB

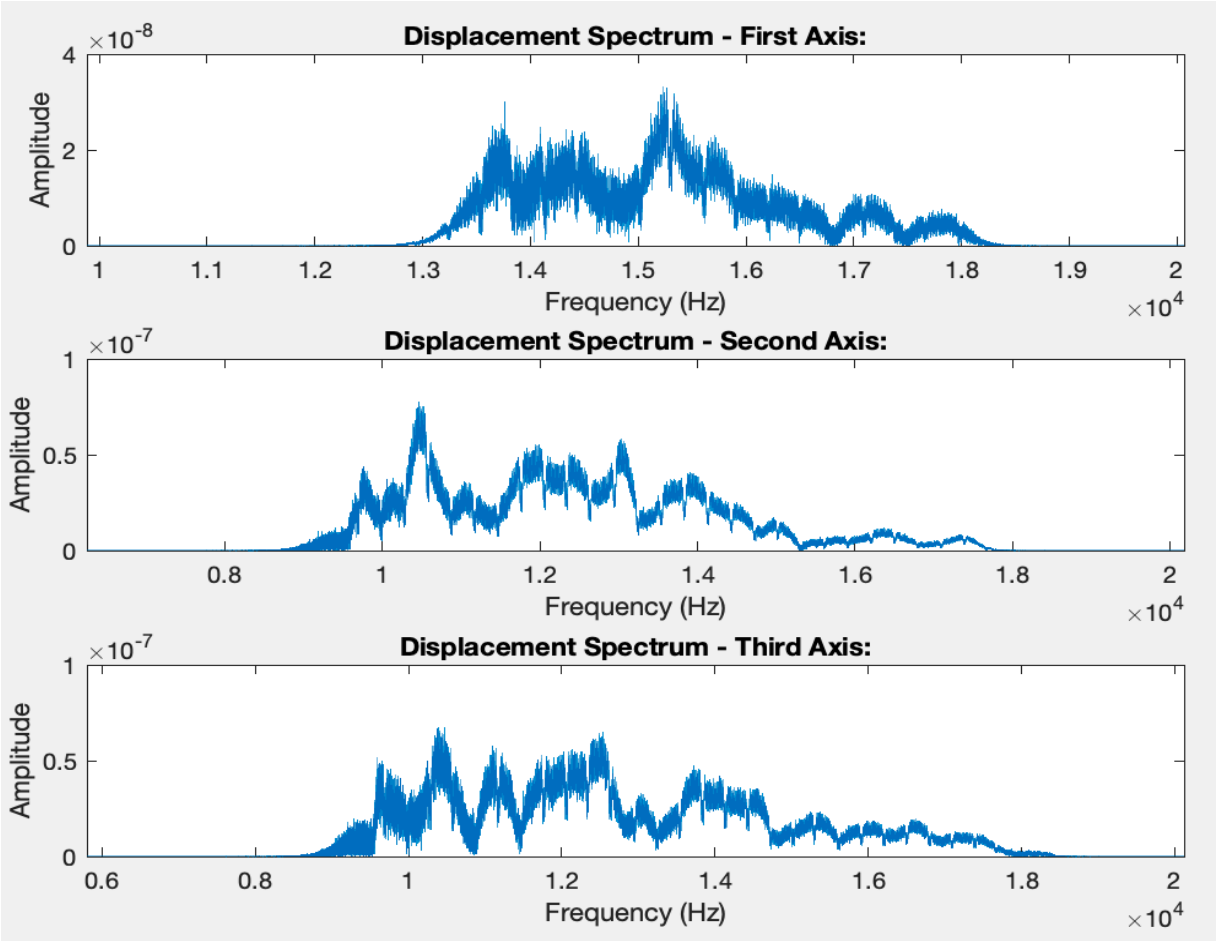

Figure 78. Displacement Spectrum for each axis plotted using MATLAB

Finally, comparing both results, the ones obtained in Ansys, which be theorical and the ones obtained using the real temporal bone in one single plot will show that the frequency margin is relatively close. Taking in consideration that the frequency peaks where the bone has its natural frequencies where it could come into resonance are similar frequency values between both plots, figure 79, 80 and 81.

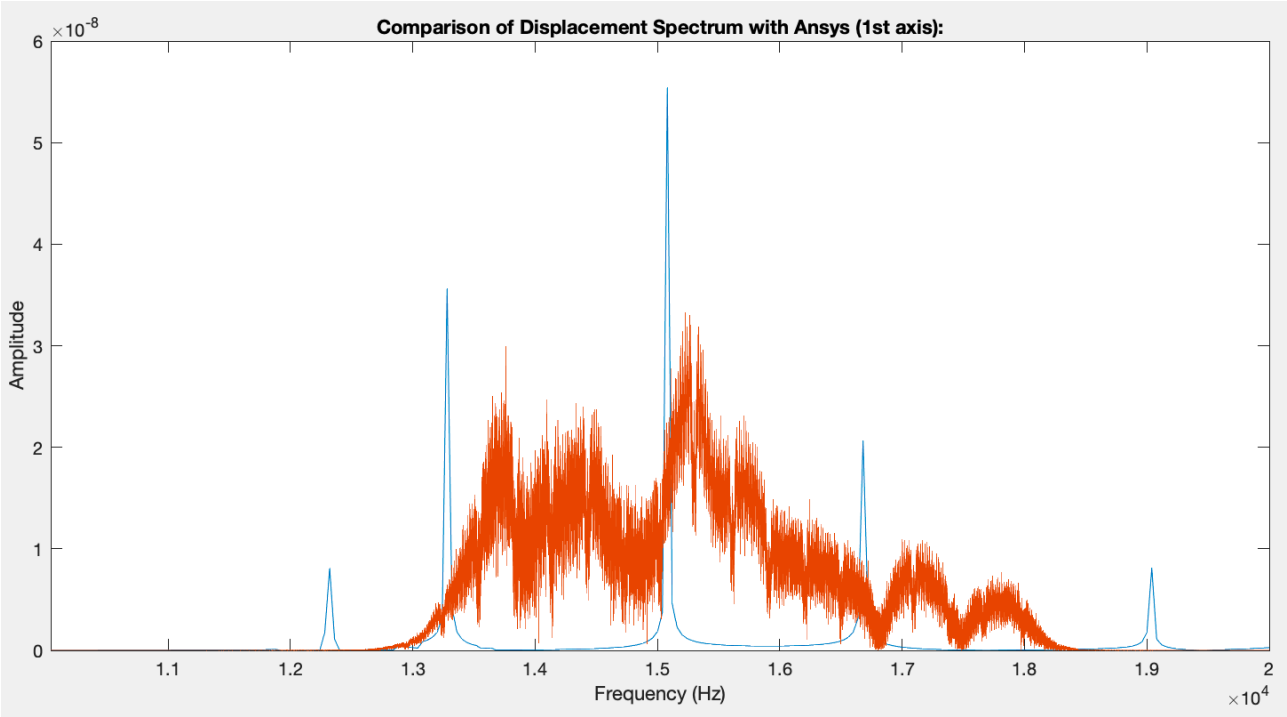

Figure 79. Comparison of Displacement Spectrum between the real bone test and Ansys FE first axis

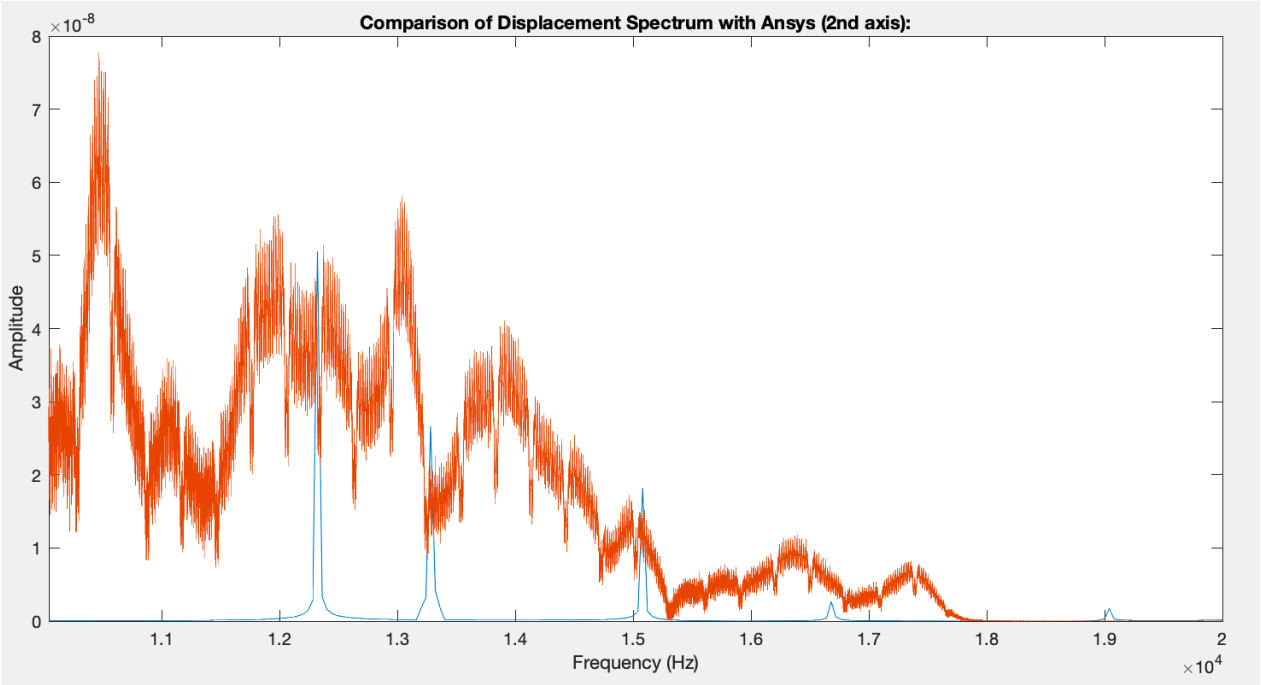

Figure 80. Comparison of Displacement Spectrum between the real bone test and Ansys FE second axis

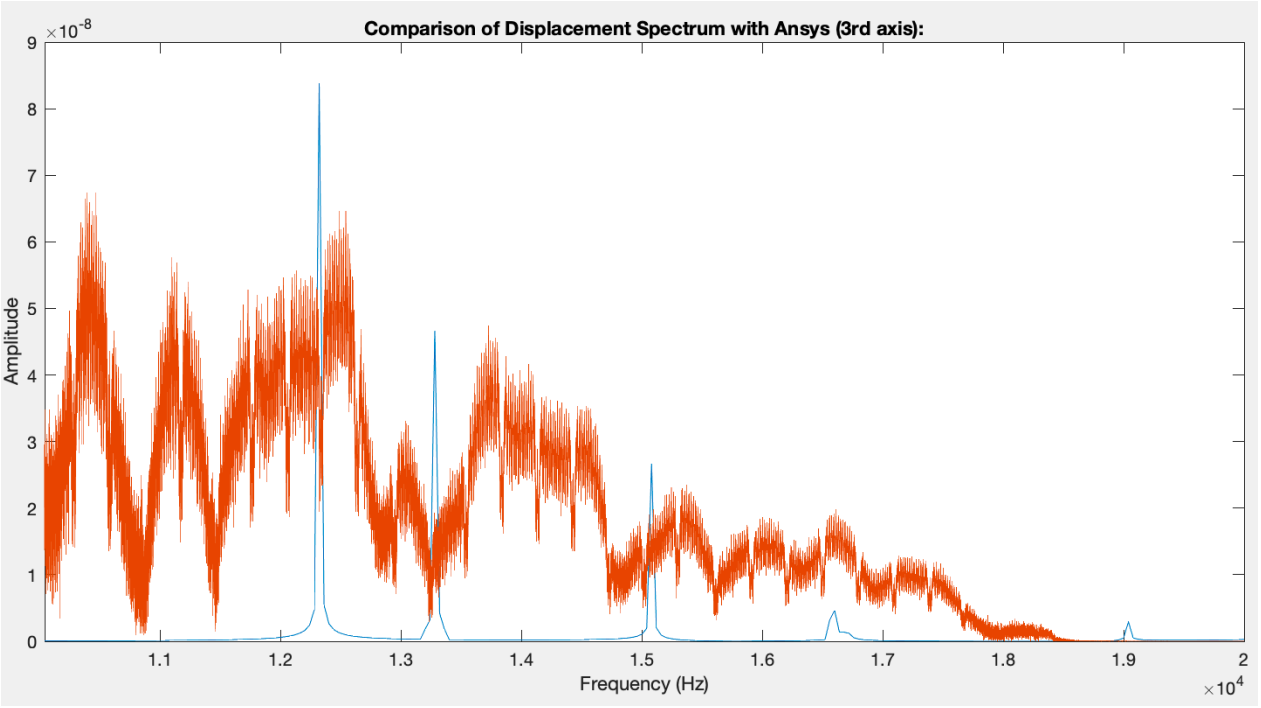

Figure 81. Comparison of Displacement Spectrum between the real bone test and Ansys FE third axis

4. DISCUSSION

The results shown in Section 3 are a comparison between both solution methods, the first one was obtained using Ansys 2017 Student Edition, where the 3D model of the temporal bone was analyzed with a pressure force of a 1.8 centimeters within a range of 10 kHz to 20kHz, and for the real bone testing, using BC headphones the same principal idea was applied using the same range of frequencies and having the 1.8 cm transducer apply a pressure force on squamous part of the bone. As seen in the figures 79, 80 and 81, for the plots, the frequency peaks for all the axis are pretty similar and lie on the same range. For all the data taken for both methods, the pressure force in conjunction with the frequency applied is producing similar displacement amplitude, which is plotting the nodal tracking point using Ansys and the triaxial accelerometer in the real bone testing, from the original position to a maximum displacement of $6e^{-8}$ meters for the first axis, 8 e^{-8} meters for the second and 9 e^{-8} meters for the third, which equals to a nanometric displacement in all axis. This is correct, as the effect the BC headphones have over the bone is imperceptible between these range of frequencies. Is important to note that Ansys is bypassing low frequencies of the first range set, applied to the 3D model of the bone, as it is obtaining vibrational modes after 10kHz, being the first vibrational mode at 12309 Hz which is in the second set of frequency range. This modal analysis results are important as the software is showing the resonance frequencies of the geometry, this correspond to the natural frequencies at which if the model is excited can be destructive or dangerous to itself. So, as the signal range applied using the Harmonic Response, which is simulating the effect of the BC headphones, it goes thru these frequencies and the temporal bone model in Ansys will react to this frequency range causing a deformation and a displacement of it shape. Certainly, this force applied to it is so minimal and by the constrains the model has by being attached virtually to the bones surrounding it, the displacement is caused is, as stated before, nanometric.

Comparing these results to the ones obtained in the study by Kim, et al (2014), results are similar in the amplitude domain and the displacement caused is also nanometric, as seen in the figure 7, and also where the peaks generated are in the frequency range from 10 kHz to 20 kHz. Even though the material used in Kim's study is polyurethane, apparently the vibrational modes will occur in the same frequency range as the one in this study. The acceleration plot showed in Kim's differ as it was extracted from a FEM software and not from a real test as the one done in this study. The BC headphones or an external vibratory system as observed in these results tend to generate vibrational modes from the applied geometries in a range from 10 to 20 kHz, this could be happening because these frequencies will be harmful for a thin layer of bone or polyurethane if the geometries are exposed for a long period of time what could be generating fissures in critical points, in the case of the temporal bone, the most critical portion is the squamous area where the section is no more thicker than 1.4 millimeters, of course this will only occur if the BC transducer is inducing vibration over the dry bone. Considering skin, muscular tissue and intercranial liquid the consequences of the BC transducer will be totally different as the vibrational modes will be much lower in range and may not have the same strong impact because of the vibrational attenuation that this layers over the bone could have.

Furthermore, in figure 77 the displacement spectrum produced using MATLAB from the real bone testing can be seen, these results show how the BC headphones caused a displacement and over what frequencies it has the higher displacement in each axis. This signal although it has been filtered has a lot of noise over it in my opinion, these must be caused by other vibrating pieces that composed the base model, or the triaxial accelerometer could have absorb vibration from the room where the test took place as it has a high sensitivity. Even though, the results display the desired frequencies and at which of them may the model get into resonance as they are comparable to the results from Ansys. Another problem which may cause

some variability on the results are the chosen mechanical properties for the temporal bone and its implementation on Ansys. As it was implied in the Section 2, bones are anisotropic materials, meaning its deformation will not occur in a similar way through all its axes, as it is directionally dependent. So, in order to gather information for these specific bones that was used for this test, it probably needed to be tested in bending and shear, and it was important to preserve the dry temporal bone in its best condition. To overcome this problem, in the literature I found several studies that have perform tests using cranial bones and more specifically temporal bones, so the mechanical properties of the bone used in Ansys is an isotropic material using the properties of the most critical part that is the squamous section of the temporal bone, which is also where the BC transducer lies down. The squamous has a low-density high porosity structure, so Ansys is analyzing the model as if all the bone has this property.

5. CONCLUSIONS

In figures 79, 80 and 81, both plots for each individual analysis can be seen. The generated plots are not similar as the one from Ansys is more of a theorical line while the one obtained using LabView got noise which plot a complex signal. In spite of this differences between both lines, these results have the same tendency and displacement peaks which shows where the vibrational modes from the natural frequencies are, which is one of the aims originally set before doing the tests. Concluding this research study, results can be compared using a FEM simulation using Ansys 2017 Student Edition and a real testing for the human dry temporal bone gathering data using a triaxial accelerometer, a DAQ, a data card and LabView 2018 Student Edition, but it is important to notice all the limitation and restrictions that using this software and also setting the parameters for testing will vary the desired results. Although the estimation of the work done using these methods are pretty similar, it should be important to use tested mechanical properties for the individual bone and also to reduce the variables of noise absorption by the accelerometers used for obtaining the data of the real tests.

It is important to keep researching about BC not only in the temporal bone, but also in all the cranial bones, as these could be developed into better devices like transducer or piezoelectric that can transmit audio frequencies in a more efficient ways having less attenuation in really low and high frequencies. BC devices have been already implemented for helping people with hearing aids, but a lot of work needs to be continuously made in order to enhance this new coming technology.

6. BIBLIOGRAPHIC REFERENCES

Stenfelt, S., and Goode, R. L. (2005). Bone-conducted sound: Physiological and clinical aspects. Otol. Neurotol. 26, 1245–1261.

Stenfelt, S. (2013) Bone Conduction and the Middle Ear. Acoust. Soc. Am. DOI: 10.1007/978-1-4614-6591-1_6

Stenfelt, S., Wild, T., Hato, N., and Goode, R. L. (2003). Factors contributing to bone conduction: The outer ear. J. Acoust. Soc. Am. 113, 902–913.

Dauman, R. (2013). Bone conduction: An explanation for this phenomenon comprising complex mechanisms., Eur. Ann. Otorhinolaryngol. Head Neck Dis., vol. 130, no. 4, pp. 209-213.

Sohmer, H. and Freeman, S. (2004). Further evidence for a fluid pathway during bone conduction auditory stimulation., Hear. Res., vol. 193, no. 1, pp. 105-0.

Ogiso, S., et al. (2014). Analysis of Sound Propagation in Human Head for Bone-Conduction Headphones Using Finite Element Method. IEEE 3rd Global Conference on Consumer Electronics. University of Tsukuba: Japan.

Tyler, D. (2009). Neuromodulation. Chapter 17 – Electrodes of the Neural Interface. Pp. 181-213. Extracted from: https://www.sciencedirect.com/science/article/pii/B9780123742483000185

Lowy, K. (1942). Cancellation of the Electrical Cochlear Response with Air and Bone Conduction. Journal of the Acoustical Society of America. pp. 156-158.

Sauren, A., Classens, M. (1993). Finite Element Modeling of Head Impact: The Second Decade. Proceeding of the International IRCOBI Conference on Biomechanics of Impacts.

Kim, N., Chang, Y., Stenfelt, S. (2014). A Three-Dimensional Finite-Element Model of a Human Dry Skull for Bone-Conduction Hearing. BioMed Research International. 2014. 1-9. 10.1155/2014/519429.

O'Brien, W., Liu, Y. (2005). Evaluation of Acoustic Propagation Paths into the Human Head. In New Direction for Improving Audio Effectiveness. pp. 15-24.

Henry, P., Letowski, T. (2007). Bone conduction: anatomy, physiology and communication. Aberdeen Proving Ground (MD): Army Research Laboratory (US).

Khetrapal, A. (2018). How Does the Ear Work? Anatomy of the ear. Taken from: https://www.news-medical.net/health/How-Does-the-Ear-Work.aspx

Encyclopedia Britannica. (n.d.). Skull. Anatomy. Taken from: https://www.britannica.com/science/skull

McBride, M., Letowski, T., Tran, P. (2006). Comparison of Bone Conduction Hearing Thresholds on Quiet and Noise Environments. The 4th Annual Meeting of the Society for Human Performance in Extreme Environments.

Jones, O. (2018). The temporal bone. Teach me anatomy. Taken from: https://teachmeanatomy.info/head/osteology/temporal-bone/

Peterson, J., Dechow, P. (2003). Material Properties of the Human Cranial Vault and Zygoma. Extracted from: https://anatomypubs.onlinelibrary.wiley.com/doi/pdf/10.1002/ar.a.10096

MathWorks. (2019). Buttord. Digital Filter Design. MATLAB Documentation. Extracted from: https://www.mathworks.com/help/signal/ref/buttord.html

MathWorks. (2019). Cumtrapz. Numerical Integration and Differentiation. MATLAB Documentation. Extracted from: https://www.mathworks.com/help/matlab/ref/cumtrapz.html?searchHighlight=cumtrapz&s_tid=doc_srchtitle

MathWorks. (2019). FFT. Fourier Analysis and Filtering. MATLAB Documentation. Extracted from: https://www.mathworks.com/help/matlab/ref/fft.html?lang=en

Cyprien. (2016). What is FEA modal analysis? Learn the basics about it. FEA Articles. FeaforAll. Extracted from: https://feaforall.com/what-modal-analysis-fea-basics/

Porschmann, C. (2000). Influences of Bone Conduction and Air Conduction on the Sound of One's Own Voice. Extracted from: https://www.ingentaconnect.com/content/dav/aaua/2000/00000086/00000006/art00018

7. ANNEXES

6.1. Photos from the Real Bone test

National Instruments DAQ and data cards

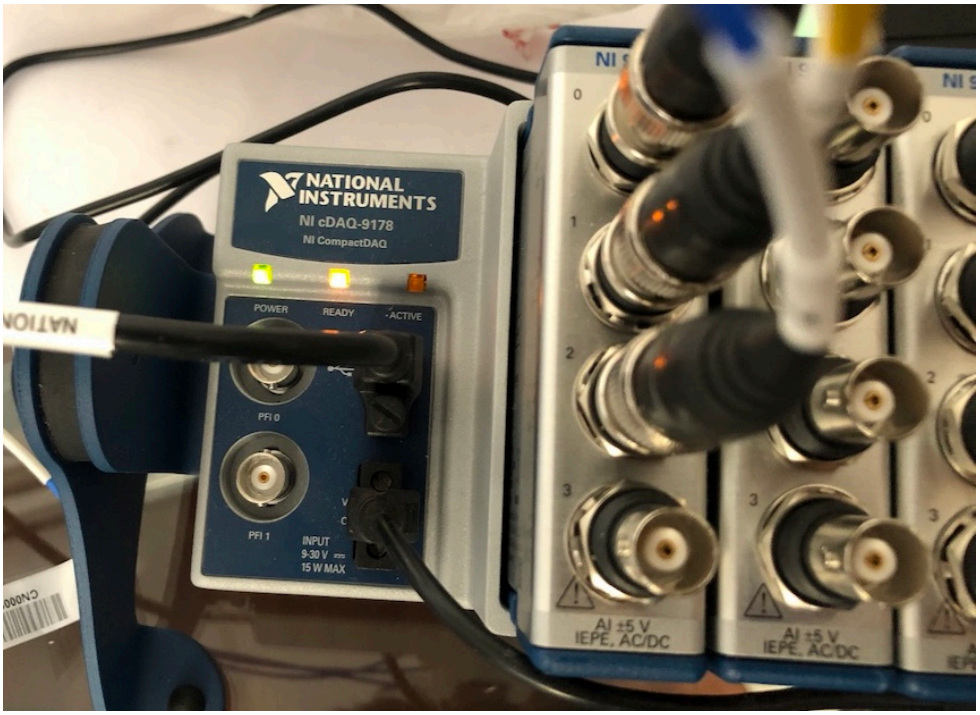

Set-up whit the 3D printed skull, real temporal bone, BC headphones and triaxial accelerometer

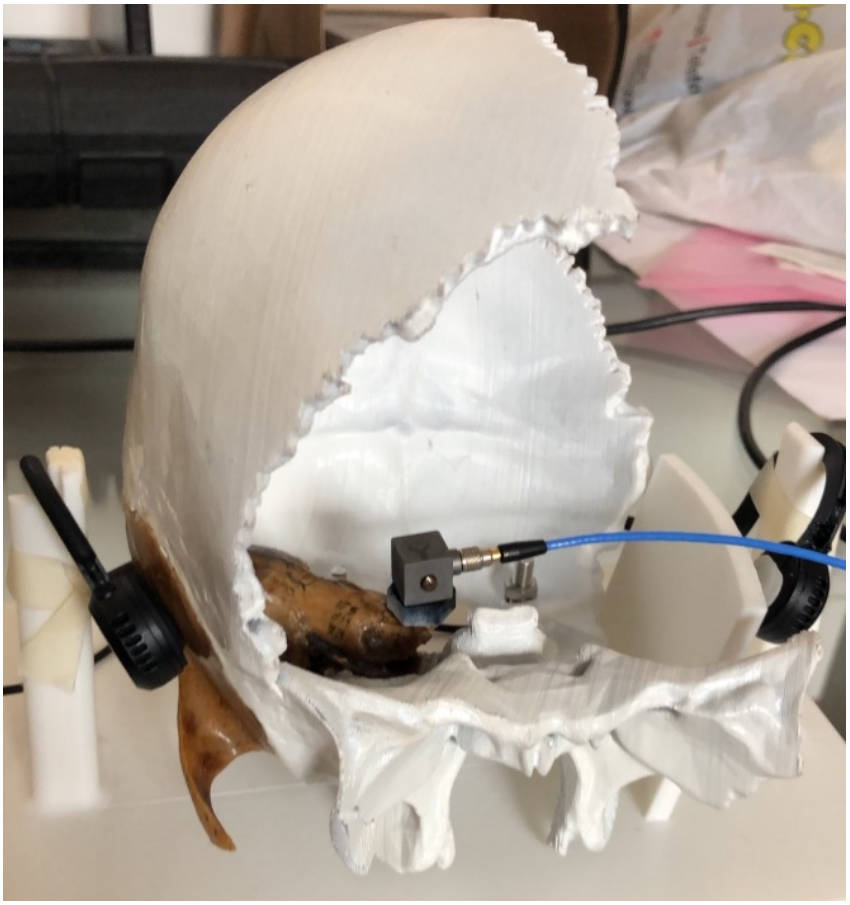

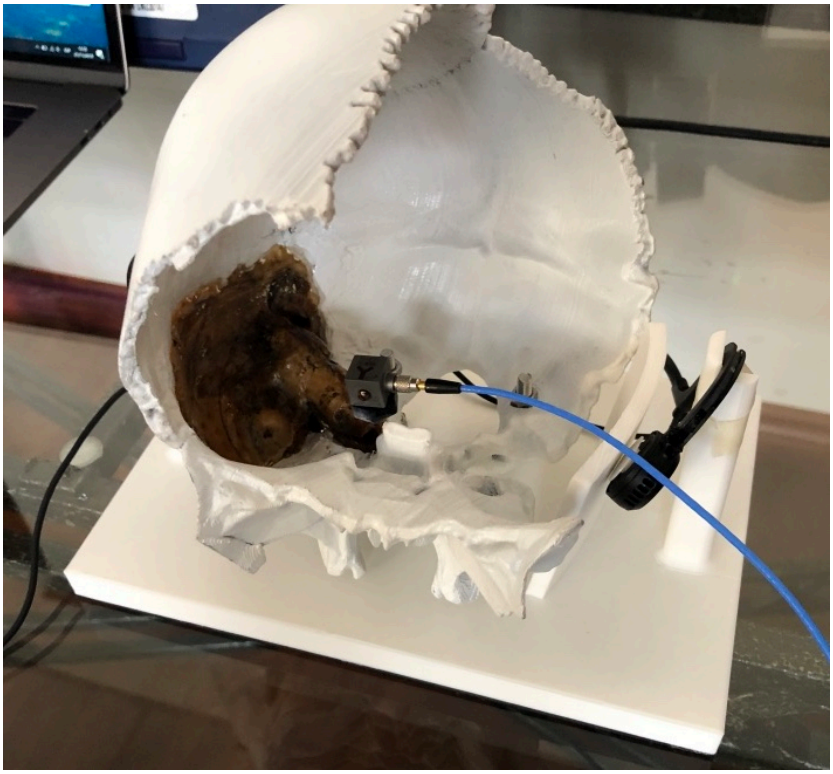

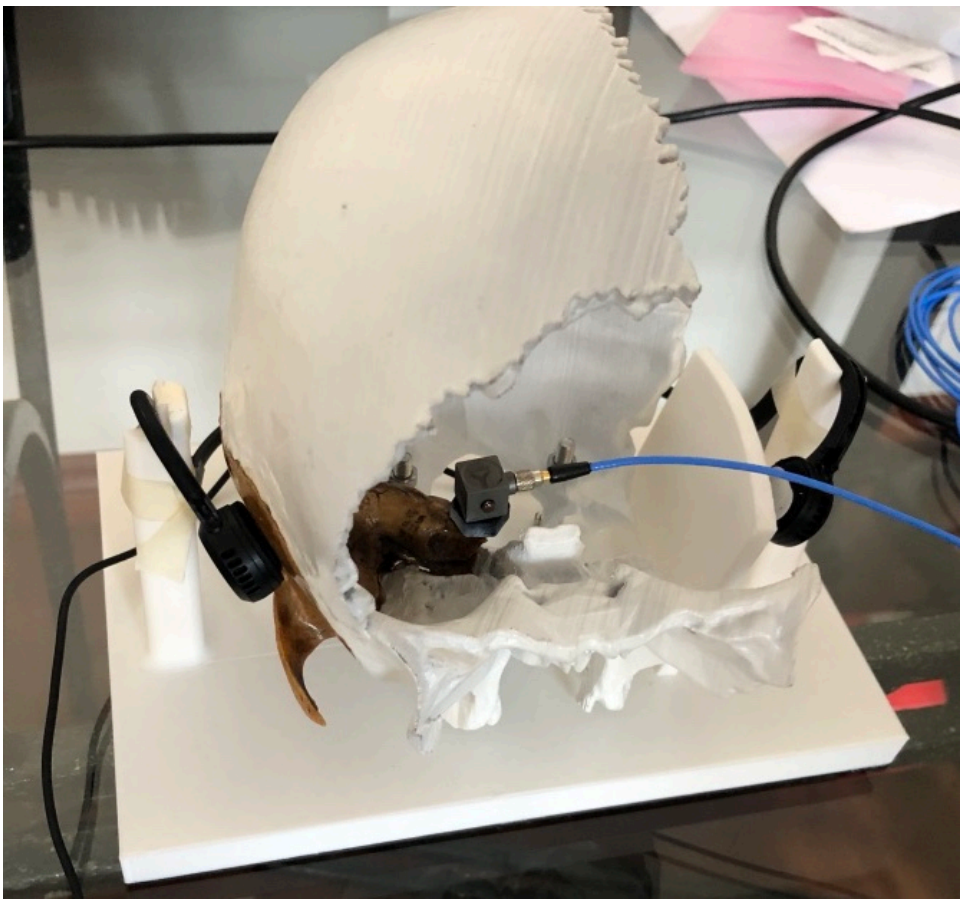

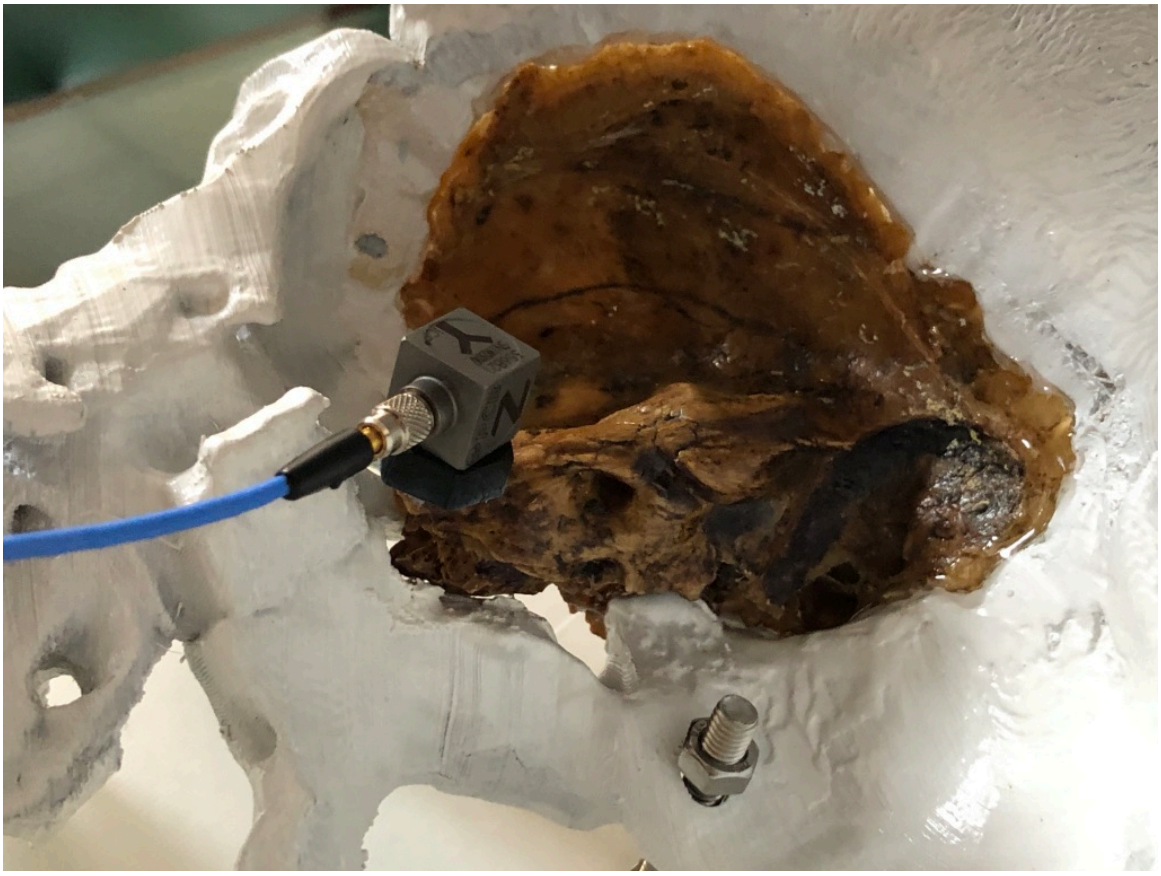

6.2. Photo of the PCB Piezotronics calibration data cards for the accelerometer

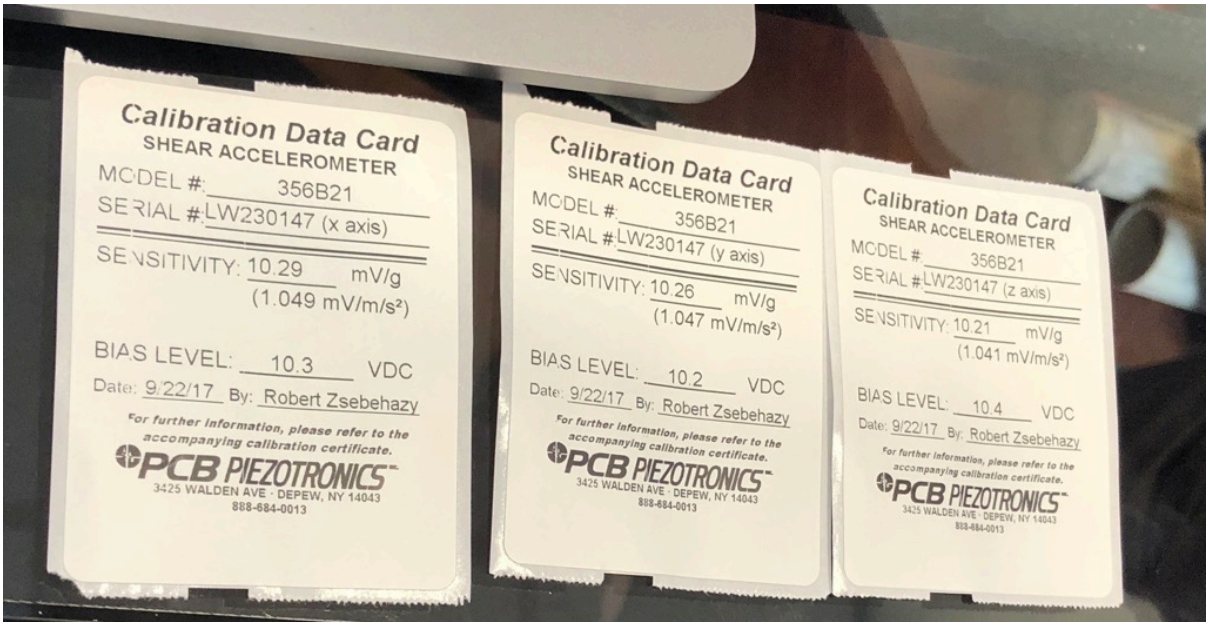

6.3. MATLAB raw acceleration data bandpass filter code

```
clc;
close all;
clear all;

acc=xlsread('raw1020.xlsx');
acc1=acc(:,1);
acc2=acc(:,2);
acc3=acc(:,3);
acc1=acc1/max(abs(acc1));
acc2=acc2/max(abs(acc2));
acc3=acc3/max(abs(acc3));

figure;
t=linspace(1,10,length(acc1));
subplot(311);
plot(t,acc1);
title('Acceleration - First Axis:');
xlabel('Time (s)');
ylabel('Acceleration');
grid on;
subplot(312);
plot(t,acc2);
title('Acceleration - Second Axis:');
xlabel('Time (s)');
ylabel('Acceleration');
grid on;
subplot(313);
plot(t,acc3);
title('Acceleration - Third Axis:');
xlabel('Time (s)');
ylabel('Acceleration');
grid on;

Fs=48000;
N=length(acc1);
w= -pi:2*pi/N:pi-2*pi/N;
f = w*Fs/(2*pi);
fft1=fft(acc1);
fft2=fft(acc2);
fft3=fft(acc3);
fft11=fftshift(fft1);
fft22=fftshift(fft2);
fft33=fftshift(fft3);

ws11=0.52;
wp11=0.57;
wp21=0.75;
ws21=0.80;
rp1=1;
rs1=50;
[Nf1,wn1]=buttord([wp11 wp21],[ws11 ws21],rp1,rs1);
[num1,den1]=butter(Nf1,wn1,'bandpass');
ws12=0.34;
wp12=0.39;
wp22=0.73;
ws22=0.78;
rp2=1;
rs2=50;
```

```
[Nf2,wn2]=buttord([wp12 wp22],[ws12 ws22],rp2,rs2);
[num2,den2]=butter(Nf2,wn2,'bandpass');
ws13=0.34;
wp13=0.39;
wp23=0.76;
ws23=0.81;
rp3=1;
rs3=50;
[Nf3,wn3]=buttord([wp13 wp23],[ws13 ws23],rp3,rs3);
[num3,den3]=butter(Nf3,wn3,'bandpass');
x1=filter(num1,den1,acc1);
x2=filter(num2,den2,acc2);
x3=filter(num3,den3,acc3);
x1=x1/max(abs(x1));
x2=x2/max(abs(x2));
x3=x3/max(abs(x3));

figure;
t=linspace(1,10,length(x1));
subplot(311);
plot(t,x1);
title('Filtered Acceleration - First Axis:');
xlabel('Time (s)');
ylabel('Acceleration');
grid on;
subplot(312);
plot(t,x2);
title('Filtered Acceleration - Second Axis:');
xlabel('Time (s)');
ylabel('Acceleration');
grid on;
subplot(313);
plot(t,x3);
title('Filtered Acceleration - Third Axis:');
xlabel('Time (s)');
ylabel('Acceleration');
grid on;
```

6.4. MATLAB filtered acceleration signal Integration and FFT code

```
clc;
close all;
clear all;

signal=xlsread('filtered1020.xlsx');
acc1=signal(:,1);
acc2=signal(:,2);
acc3=signal(:,3);
acc1=acc1/max(abs(acc1));
acc2=acc2/max(abs(acc2));
acc3=acc3/max(abs(acc3));

Fs=48000;
N=length(acc1);
w= -pi:2*pi/N:pi-2*pi/N;
f = w*Fs/(2*pi);

v1=cumtrapz(t,acc1);
d1=cumtrapz(t,v1);
v2=cumtrapz(t,acc2);
d2=cumtrapz(t,v2);
v3=cumtrapz(t,acc3);
d3=cumtrapz(t,v3);

figure;
subplot(311);
plot(t,d1,'linewidth',1.5);
title('Displacement - First Axis:');
xlabel('Time (s)');
ylabel('Displacement');
grid on;
subplot(312);
plot(t,d2,'linewidth',1.5);
title('Displacement - Second Axis:');
xlabel('Time (s)');
ylabel('Displacement');
grid on;
subplot(313);
plot(t,d3,'linewidth',1.5);
title('Displacement - Third Axis:');
xlabel('Time (s)');
ylabel('Displacement');
grid on;

dFFT1=fft(d1);
dFFT2=fft(d2);
dFFT3=fft(d3);
dFFT1s=dFFT1(1:N1);
dFFT2s=dFFT2(1:N1);
dFFT3s=dFFT3(1:N1);

figure;
subplot(311);
plot(f1,abs(dFFT1s));
title('Displacement Spectrum - First Axis:');
xlabel('Frequency (Hz)');
ylabel('Amplitude');
```

```
subplot(312);
plot(f1,abs(dFFT2s));
title('Displacement Spectrum - Second Axis:');
xlabel('Frequency (Hz)');
ylabel('Amplitude');
subplot(313);
plot(f1,abs(dFFT3s));
title('Displacement Spectrum - Third Axis:');
xlabel('Frequency (Hz)');
ylabel('Amplitude');
```